The overall objective of the Famega project was to identify the mechanisms controlling liquid metal assisted cracking (LMAC) of high-strength structural steels during hot-dip galvanising.

Sixteen steel sections were obtained and classified in terms of chemical composition, microstructure and mechanical properties, including high-temperature properties as inputs for FE modelling. Measurements of web residual stress showed predominantly compressive values of up to 50 % of yield. In contrast, welding processes resulted in tensile residual stresses close to yield near the weld.

Details of the galvanising process considered important to FE models were obtained from operators in Germany, Spain, Luxembourg and the United Kingdom.

Eighty full-scale galvanising tests were carried out on 2 m long beams with welded half-cover plates. Beams without welded plates did not crack. Techniques to reduce LMAC showed that thermal stress relief with a hand-held torch was highly effective, while sand blasting, ultrasonic peening and additional weld beads proved ineffective with compressive stresses confined to surface layers.

LMAC tests in three laboratories were carried out using newly developed and conventional test piece types and a variety of Zn alloys. Factors which contributed to LMAC included: Zn–Sn baths, lower strain rates and steel. High hydrogen levels were found at the steel/zinc alloy interface but did not contribute to cracking. Combining threshold stress and stress intensity using an FAD approach showed that fracture mechanics was only appropriate for cracks > 2 mm.

Modelling of welding and galvanising showed the importance of stress concentration near the half cover plate, residual stress, dipping speed and angle, and the heat transfer coefficient associated with a Zn–Sn alloy bath.

Price (excluding VAT) in Luxembourg: EUR 20

Publications Office
Publications.europa.eu

ISBN 978-92-79-08171-2

KI-NA-23195-EN-S

EC

Failure mechanisms during galvanising

EUR 23195

EUROPEAN COMMISSION

Community research

Failure mechanisms during galvanising

PROJECT REPORT

Research Fund for Coal & Steel

Interested in European research?

RTD info is our quarterly magazine keeping you in touch with main developments (results, programmes, events, etc.). It is available in English, French and German. A free sample copy or free subscription can be obtained from:

Directorate-General for Research
Information and Communication Unit
European Commission
B-1049 Brussels
Fax (32-2) 29-58220
E-mail: research@ec.europa.eu
Internet: http://ec.europa.eu/research/rtdinfo/index_en.html

How to obtain EU publications

Our priced publications are available from EU Bookshop (http://bookshop.europa.eu/), where you can place an order with the sales agent of your choice.

The Publications Office has a worldwide network of sales agents. You can obtain their contact details by sending a fax to (352) 29 29-42758.

EUROPEAN COMMISSION
Directorate-General for Research
Research Fund for Coal and Steel Unit

Contact: RFCS publications
Address: European Commission, CDMA 0/124, B-1049 Brussels
Fax (32-2) 29-65987; e-mail: rtd-steel@ec.europa.eu

European Commission

Research Fund for Coal and Steel

Failure mechanisms during galvanising

W. J. Rudd, S. W. Wen
Corus UK
Swinden Technology Centre, Moorgate, Rotherham S60 3AR, United Kingdom

P. Langenberg
IWT Aachen
Malmedyer Straße 30, D-52066 Aachen

B. Donnay
Arcelor Profil Luxembourg
66, rue de Luxembourg, L-4009 Esch-sur-Alzette

A. Voelling
RWTH
Intzestraße 1, D-52072 Aachen

T. Pinger, M. Feldmann
Universität Kaiserslautern
Stahlbau, Bauingenieurwesen, Gebäude 14, Zimmer 503, Erwin-Schroedinger-Straße, D-67663 Kaiserslautern

J. Carpio, J. A. Casado, J. A. Alvarez, F. Gutierrez-Solana
Universidad de Cantabria
Departmento de Ciencia e Ingenieria del Terreno y de los Materiales
ETS de Ingenieros de Caminos, Canales y Puertos, Avenida de los Castros s/n, E-39005 Santander

Contract No RFSR-CT-2003-00021
1 September 2003 to 28 February 2007

Final report

Directorate-General for Research

2008 EUR 23195 EN

Europe Direct is a service to help you find answers to your questions about the European Union

Freephone number (*)**:**

00 800 6 7 8 9 10 11

(*) Certain mobile telephone operators do not allow access to 00 800 numbers or these calls may be billed.

A great deal of additional information on the European Union is available on the Internet. It can be accessed through the Europa server (http://europa.eu).

Cataloguing data can be found at the end of this publication.

Luxembourg: Office for Official Publications of the European Communities, 2008

ISBN 978-92-79-08171-2

ISSN 1018-5593

Printed in Luxembourg

PRINTED ON WHITE CHLORINE-FREE PAPER

Contents

	Final summary report	5
1.	Introduction	15
2.	Objectives	15
3.	Background	16
4.	Comparison of initially planned activities and work accomplished	16
5.	Characterisation of materials (Work Package 1)	17
6.	Industrial process reviews (Work Package 2)	17
6.1	Residual stresses associated with manufacture and fabrication	18
6.2	Review of galvanizing procedures	19
7.	Experimental methods	21
7.1	Full scale trials and simulations (Work package 3)	21
7.2	Laboratory tests (Work Package 4)	25
7.3	Modelling	29
8.	Results	32
8.1	Full scale trials and simulations (Work Package 3)	32
8.2	Laboratory tests (Work package 4)	37
8.3	Modelling (Work Packages 5 and 6)	42
9.	Discussion	48
9.1	Materials	48
9.2	Galvanizing	49
9.3	Geometry	50
9.4	Strain rate	50
9.5	Residual stress	50
9.6	Dipping angle	51
9.7	Bath composition	51
9.8	Preheating	52
10.	Conclusions	52
11.	Exploitation and impact of the research results	53
11.1	Guidelines for the Avoidance of LMAC During Hot Dip Galvanizing of Steel Structural Components	53
12.	List of Tables and Figures	59
13.	References	63
	Tables	67
	Figures	87

FINAL SUMMARY REPORT

1. Introduction

Hot dip galvanizing (HDG) is a highly cost effective process to protect steel from atmospheric corrosion, with many advantages to service life and maintenance of steel structures. HDG is increasingly specified by architects and designers for the protection of steelwork in steel framed buildings such as multi-story car parks, offices and sports stadia, where the industrial finish is often appreciated for its modern aesthetic appearance as well as its corrosion protection properties.

Within the last decade there have been reports of cracks in steel after galvanizing which have been attributed to liquid metal assisted cracking (LMAC). These reports are still rare, and there is a view expressed in a recent review by Kinstler that the frequency of failures has not increased, but they are reported more [1]. In contrast other workers consider that the greater use of larger sections, higher strength steels, complex welding and the use of new zinc alloys has resulted in an increased occurrence of cracking. There has been economic and ecological pressure to substitute Zn-Pb alloys with those containing Sn and Bi. These alloys produce a desirable aesthetic appearance with a shiny surface and have economic advantages by controlling zinc thickness.

Sporadic outbreaks of LMAC have occurred throughout Europe over the last few years and, whilst a number of investigations have been carried out, the problem is not fully understood, cracking cannot be controlled and incidents continue to occur. Cracks formed by LMAC are sometimes observed immediately after galvanizing. In other cases cracks can be extremely difficult to detect by normal inspection methods and may become apparent only during the loading of a structure. There have also been occasions when substantial cracks have been discovered in load bearing members by routine inspection some time after the erection of the structure. In extreme cases galvanizing cracks approaching a metre in length have been observed and have serious implications on the structural integrity of an engineering structure. Even small galvanizing cracks may reduce the design lives of structures subjected to fatigue loads. The risk of structural failure must be reduced to acceptable levels, particularly where public safety is an issue, and the possibility of steel structures going into service whilst containing pre-existing cracks is clearly unacceptable. To achieve this it is necessary to understand the circumstances under which the cracks are initiated during the galvanizing process and to make recommendations that will help to avoid these failures.

2. Objectives

The overall objective of the project was to identify and understand the mechanisms controlling LMAC during hot-dip galvanizing by increasing the understanding of the phenomenon and the main factors controlling cracking, and thereby enable the safe galvanizing of higher strength steel components and fabrications without risk of cracking. The main objectives are summarised below:

- Identify the factors leading to the onset of cracking in the hot dip galvanizing process.
- Understand the microstructural mechanisms by which cracking occurs.
- Develop models of the failure mechanisms.
- Develop tests that allow reproducible tests for crack susceptibility of Zn-alloys under variation of important parameters.
- Modify products and processing methods to avoid the conditions that result in cracking.

3. Programme of work

Reviews suggest that three consistent factors are observed for liquid metal assisted cracking (LMAC):

- The cracks are almost always intergranular
- The cracks are the result of or at the location of some thermal or cold forming process
- The crack surface is coated with zinc or zinc reaction products

LMAC is considered to require the conjoint action of three factors: stress, environment and material, to which a recent review by Kinstler added time, making the requirements (Fig. 1):

- A tensile stress field
- A specific liquid metal
- A material condition or processing-induced sensitivity
- Time for the nucleation and growth or propagation processes to reach critical threshold levels

The factors affecting LMAC are not isolated; they have various interactions. Factors such as welding may influence the stress concentration, the residual stress, the surface roughness, the hardness and microstructure.

The FAMEGA programme was not aimed at an understanding of the chemistry and micro mechanism of LMAC, but was aimed at the more practical aspects, which would allow manufacturers, fabricators and galvanizers to avoid cracking. A combination of assessment of residual stress in sections, full scale tests, laboratory tests, and finite element modelling of welding and galvanizing allowed many of the factors influencing LMAC to be identified as described below.

The research programme was divided into 7 work packages:

- WP 1: Procurement and characterization of materials.
- WP 2: Industrial process reviews.
- WP 3: Full scale trials and simulations
- WP 4: Laboratory tests
- WP 5 Modelling of fabrication processes
- WP 6: Modelling of galvanizing processes
- WP 7: Co-ordination of programme

Obviously it is important for this type of research to develop means of dissemination into practice. This was done by producing practical guidelines which summarise the most important findings for practical use.

The technical work packages are described in detail below:

4. WP1 Procurement and characterization of materials

16 steels were obtained for the programme, with a range of strengths and toughness values. Six steels were obtained specifically for the lab programmes, with 10 steels obtained from a variety of sources for the full-scale tests. Manufacturers' information is always determined from material obtained from the flange of sections and this basic information was presented for the steels used in the full-scale tests. For the laboratory programmes the material was selected from the web, where LMAC usually occurs. All laboratory scale tests whether, tensile, Charpy, fracture toughness or LMAC were conducted with a stress applied transverse to the web and cracking running parallel to the web.

The microstructures of the steels ranged from large ferrite grains in S235J0 material to finer grained ferrite-pearlite steels for as-rolled and controlled rolled steels.

5. WP2 Industrial process reviews

This work package was primarily aimed at measurements of residual stresses and overlapped with the full-scale trials and modelling.

Residual stress measurements on the webs of as-rolled and straightened sections showed very low transverse residual stresses (Fig. 4). A series of sections collected from various European manufacturers for the full-scale trials also showed relatively low compressive residual stress, with a maximum of 50% of yield in the web (Fig. 7). In contrast, residual stress measurements associated with individual butt welds and on half plate test sections for the full scale tests showed tensile residual stresses close to yield either in the weld or adjacent to the weld.

The influence of residual stress on LMAC has been shown by full-scale tests and modelling and is described in Sections 6 and 8.

6. WP3 Full-scale trials and simulations

In each of the eight galvanizing trials 10 off 2 m lengths were tested together on an industrial scale (Fig. 11). The performance of these galvanizing trials allowed an improved understanding of the effects of processing and metallurgical variables on the cracking during hot dip galvanizing.

Ten sections, in steel grades ranging from S275 to S460, including thermomechanical, normalised rolled and conventional steels, were used to examine the following cases leading to cracking after galvanizing:

- Half cover plate welded on the web at the end of beams, which constitutes one of the most severe case in term of constraint and residual tensile stress. In some cases, half cover plates were welded without de-scaling and contained deliberate defects (saw cuts) and these were compared with properly welded plates.
- Flame-cutting of the flange, known as a “cope cut”.
- Plate welded on the flange.
- Drilling and oxy-cutting of holes of various diameters in the web.

The tests were carried out by using different processing parameters, namely:

- Classical zinc baths with usual pickling and over-pickling
- Zinc baths alloyed with tin with or without bismuth (usual pickling).

The test results allowed the identification of some factors leading to the onset of cracking during hot dip galvanizing. A combination of causes generated the cracks on assemblies, which can originate from:

- The high stress level following the design and the fabrication method.
- The steel grade or material susceptibility.
- Galvanizing processes.

Welding and finishing operations such as flame cutting or drilling inevitably generate high tensile residual stress. Actions aimed at reducing the level of residual stress in the critical area prior to galvanizing included:

- Application of thermal stress relieving at temperatures ranging between 550 and 700°C, with and without a holding time of 2 minutes.
- Application of mechanical stress relieving by sand blasting and ultrasonic shot peening.
- Modification of the welding sequence and the welding of additional weld beads under the half cover plates.

The analysis of the test results allowed the following conclusions to be drawn:

- Sections with half cover plates welded on the ends were very sensitive to LMAC and provided a good test model in this research to study the sensitivity to cracking in hot dip galvanizing. Cracks, always filled with zinc, were systematically located in the web at about 15 mm below the half butt plate and their length varied from a few mm to 700 mm following the galvanizing process.
- The steel variant combining a high strength and relatively low toughness level (S460J0: Charpy V at 0°C) presented the greatest sensitivity to cracking after galvanization. This section also had a highly sensitive geometry (see below)
- Compact sections appear to be less sensitive to cracking compared with high and slender sections with weaker moment of inertia.
- The thickness of the cover plate appeared to have no influence on LMAC - a 40 mm thick welded butt plate was no worse than a 25 mm thick plate.
- A mechanical defect, like a saw cut, may increase the sensitivity to cracking. This indicates that it is necessary to take care in the preparation of the welded joints prior to galvanizing.
- The magnetic particle inspection (magnetoscopic) technique is the most suitable NDT method; visual inspection and the dye penetrant test are insufficiently accurate and do not allow the systematic detection of all cracks.
- Over-pickling did not appear to have any detrimental effect on the structural steels tested.
- There was a clear increase in the values of residual stresses measured on welded sections compared to the as-rolled state. The tensile residual stresses associated with welding approached the yield strength level.
- A thermal stress relieving process prior to galvanizing was carried out using a hand-held torch at 550-600°C and a small holding time. This technique was shown to reduce the residual stresses of welded sections and to considerably reduce or avoid cracking. Mechanical stress relieving using ultrasonic peening was not successful and had only an impact on the product surface, while thermal stress relief acted more deeply.
- By comparing LMAC occurring in different galvanizing baths it was apparent that the beams galvanized in a zinc bath alloyed with tin presented a greater sensitivity to cracking at the beam end (with or without a mechanical defect). A bath containing a minimum amount of (or no) lead (Pb) and tin (Sn) could be very useful in galvanizing complex welded joints or designs, where a thermal stress relief treatment cannot be applied.

7. WP4 Laboratory programmes

LMAC tests were carried out at the University of Cantabria (UC), RWTH Aachen University (UA) and Corus RD&T. Each establishment concentrated on various aspects, which resulted in a better understanding of the factors controlling LMAC.

The University of Cantabria examined the following aspects:

- Material properties before and after galvanizing
- Surface roughening and surface deposits during pickling and fluxing pre-treatment
- Hydrogen uptake during acid pickling and during fluxing.
- LMAC tests on notched tensile and fracture mechanics tests pieces
- Energy dispersive analysis (EDA) of cracked samples to show the concentration effects associated with Zn-Pb and Zn-Sn baths

All materials suffered a decrease of strength and toughness in air at 450ºC compared to room temperature. The decrease was higher in liquid Zn. The average loss in mechanical properties was 24%, but in some cases values exceeded 30%. Steel J, which was the most susceptible to LMAC in full-scale tests (Section 8.1), had the lowest Charpy energy, but the loss of tensile and impact properties was similar to other steels. Surface roughness and hydrogen content increased after fluxing. After galvanizing tensile and impact properties recovered, becoming similar to the non-galvanized material.

The RWTH University of Aachen programme developed a new test method using a modified compact tension test piece with a 3 mm radius notch (LNT specimen). This had several advantages including

constraint at the notch. With only the test piece immersed, bath chilling was minimised yet direct measurements could be made on load-line displacement, with a clip gauge, which was not immersed in the zinc bath. The measurements of load and load line displacement allowed the assessment of failure to be made in terms of Mises stress and strain via finite element analysis. The results from these tests showed:

- For a given steel LMAC occurred at lower stresses and strains in Zn-Sn alloy compared to Zn-Pb alloy.
- There was a definite concentration of Sn at the tips of cracks and notches which suffered LMAC in Zn-Sn baths
- Stress and strain for failure depended on loading rate. There appeared to be a critical loading rate at which failure stress and strain was a minimum.
- The steel had a secondary effect, with no influence of strength. Higher levels of susceptibility to LMAC were associated with inclusion content, in particular elongated MnS particles.
- The test set up with the new LNT specimen gave reproducible results showing the influence of various Zn alloys on susceptibility to LMAC.

Tests at CRD&T on a range of test piece types showed the following:

- Threshold stress occurred above the yield stress (at 450°C) and hence stresses were lower for lower strength steels. The most resistant steel had low S and higher toughness, which agreed with the effect of inclusions observed at RWTH Aachen University.
- No difference in threshold stress/strain was obtained between machined test pieces and those with a flame-cut edge.
- Threshold stress values were reduced as the strain rate reduced, which was in line with results predicted by modelling.
- Failure analysis diagrams combining threshold stress intensity and threshold stress showed that threshold stress was the more important factor for cracks < 2 mm.

8. WP5 and WP6 Modelling

Modelling work was carried out at Technical University of Kaiserslautern (TUKL) predominantly using ANSYS software, with SYSWELD used for weld analysis. CRD&T used ABAQUS which required a number of input parameters to be determined experimentally including high temperature tensile data, Young's modulus and thermal strain.

TUKL analysed the round notch tensile specimen used by RWTH Aachen Univeristy, while Corus analysed key-hole test specimen used in the laboratory programme.

TUKL used a FE model to re-analyse data and obtain a heat transfer coefficient, whereas CRD&T used the heating of a channel section containing thermocouples and hot strain gauges in a validation exercise. TUKL also used a validation experiment on a beam section, using displacement transducers to determine the dynamic change of strains during galvanizing.

The TUKL programme examined several geometries including:

- Half-cover plate
- Drilled holes
- Cope cut

Factors which were modelled included:

- The influence of zinc bath composition
- Dipping speed
- Angle of dip – horizontal, 15° and 30°

The finding were summarised as follows:

1. Previously stress and strain were often considered to be constant or quasi constant during galvanizing. The modelling work has shown that high transient stresses are produced during galvanizing due to differential expansion within a complex shaped product

2. Construction details like stiffness changes or drilled holes are defined points with a high potential for deformation concentration.

3. Local areas of plasticity were formed giving residual strains in a range of 2 – 20% depending on the specific construction detailing.

4. The development of temperatures and the coincident stresses/strains strongly depends on the parameters chosen in the galvanizing process.

The CRD&T programme modelled the TUKL galvanizing experiment i.e.

- Half-cover plate
- Drilled holes

The following details were examined:

- Angle of dipping – horizontal, 45°, upside down (this models the back end).
- Effect of weld residual stress.
- Effect of mesh density on temperature, stress and strain prediction.

The conclusions drawn from this work are summarised below:

- The current work has shown that the galvanizing dipping orientation has an effect on the stress and strain history near the galvanizing cracking susceptible zone, and hence influences the cracking susceptibility.
- It has been demonstrated that using FE simulation the galvanizing cracking susceptible zones of a structure can be easily identified in relation to galvanizing process parameters, which would provide valuable information for the galvanizing practitioners.
- It has also been shown that weld residual stress has a detrimental effect on galvanizing cracking. The effect of residual stress is to increase the time spent at high stress, which allows time for LMAC to occur.
- It has been recognised that the values chosen for the heat transfer coefficient were artificially high. It has also been demonstrated that the discrepancies between the FE prediction and experimental measurements in terms of temperature and strain history during galvanizing are largely attributed to the fact that the metallurgical and fluid dynamic effect was not sufficiently considered in the heat transfer modelling. Furthermore, the density of the FE meshes employed might not be high enough, particularly near the surface. This suggests that further refinements could be made to modelling.

9. Synthesis of different work packages

All of the work packages have added to the knowledge of factors controlling LMAC. The following section attempts to bring this knowledge together under general headings.

9.1 Steel type

The highest strength lowest toughness material showed the greatest propensity for failure in full-scale tests. However, laboratory tests at UC failed to show an unusual susceptibility of this steel to LMAC. The implication is that the particular susceptibility of this beam is due to its slender geometry rather than material properties.

LMAC always occurred at stresses above the yield stress and hence higher stresses were required for higher strength steels. However, there was a wide range of critical strains and these depended on bath composition (UA), strain rate (CRD&T) and cross-head rate (UA)

9.2 Pre-galvanizing treatment

Fluxing rather than pickling increased surface roughness and hydrogen concentration (UC). A salt bath containing $ZnCl_2 \cdot 4NH_4Cl$(500 g/l) was, at the same molar concentration, more aggressive than $ZnCl_2 \cdot 2NH_4Cl$ salt (360 g/l).

The roughness increase was evidence of a deleterious effect in the quality of the surface, as well as the presence of small superficial defects that could act as micro-notches and, as a consequence, increase sensitivity to LMAC.

Hydrogen content after galvanizing was extremely high and hydrogen appeared to have accumulated in the steel base-Zn layer boundary, especially in the microcracks of Zn-Fe compound layers. There was, however, no evidence of hydrogen embrittlement in the structural steels examined in FAMEGA.

9.3 Galvanizing

The detrimental effects of Zn-Sn baths were shown by:

- The greater occurrence of cracking and greater crack lengths associated with LMAC during full scale tests in Zn baths containing additions of Sn and Sn-Bi compared to baths containing Zn-Pb or Zn alone
- Lower failure stress/strain in steels tested in Zn-Sn alloy baths during laboratory tests (UC and RWTH Aachen University)
- The observation of high Sn concentration at LMAC crack tips and a rich Sn-Pb layer between δ and ζ galvanizing layers suggested that Sn was able to concentrate and corrosively attack the GB region (UC)
- Sn concentrates at the tip of notches, cracks and other defects on the steel, both artificially introduced or produced by LMAC.
- Sn-rich baths increase the heat transfer coefficient resulting in greater thermal differences and hence increasing the stress and strain over the height of the component (TUKL) Fig. 103.

9.4 Geometry

A distinction should be made between stress concentration from joint geometry and micro-notches. Stiffness changes and holes have been examined during the FAMEGA programme and are considered to be one of the most important factors in LMAC as summarised below:

- The full-scale tests on beams with and without half cover plates showed no cracking without a cover plate. Stress concentrators such as holes also showed little cracking (see residual stress).

- Validation tests carried out at TUKL and RD&T showed that when simple sections were galvanized the measured and modelled stresses were elastic and relatively low. In contrast, for the half-cover plate geometry stresses well above yield were developed in the region where cracking was observed in full-scale tests (in the web 10-15 mm beneath the half cover plate weld).
- Models both at TUKL and CRD&T showed the large stress concentration effect of the half cover plate geometry.
- Holes also showed stress concentration effects but rarely cracked in full-scale tests (see residual stress).

The influence of micro-notches has not specifically been examined in the FAMEGA programme.

- The failure assessment diagram (FAD) analysis suggested that microcracks less than 2 mm should have little influence for the steels tested (Fig. 81).
- The literature suggests that flame cut edges reduce the stress required for LMAC. This was not proved in the FAMEGA programme and no real difference could be determined between machined and flame cut test pieces (Fig. 76).

9.5 Strain rate

Laboratory tests at CRD&T displayed lower threshold stress values for LMAC at lower strain rates (Fig. 77), although all values were above the yield stress of the steel at 450°C. The influence of loading rate on round notched samples studied at RWTH Aachen University (Figs. 59-63 and 65-71) suggested the lowest threshold strain values were produced at critical cross head rates. For practical purposes when galvanizing thin sections the dipping speed is the factor with the most impact on the stresses and strain rates (Fig. 100). An increase in dipping speed can be beneficial in lowering the maximum stress and strain rate underneath the half cover plate.

9.6 Residual stress

Residual stress measurements on as-rolled and straightened sections showed very low transverse web residual stresses (Figs. 3 and 4). A series of sections collected from various European manufacturers also showed relatively low web residual stress, with a maximum of 50% (compressive) of yield (Fig. 7). In contrast, residual stress measurements associated with welds and on half plate test sections showed tensile residual stresses close to yield either in the weld or adjacent to the weld (Figs. 5 and 7).

The influence of residual stress has been shown by full-scale tests and modelling.

- In full-scale tests heat treatment on the half-cover plate geometry reduced measured residual stress in the critical region and this was reflected in better LMAC resistance (Tables 20, 21 and 26).
- Modelling showed the residual stress of a welded half cover plate geometry had almost no influence on the peak stress and the time to reach the peak stress, but it had a considerable influence on increasing the time at high stress (Fig. 119). Without residual stresses the peak stresses above yield last only for a few seconds, while with residual stresses a beam would spend a longer time above yield, producing the appropriate stress/strain conditions for LMAC to occur.

9.7 Dipping angle

The TUKL model showed that changing the angle up to 30° resulted in a lower maximum strain (Fig. 101). In the specific position 13 mm below the half cover plate, the CRD&T model with a different geometry showed that dipping at 45° resulted in a slightly higher peak stress, but this peak stress lasted a matter of seconds (Fig. 111). In contrast a horizontal dip produced a marginally lower peak stress (but above the yield stress) for a much longer period. The implication from both models is that horizontally dipped beams with a half cover plate will be more prone to LMAC.

9.8 Preheating

Preheating reduced the temperature differences before and after heating. It therefore resulted in a significant reduction of the stress gradient across the section as well as across the thickness. Using Finite Element simulations a linear dependence between the preheating temperature and the occurring stresses and respective strains was verified (TUKL), see Fig. 104.

10. Guidelines

In addition to the scientific report, practical guidelines have been produced for public use. Every partner shall submit these guidelines to the interested industries and associations.

11. Conclusions

1. Measurements of web residual stress showed low or compressive transverse values, with a maximum up to 50% of yield. In contrast welding processes resulted in tensile residual stresses close to yield.

2. Full-scale tests, predominantly on beams with a half-cover plate, were successful at producing LMAC during galvanizing. Joint stiffness and residual stress are important and these parameters have been modelled (see below). Techniques to reduce LMAC showed that thermal stress relief with a hand-held torch was highly effective while sand blasting, ultrasonic peening and additional weld beads proved ineffective with the induced compressive stresses confined to surface layers.

3. Small scale laboratory tests show that LMAC occurs above the yield stress, but there is a drastic loss of ductility of steel under combined mechanical and corrosive loading which can manifest itself as a lower strain in tensile or round notch tests, or as reduced J integral in fracture mechanics based tests.

4. Fluxing was shown to produce high hydrogen levels at the steel-zinc interface, but this was not considered to influence cracking in the structural steels examined.

5. EDA studies showed a concentration of Sn at the crack tip in Zn-Sn baths and the constant presence of Sn and Pb above the δ layer close to the steel surface.

6. With regard to surface quality: a high presence of inclusions, poor welds, fluxing with excess of NH_4Cl, etc., may create small defects which make liquid metal penetration easier, especially liquid Sn penetration.

7. Combined tensile and fracture mechanics data showed that a level 2 FAD approach could be used for LMAC. The propagation of LMAC from control by threshold stress to stress intensity for cracks > 2 mm in S460ML steel was investigated. This fully justified the use of a threshold stress or strain in the modelling work.

8. The simulation of realistic steel structures created an understanding for the unsteady character of the stress/strain state during the galvanizing process. The development of high stresses or strains for a sufficiently long period is the basis to define an ultimate limit state against LMAC.

9. The combination of data obtained from laboratory scale tests and modelling simulation allowed the classification of multiple effects and influences contributing to LMAC initiation.

   Factors considered to have a large detrimental effect included:

- Stiffness of joint combined with residual stress – the geometry produced a high stress concentration, while the residual stress caused the stress/strain to remain high for a longer period of time.
- The zinc bath composition – Sn-rich baths influenced the concentration of Sn at the steel interface and increased corrosivity. In addition Sn additions had a large influence on heating rate by increasing the heat transfer coefficient.
- Dipping speed - this controlled both the maximum strain and the strain rate, with a reasonable correlation with laboratory tests. Higher dipping speeds could be used to prevent LMAC in critical situations.

Factors considered as having a secondary detrimental effect included:

- The base material - strength of the base material (S355 and S450/460 grades) appeared to be relatively small. There was some influence of toughness with lower critical strains associated with lower toughness steels.
- Preheating - modelling showed a linear effect of preheating. In practice preheating is not widely practiced and may be little more than a drying operation. If it involves suspending above the zinc bath it is not well controlled.
- Dipping angle - the influence on strain was relatively small

1. Introduction

Corrosion protection of steel by hot dip galvanizing has been practiced for about 100 years. It is a highly cost effective process with many advantages to service life and maintenance of steel structures. Hot dip galvanizing is used in many familiar items such as electrical transmission pylons, highway barriers, lamp posts, other street furniture and bridge wires. Architects and designers increasingly use it for protection in steel framed buildings such as multi-story car parks, offices and prestigious buildings such as sports stadia, where the industrial finish is often regarded as a modern desirable appearance.

Within the last decade there have been reports of cracks in steel after galvanizing which have been attributed to liquid metal assisted cracking (LMAC). These reports are still rare, and there is a view expressed in a recent review by Kinstler that the frequency has not increased, but they are reported more [1]. In contrast other workers consider that the increased use of larger sections, higher strength steels, complex welding and the increased use of new zinc alloys has resulted in an increased occurrence of cracking. The more usual Zn-Pb alloy has in some cases been substituted with Zn alloys containing Sn and Bi due to ecological pressure to remove Pb, aesthetic pressure because of the desirable appearance of the shiny spangle surface and economic pressures to control zinc thickness.

Sporadic outbreaks of LMAC have occurred throughout Europe over the last few years and, whilst a number of investigations have been carried out, the problem is not fully understood, cracking cannot be controlled and incidents continue to occur. Cracks formed by LMAC are sometimes observed immediately after galvanizing. In other cases cracks can be extremely difficult to detect by normal inspection methods and may become apparent during the loading of a structure, while there have been are occasions when substantial cracks have been discovered in load bearing members by routine inspection some time after the erection of the structure.

Galvanizing cracks approaching a metre in length have been observed in extreme cases and the implications of these on the structural integrity of an engineering structure are obvious. Even small galvanizing cracks may reduce the design lives of fatigue-loaded structures. The risk of structural failure must be reduced to acceptable levels, particularly where public safety is an issue, and the possibility of steel structures going into service whilst containing pre-existing cracks is clearly unacceptable. To achieve this it is necessary to understand the circumstances under which the cracks are initiated during the galvanizing process and to make recommendations that shall help to avoid these failures.

2. Objectives

The overall objective of the project was to identify and understand the mechanisms controlling LMAC during hot-dip galvanizing. This project aimed to increase the understanding of the phenomenon and the main factors controlling cracking and thereby enable the safe galvanizing of higher strength steel components and fabrications without risk of cracking. The main objectives and deliverables are summarised below:

Objectives:

- Identify the factors leading to the onset of cracking in the hot dip galvanizing process.
- Understand the microstructural mechanisms by which cracking occurs.
- Develop models of the failure mechanisms.
- Modify products and processing methods to avoid the conditions that result in cracking.

Deliverables:

- Improved understanding of the effects of processing and metallurgical variables on cracking during galvanizing.
- Models of the microstructural behaviour during galvanizing.
- Understanding of the interactions between material properties, fabrication methods and galvanizing processes, which result in cracking.
- Guidance for the avoidance of cracking.

3. Background

A number of reviews of LMAC have been carried out [1-5], the most recent by Kinstler on behalf of the American Institute of Steel Construction (AISC) [1,5]. This section is not designed to be a review but is designed to highlight and summarise the major findings. According to Kinstler [1,5] three consistent factors are observed for liquid metal assisted cracking (LMAC):

- The fractures are almost always intergranular.
- The fractures are the result of or at the location of some thermal or cold forming process.
- The fracture surface is coated with zinc or zinc reaction products.

In a similar manner to stress corrosion cracking many workers have considered that the phenomenon of LMAC is related to the conjoint action of three factors: stress, environment and material, to which Kinstler added time, making the requirements:

- A tensile force field.
- A specific liquid metal.
- A material condition or processing-induced sensitivity.
- Time for the nucleation and growth or propagation processes to reach critical threshold levels.

The conjoint action of the different factors is shown schematically in Fig. 1.

The factors affecting LMAC are not always isolated and factors such as welding may influence the stress concentration, the residual stress, the surface roughness, the hardness and the microstructure. The factors contributing to the problem are summarised in Table 1.

4. Comparison of initially planned activities and work accomplished

The project was originally divided into 7 different work packages. At the proposal stage of this investigation the literature suggested that residual stresses played a dominant role in LMAC, and this was due for investigation in WP3 and WP 5. The modelling work suggested that the dipping operation had a large influence, with welding playing a secondary role for thin sections. It appeared appropriate, therefore, to combine all modelling into one section and concentrate on the mechanisms which were most important to LMAC. A full description of the original working packages can be found in the technical annex in Appendix 1. WPs 5and 6 have been amalgamated and modified to include data required for all modelling work as shown below:

- WP1: Procurement and characterisation of materials.
- WP2: Industrial process reviews.

- WP3: Full-scale trials and simulations.
- WP4: fracture and microstructure modelling.
- WP5 and 6 Modelling of welding and galvanising + material data for modelling.
- WP7: Co-ordination.

A full description of the tasks within each Work Package is shown in Table 2, together with an assessment of whether these tasks have been accomplished and how successful they were.

5. Characterisation of materials (Work Package 1)

Work Package 1: Procurement and characterisation of materials

The list of materials is shown in Table 3. Steel sections were obtained from various European sources. Some of the steels were tested in all three laboratories undertaking the experimental programme.

The compositions of the steels are shown in Table 4, with the web mechanical properties in air at room temperature and 450°C shown in Table 5. Sections are normally characterised by flange properties, but web properties were also evaluated because LMAC occurs frequently there. All tested steels suffered a loss in strength and Charpy energy values at 450°C. The mean drop was 24% but values of more than 30% were found. Steel J, which was the most susceptible to cracking in full-scale trials, showed the lowest results in Charpy tests, but its behaviour was similar to other materials. All the mechanical properties were recovered after galvanizing, as shown in Table 6. Flange properties are quoted for the full-scale test programme in Table 7.

Typical microstructures are shown in Fig. 2, and range from low strength steels with a large grain size and predominantly ferrite microstructure, to micro-alloyed steels with fine grains and higher pearlite, though to controlled rolled steels where a degree of strength is conferred by the lower rolling temperature as well as micro alloying.

6. Industrial process reviews (Work Package 2))

The original work package sub-divided the tasks into:

- 2.1. Review of steel product manufacturing processes.
- 2.2. Review of typical customer fabrication procedures.
- 2.3. Review of galvanizing procedures.

Task 2.1. was mainly concerned with the measurement of residual stresses from manufacture, with task 2.2 being a review of processes such as cutting, welding etc. The influence of some of these processes on residual stress is covered in the large-scale testing of Sections 7.1 and 8.1. Auditing these processes with external manufacturers was very difficult because of confidentiality issues and some means of quantifying the procedures. The measurement of residual stress through the entire manufacturing process would appear to be a useful procedure and this has been undertaken for full-scale tasks by Arcelor Profil Luxembourg and Corus RD&T. Hence tasks 2.1. and 2.2 have been combined and include residual stress measurements after galvanizing. However, task 2.3, a review of galvanizing procedures, was carried out as planned for Germany, Luxembourg, Spain and the UK. The authors would like to thank various galvanizers and galvanizing associations for their help in carrying out this survey.

6.1 Residual stresses associated with manufacture and fabrication

The residual stress profile of a section is generated by a sequence of processes, which include:

- Rolling
- Cooling
- Lifting
- Straightening
- Fabrication (cutting and welding)
- Galvanizing

Some of these processes have been examined by finite element (FE) analysis and by measurements. This section deals primarily with measured residual stress. The development of stresses from welding and galvanizing is also covered in the sections on modelling i.e. Sections 7.3 and 8.3.

6.1.1 As-rolled and straightened sections

Residual stresses within sections have been modelled using Abaqus finite element modelling and direct measurements. Corus RD&T made measurements using a 3MA meter, which measures residual stress using the magnetic properties of a material. By measuring eddy current, upper harmonics, incremental permeability and Barkhausen noise, all of which vary with the stress state of the material, the 3MA meter calculates a residual stress value based on interpolation. The accuracy of the reading is closely dependent on the calibration for a particular grade of steel. A sample having identical composition and surface-finish as the test object is required for calibration. This sample is then loaded to a known stress allowing the 3MA meter to measure the different material properties at that stress. This is repeated over the range of stresses likely to be experienced by the material.

After rolling and cooling, the highest tensile stresses were observed at the web/flange junction. The web tended to have relatively low compressive stresses (Fig 3), with an even lower value at the end. The stresses were modified by lifting and straightening, but remained compressive or relatively low tensile stresses in the web (Fig. 4).

6.1.2 Residual stresses associated with welding

Measurements were made across a multiple pass double V butt weld on a 25 mm thick section using X-ray techniques. This required calibration using a 4-point bend test. Residual stresses were measured 80 mm either side of the horizontal weld for longitudinal and transverse stresses. Electro polishing was always used to remove surface residual stresses from preparation such as grinding. The results show values at a maximum in the centre of the weld with tensile values approaching the yield strength of the steel (Fig. 5).

6.1.3 Residual stresses for half cover plate

Arcelor Profil Luxembourg used SONATS equipment, which measures residual stress by X-ray diffraction (Fig. 6). It is a statistical method leading to the determination of the medium deformation of crystallographic planes (in the analysed volume), as a function of their orientation. Measurements of residual stresses were carried out in following conditions:

- As-rolled state
- Welded state
- Welded state + stress relieved
- Welded state + shot blasted

The measurements of residual stresses were carried out in the web of sections in the zone located below the welded half butt plate (Fig. 7). The measurements were made parallel and perpendicular to the rolling direction on two positions in the web, on the face and on the edge.

The following conclusions were made:

- In the as-rolled state, the residual stresses have levels of compression corresponding to a maximum 50% of the values of the yield strength of the steels measured.
- In the welded state, tensile residual stresses, which may approach the yield strength, were measured.

These aspects are covered in greater detail in Section 8.1, which also examines techniques to reduce residual stress and the subsequent influence on LMAC.

6.2 Review of galvanizing procedures

For beams and other large structural steel components batch hot-dip galvanizing is the process usually chosen. A schematic of an industrial process is presented in Fig. 8 [1-3].

The first step is washing, usually in an alkaline bath at a temperature between 65 and 80ºC in order to clean the beam of organic contaminants. Abrasive cleaning, which is sometimes used for galvanizing cast iron and steel, is less recommended for steel components because it can result in an excessively thick zinc coating.

After washing, articles must be rinsed with water. This is usually carried out at room temperature for at least one minute. Mineral salts in the water should be controlled to avoid further secondary reactions.

The next step is pickling in hydrochloric acid (5-15% wt.) at 25-40ºC (to avoid excessive foaming) or in sulphuric acid (3-14% wt.) at 60-80ºC. The main objective is to eliminate rust and oxides, common in hot-rolled products, and deleterious to surface coatings such as galvanizing. In this step, hydrogen (H) could penetrate the steel and cause embrittlement. With current techniques in galvanizing mills this problem is minimized, but not totally eliminated.

After a new rinsing to eliminate all the acid from pickling, there are two possible hot-dip galvanizing processes: Wet galvanizing and dry galvanizing.

In dry galvanizing, which is the more traditional process, the surface of the steel is activated by fluxing in an aqueous solution of zinc ammonium chloride, with additions of a wetting agent, at a temperature of 25-80ºC. Varying concentrations and types of salt may be used here.

After fluxing, drying the steel component is very important to avoid splashes on the steel surface and possible explosions of water vapour in the galvanizing bath. Some manufacturers have ovens designed for this process, while others rely on the heat from the flux bath and/or suspending the objects over the zinc bath. This drying step makes it easier to eliminate H picked up from pickling/fluxing of steel. After drying, steel components are dipped in the galvanizing bath at 440-460ºC. The usual immersion time is between 3 and 6 minutes, but some operations use up to 10 minutes.

In wet galvanizing, which is a relative new technique, a flux blanket of liquid ammonium chloride with additions of sodium aluminium fluoride (cryolite) or zinc ammonium chloride, covers the liquid zinc bath at 440-460ºC. When the steel component is introduced, it crosses the flux blanket, which eliminates the impurities on the steel and activates its surface. The galvanizing bath is the same as in the dry process. Wet galvanizing allows cost savings in both equipment and space, but as a new technique it is not present in all countries yet.

The modelling work (Section 8.3) indicated that the most important areas within the galvanizing process, which could influence LMAC were:

- Speed of dipping.
- Bath composition.

- Preheating.
- Temperature of bath.

The FAMEGA team have conducted surveys within their own countries to look at these variables, which are summarised in Table 9, and discussed in greater detail below.

Speed of dipping

Most galvanizers have very rudimentary control over dipping speed. Crane hoists usually have 2 speeds, namely fast and slow, and hence the speed may differ between galvanizers depending on the equipment available and the article itself. Withdrawal speed is generally considered important for the appearance of the finished article with withdrawal speed matched to good drainage to avoid sheeting or puddles of zinc. However, the modelling work suggests that LMAC is most strongly associated with differential thermal expansion during the dipping process.

The angle of dipping is also important. This tends to be based on removal of gases and ash, but occasionally angle and orientation have been used to reduce the effects of stresses.

Bath composition

Galvanizers have often evolved bath compositions and regard this as a highly confidential area. However, it is known that baths high in tin are more prone to cause cracking. Continental operators in particular noted this problem and reduced the levels of tin used. The modelling work suggests that small quantities of tin have a large influence upon heat transfer coefficient (Section 8.3.). There may be other effects of tin with high concentrations observed at the tips of LMAC (Sections 8.1 and 8.2). Zinc galvanizing baths for sections often contain small quantities of aluminium to improve brightness, nickel to improve reactivity in formation of the alloy layer and tin to retain the spangle finish and improve flow of the solution around work piece contours. The effects of elements other than tin and bizmuth have not been associated with an increased risk of LMAC.

Preheating

Few galvanizers deliberately preheat sections prior to galvanizing. However, one operator had a 30-minute drying operation at 60-70°C. The fluxing operation itself is usually carried out at ~60°C, but drying temperature has to take into account the thermal stability of flux salts [6]. It is common practice to suspend the articles over the galvanizing bath to complete drying, usually for 2-10 minutes. Hence articles are usually well above room temperature when dipped in the zinc bath. Corus was allowed to monitor operations at one galvanizers and recorded temperatures with an optical pyrometer. Web temperatures between 90 and 140°C were recorded for hold times of 10 minutes. It would appear that this part of the operation might result in a considerable amount of variability.

Bath temperature

Bath temperatures are fairly well controlled at individual galvanizers. Table 9 shows that the ranges are fairly limited even over a wide range of operators in different countries. Although bath temperature is one of the factors in modelling, it is considered that there is little scope to control LMAC with bath temperature.

7. Experimental methods

7.1 Full scale trials and simulations (Work package 3)

7.1.1 Objectives

The objectives of the work package were:

- Measure stresses imposed and changes to original product by downstream processes: cutting, drilling, welding.
- Perform monitored full-scale galvanizing trials.
- Determine optimum technique for post-galvanizing crack detection.

7.1.2 Working programme

Full scale trials were carried out by Arcelor Profil Luxembourg in order to determine the probable mechanisms of cracking when galvanizing sections. It was intended to study the effect of various parameters of the fabrication and galvanizing operations as well as the characterisation of the steels.

The selected assembly consisted of beams welded with half cover plates, as this geometrical configuration was known from the literature to be highly sensitive to LMAC during galvanizing. Thermo mechanical steel grades were compared with normalised and conventional steels. Ten different grades of sections ranging from S275 to S460 were used to assess the effects of strength, toughness and process route (Table 8).

As far as possible, sections with identical geometries were selected to avoid dimensional influences in the full-scale trials. IPE sections were chosen as the basic geometry (with height ranging between 600 and 750 mm). These profiles are used in real applications with the critical design reproduced in these full-scale trials (welded half cover plate). Unfortunately, it was not possible to obtain this geometry in all cases.

An example of an assembly composed of half cover plates welded on a beam is illustrated in Fig. 9. In this case one end with a half cover plate had deliberate defects (scale + mechanical defect), whereas the other end reflected good practice.

The dimensions of the welded joints were chosen with the section length at least twice the section height. This allowed the test samples to accurately simulate the galvanizing of long sections.

Beside the half-cover plate, other cases investigated included:

- Sections where the flange was partially removed by oxy-cutting or by other means.
- Sections with boreholes or flame cut holes.

7.1.3 Choice of welding conditions

A welder qualified according to EN287-1 performed the fillet welds, connecting the half cover plates on the section ends in the finishing department of Arcelor Profil Luxembourg-Differdange. In these tests the welding procedure corresponded to that usually performed by a commercial workshop for the welding of half cover plates.

25 mm thick grade S355 half cover plates were attached by 6 mm thick fillet welds to the sections using the following welding procedure:

- MAG (metal active gas) process 135, EN ISO 4063, with wire of diameter 1.2 mm, trade mark ESAB OK Autrod 12.51, gas protection: 82% argon and 18% CO_2 (standard identification: EN 440 G3Si1 and AWS A/SFA 5.18 ER 70S-6).

- Average heat input 21 kJ/cm
- Welding without preheating (according to EN 1011-2).
- Welding in flat position (position PA according to EN 287).

The welding parameters and the position of the section during the welding of the half cover plate are given in Table 10.

The welding parameters of the fillet welds were checked and validated according to the requirements of standard EN ISO 15614-1. This standard requires the establishment of a WPQR (welding procedure qualification report) for the welded joint and a WPS (welding procedure specification) necessary to produce all of the weld joints. The standard (EN ISO 15614-1) requires a macrographic section and HV10 hardness measurements on precise positions in the fillet welded joints as shown in Fig. 10.

The metallographic examination was carried out on the section web, as this is the usual place that LMAC is observed after galvanizing. The results of the metallographic examinations for the three sections identified D, F and I (S355 to S460) are given in Table 11. The purpose was to check the requirements of EN ISO 15614 i.e. 6 mm weld bead height and HV10 max. = 380 for a single pass.

The visual examinations after the dye penetration test and the metallographic examination showed that the weld beads did not contain macroscopic or microscopic cracks. It was considered that typical commercial welding conditions had been accurately simulated.

7.1.4 Industrial galvanizing tests

In this research programme 8 series of galvanizing tests were carried out. The galvanizing variants are summarised in Table 12. The experimental parameters evolved throughout the research programme to reflect current ideas and react to some of the industrial changes occurring in the galvanizing industry.

7.1.4.1 Industrial galvanizing tests: No. 1 to No. 3

At the beginning of the research programme three full scale galvanizing tests were performed where the effect of two processing parameters were examined (Test numbers 1-3, Table 12):

- Pickling time: standard pickling time (2 hours) was compared with over-pickling (17 hours).
- Analysis of galvanizing bath: conventional bath was compared with tin alloyed bath.

The common galvanizing procedure for the first three tests is described below:

- 10 section lengths were fixed on one gantry crane (see Fig. 11).
- Pickling was carried out in hydrochloric acid (HCl), with pickling times for variant 1 = 17 hours, variant 2 = 120 minutes, variant 3 = 50 minutes. Acid concentration ranged between 100 and 150 g/l.
- Sections were rinsed with water.
- Fluxing was carried out in a bath of "double salt $ZnCl_2$-NH_4Cl" for 7 minutes at a temperature of about 40°C.
- Dipping speed in the zinc bath was 1 m/min.
- Holding time in the zinc bath was 7 minutes.
- Temperature of the zinc bath was 448 to 450°C.
- Extraction speed from the zinc bath was 0.4 m/min.
- Natural cooling was carried out after galvanizing.

This procedure ensured identical galvanizing conditions for three tests.

7.1.4.2 Industrial galvanizing tests 1 and 2

Figure 12 illustrates the detail of the preparation of the welded joints for galvanizing tests 1 and 2. In order to obtain a similar level of residual stresses for the various sections heights, it was decided to weld a half cover plate corresponding to half the section height for beams greater than 600 mm and to weld a cover plate corresponding to 3/4 of the section height for the 350 mm beams. This situation was then kept throughout the programme. 25 mm thick butt plates in grade S355 were used throughout, as this is common industrial practice.

Two methods for joint preparation were studied for these first galvanizing tests:

- At one end of the beam, good practice was performed on all pre-and post-welding operations
- At the other end of the beam, the welding was carried out without removing the scale prior to welding, and a deliberate 2 mm saw cut was introduced 10 mm below the half cover plate. This position corresponds to the position where LMAC has been observed in sections with half cover plates and is shown in Fig. 13.

Welding parameters were recorded during the execution of the 6 mm fillet welds between plate and section for the first two series of tests. For the properly executed weld, heat inputs of about 21 kJ/cm, were recorded i.e. the same as noted for the establishment of the WPQR. For poorly executed welds higher heat inputs were recorded with values reaching 28 kJ/cm. This was attributed to the lower welding speed required as the scale had not been removed by grinding prior to welding.

7.1.4.2 Industrial galvanizing test no. 3

Compared to the two preceding test series, modifications were made for the preparation of the welded joints for each steel variant, namely:

1. A 25 mm thick cover plate was welded on one beam end while the other end was fitted with a 40 mm thick plate. Such designs may be used commercially and there was some concern that a higher thickness ratio with the web may induce greater cracking sensitivity due to higher thermal heterogeneities.

2. No mechanical saw notch was used.

3. The welding was properly carried out for both thickness variants (25 and 40 mm thick plates in S355). The same welding parameters were applied as for the first test series, where the heat input of 21 kJ/cm was used to execute 6 mm fillet welds.

Figure 14 illustrates the welded assembly design for galvanizing test no. 3.

7.1.4.3 Industrial galvanizing test no. 4 – residual stress measurements

The main objective of this part of the research programme was to find solutions to avoid LMAC in beams welded with half cover plates. A combination of causes is likely to generate LMAC on these assemblies, but one of the principal reasons is considered to be the residual stresses generated by the welding of the half cover plate. It was decided to assess the residual stress pattern in the area where the cracks originate, using a non-destructive technique. Residual stresses were measured before and after mechanical or thermal treatments, which were used to modify the residual stress pattern in an attempt to reduce the sensitivity to LMAC.

The following potential stress relief methods were tested:

- Thermal stress relieving using a torch to apply at temperatures ranging between 600 and 700°C, without applying any holding time (Fig. 17).
- Mechanical stress relieving by sand or by shot blasting, a process called Stressonic carried out by the Sonats company.
- Modification of the welding sequence and the welding of additional weld beads (Fig. 16).

For galvanizing test no.4 three steel grades were used: S275J0, S450J0 and S355ML. In particular, S450J0 was selected due to its high susceptibility to LMAC in previous trials.

Sections with half cover plates were manufactured according to Fig. 15. Details of the equipment (Fig. 6) and procedure are contained in section 6.1.3. Measurements of residual stresses were carried out in following conditions:

- As-rolled
- Welded
- Welded + stress relieved
- Welded + shot blasted or peened

7.1.4.4 Industrial galvanizing test no. 5

The principal aim of this trial was to validate the test results of trial no. 4, which indicated that thermal stress relieving could be a good remedy to avoid LMAC in welded and galvanized sections. For galvanizing test no. 5, test specimens in different grades were prepared by applying the correct welding rules during the welding of half cover plates on each beam ends. For grades S275J0 and S450J0 one extremity of the beam was not fitted with a cover plate. A comparison with the welded side would reflect the importance of welding stresses and geometry. The galvanizing process was identical to test no. 4.

In addition test no. 5 also studied the following variations:

- The welding of a weld seam below the half cover plate.
- The effect of thermal stress relieving at 600°C with a holding time on temperature of 2 minutes on each of the beam ends covered by a welded plate.
- The welding of a plate in the flange.
- The use of a protective coating to decrease the thermal shock.

Figure 18 shows the aspect of welded assemblies.

It was considered that the addition of a 5 cm long weld bead under the ½ cover plate, would have the following effects:

- Add compressive residual stresses in this area.
- Strengthen this zone by a local increase of the web thickness.
- Prevent the dissolution of surface MnS particles during pickling, as these could be initiation sites for the development of cracks.

Figure 19 shows a scanning electron microscope SEM (100x) picture of a web section of grade S460ML (C-steel, low sulphur) after pickling with hydrochloric acid. In this case pits were observed corresponding to manganese sulphides.

7.1.4.5 Industrial galvanizing test no. 6

In galvanizing trial no. 6 the aim was to study the influence of reduced residual stress on LMAC. Finishing operations such as drilling or flame cutting can generate residual stresses. Different test specimens were used (half cover plate, cope cut, burned and drilled holes of different diameters) in order to study the effects of thermal stress relieving on these different parameters. Tests were undertaken as follows:

- Beams with welded ½ cover plate: addition of a compression weld bead or application of a 2 minute thermal treatment at 600°C in the critical cracking zone.
- Beams with plate welded on beam flange: no action.

- Beams with flame-cut flanges (cope cut) and beams affected with oxy-cut (ø150 mm) and drilled holes (ø 22, 29 mm): one half of the beam was heat treated at 600 °C for 2 minutes; the remaining half beam was not thermally treated.

The different assemblies are shown schematically in Fig. 20.

Galvanizing was carried out using a zinc bath alloy with a higher tin content. The flux can be a significant parameter for avoiding LMAC and an optimised flux was proposed by the producer of zinc alloy with a view to counteract the effect of tin. This optimised flux was adapted for this test.

The other galvanizing parameters were as follows:

- Slope of galvanized pieces: a low angle (8 -10°) was selected.
- Dipping speed: as fast as possible (8 m/min).
- Zinc bath temperature of 442 °C (lowest possible choice).
- Dipping time (unknown).
- Bath composition: Pb 0.95 %, Sn 0.81 %, Bi 0.018 %.

Fifteen sections of finished beams were galvanized under these conditions; 10 beams with welded ½ cover plates, 3 beams with cope cuts and 2 beams with oxy-cut and drilled holes.

All beams were visually examined after galvanizing. In addition, all beams were checked by the magnetoscopic technique in order to detect non-visible cracks.

7.1.4.6 Industrial galvanizing tests no. 7 and 8

The main aim of these tests was to investigate the efficiency of heat treatment at the slightly lower temperature of 550°C and perform further work at 600°C.

The composition of the galvanizing baths contained tin but not lead for the first test and had neither lead nor tin in the second test. The different compositions of zinc baths for both tests are shown in Table 12.

Test nos. 7 and 8 used 10 welded joints covering all the steels used in this project (Table 7), and each end of the beam was welded with a ½ cover plate. Welding was correctly performed according to the usual procedure required for the welding of half cover plates. After welding, one end was left in the as-welded condition, whereas the other end was thermally treated in the critical cracking zone at temperatures of 550°C and 600°C respectively for 2 minutes duration.

7.2 Laboratory tests (Work Package 4)

The main objectives for this task were:

- Characterise LMAC in terms of threshold stress/strain and in fracture mechanics terms (K, J).
- Modelling of fracture mechanisms in the zinc bath to establish the critical parameters for fracture.
- Metallurgical assessment to determine the microstructures most susceptible to cracking.

LMAC tests in liquid zinc were undertaken at the Universities of Cantabria and Aachen and at Corus RD&T.

7.2.1 University of Cantabria programme

A test matrix was developed in order to evaluate the influence of each galvanizing step and other variables such as temperature on the mechanical, chemical and surface properties of the steel grades tested at full scale (See Table 14). All the tests of the matrix were applied to steel grade J, which was the most sensitive to cracking in full-scale trials (see Sections 7.1 and 8.1).

Some tests were performed on other steels for comparison with steel J: steels A, B, C, L and M were chosen for tensile and Charpy tests, steel B for crack characterisation tests and steel C for fracture (J-integral) tests.

Chemical analysis, microstructural, tensile and Charpy tests in as-received conditions at 20ºC and 450ºC and in galvanizing conditions (using a galvanizing bath with 1.1% Sn) were performed to obtain a material database whose results are shown in Section 8. The different specimens used in the complete experimental programme also appear in Section 8 (Fig. 22).

As shown in Table 14, the tests were performed using different conditions:

- As received condition: at 20ºC and 450ºC (galvanizing temperature).
- Pickling condition: after immersion for 2 hours in a 15% HCl aqueous solution at 35°C with 100 ppm of hexamethilentetramine inhibitor (usual pickling conditions in industry).
- Fluxing conditions: Two kinds of flux baths were used in this programme [6]:
  - $ZnCl_2 \cdot 2NH_4Cl$ salt flux: 360 g/l aqueous solution, duration of 10 minutes at 50ºC. This salt composition is typically used in Europe.
  - $ZnCl_2 \cdot 4NH_4Cl$ salt flux: 500 g/l aqueous solution, duration of 10 minutes at 50ºC. This salt composition is typically used in North America.
  - Except where indicated, pickling was applied before fluxing.
- Galvanizing baths: Two kinds of galvanizing baths were considered in this programme; the traditional Zn-Pb compositions and a Zn-Sn bath, which is representative of that used in the last decade. The compositions are shown in Table 15. The temperature for galvanizing was 450ºC and immersion time was 5 minutes.

Steel surface roughness was measured in the as-received condition to establish a reference. The same measurement was performed after pickling, and after fluxing with $ZnCl_2 \cdot 4NH_4Cl$ salt. The experimental equipment used to measure the roughness was a PERTHOMETER PRK.

Hydrogen concentration tests were performed on prismatic specimens of 6 x 6 x 10 mm, which were submitted to the different pre-galvanizing and galvanizing processes indicated in Section 8.1. Figure 21 shows a schematic of the specimens used to carry out the hydrogen concentration tests and a photograph of the LECO RH-402 machine used for these tests.

J-integral fracture tests using compact tension (CT) specimens (Fig. 22) from steels J and C were performed following the ESIS P-2 standard [7]. Several were considered:

1. As received at 20ºC.
2. As received at 450ºC (galvanizing temperature).
3. Fluxed with $ZnCl_2 \cdot 4NH_4Cl$ salt and immersed in a Zn-Sn bath at 450ºC.
4. Fluxed with $ZnCl_2 \cdot 4NH_4Cl$ salt and immersed in Zn-Pb bath at 450ºC.

Slow strain rate tests (0.002 mm/s displacement rate) on round-notched axi-symmetric specimens (Fig. 22) from steel J were performed in the following conditions:

1. As received at 20ºC.
2. As received at 450ºC.
3. Fluxed with $ZnCl_2 \cdot 4NH_4Cl$ salt and immersed in a liquid Zn-Sn bath at 450ºC.

Crack characterisation tests using double cantilever beam (DCB) specimens (Fig. 22) made from steels B and J were performed in liquid Zn. The steel B specimens were machined with different notches in order to analyse the notch geometry effect in crack initiation during galvanizing. A value of K_I = 120 MPa $\sqrt{m}$ was applied to the pickled and fluxed DCB specimens using bolts, as shown in Fig. 23. The specimens were then immersed in Zn-Sn or Zn-Pb galvanising baths for five minutes before being extracted and cut to be examined by scanning electron microscope (SEM).

7.2.1.1 LMAC testing

Several types of test piece were used for the UC LMAC test programme, as illustrated in Fig. 22.

A 100 kN capacity Instron universal testing machine with a specially designed loading rig was used by UC for these tests. The loading device was needed to transform the vertical load from the universal testing machine into a horizontal one directly applied to the specimens immersed in the Zn bath. Moreover it had to satisfy the following requirements:

- Be rigid compared to the specimens.
- Resist the 450°C of the Zn bath.
- Transmit the loads without losses by friction.
- Adapt to the CT and axi-symmetric specimens used in the Zn bath tests.
- Permit the use of measuring devices (clip gauges, etc).

Photographs of the loading device are shown in Fig. 23, and schematically in Fig. 24. A 250 mm high cylindrical furnace with an internal diameter of 210 mm was specially designed for the tests. The furnace included exchangeable crucibles made of boronsilicate glass (Pyrex ®), which resisted the temperature of the bath without contaminating it. Appropriate software was used to control the heating process and to maintain the temperature at constant values (450 ± 5°C) for the LMAC tests.

All specimens tested in liquid Zn baths were examined in a JEOL scanning electron microscope (SEM) incorporating an energy dispersive X-ray spectroscopy (EDS). The analysis included:

- Study of industrial Zn layers on galvanized steel with Zn-Sn baths versus conventional Zn-Pb baths.
- EDS spectrum of Zn layers at crack tips and machined notches CT and DCB specimens.
- Study of the composition of the metal which penetrated and solidified in the cracks propagated in the specimens tested in liquid Zn.

7.2.2 RWTH Aachen University programme

Factors considered to influence the development of LMAC include:

- Surface condition (roughness, hardness).
- Microstructure.
- Micro-notches on the surface, which can act as local stress concentrators and facilitate the penetration of liquid zinc at the grain boundaries.
- Impurities, especially elongated inclusions such as sulfides.

7.2.2.1 Test specimen

To reproduce these effects in laboratory testing a new specimen {long notch tension; L-N(T)} was designed to investigate the different and interacting influences. The test piece was based on compact tension type test pieces with a key-hole notch (Fig. 25). At the tip of the machined notch a drilled hole was inserted to enable local stress concentration and development of a stress hot spot. Cracks grow along beams in a longitudinal direction, hence the specimen was extracted from the web of rolled I-beams in full thickness with a T/L orientation.

7.2.2.2 Test equipment

In the LMAC test setup a 60 kN hydraulic universal testing machine was used. The hydraulic cylinder was operated horizontally and provided a maximum displacement of about 28 mm in load control and about 20 mm in displacement controlled testing. An electrical furnace containing a graphite crucible with a capacity of about 12 litres of liquid zinc was placed beneath the loading arms. In the top cover

of the furnace a rectangular slot was placed to insert the L-N(T) specimen for dipping which was achieved done simply by lifting the whole furnace with a hydraulic lifting table (Figs. 26 and 27).

7.2.2.3 Specimen preparation

Each specimen was taken individually through the following steps:

- Sandblasting to remove any residue from machining and get a clean surface.
- Pickling with 10% hydrochloric acid for 10 minutes.
- Rinsing in distilled water and drying with cool air stream.
- 5 minutes fluxing in 60% ZnCl+40% NH_4Cl.
- Drying at room temperature.

7.2.2.4 Testing parameters

The starting temperature for testing was 445°C. Due to dipping of the L-N(T) specimen the temperature then dropped by about 5 to 8°C. The following measurements were made:

- Machine load.
- Machine displacement.
- Bath temperature.
- Load line displacement of the specimen, using a high temperature clip gauge.

Due to safety regulations an exhaust system was installed and operated just above the L-N(T) specimen to extract any air pollution. The universal testing machine was operated under both constant load and constant displacement rate.

7.2.2.5 Zinc alloys investigated

Three different zinc alloys were used for testing. The alloying concept of a0 was mainly based on tin and bismuth supported by small parts of nickel, iron and aluminium. Alloy a1 was a classical composition containing basically lead alongside small amounts of iron and aluminium. Complementary alloy a2 contained mainly lead and tin with small amounts of bismuth nickel, iron and aluminium. Table 16 gives the bath compositions.

7.2.3 Corus RD&T programme

7.2.3.1 Test piece type

Steels A, B and C (Table 3) were used in the Corus programme. Several test piece designs were used (Fig. 28).

(a) Tensile test piece: Surface finish, microstructure and hardness were compared by using machined test pieces and flame cut test pieces.
(b) Compact tension test pieces: These were used in the fatigue pre-cracked condition to determine the threshold stress intensity for LMAC.
(c) Keyhole test pieces: These were used to determine a threshold stress, as direct measurements could be made on the test piece. The disadvantage was the complex analysis, which required FE
(d) Short crack fracture mechanics test pieces: These were used to determine if a type 2 FAD approach could be used for LMAC.

7.2.3.2 LMAC test equipment

A 100 kN hydraulic test frame was used horizontally. The zinc bath was manufactured from mild steel used by industrial galvanizers, and contained approximately 2.5 litres of zinc. The experimental set up is shown in Fig. 29.

All test pieces were loaded via a set of horseshoe grips, with the entire furnace and bath raised and lowered into position via a standard automotive screw jack. Both the standard compact tension test piece and ones with key holes had advantages over the other tests in that the horse-shoe grips were not immersed in the zinc bath (avoiding the chilling effect) and direct measurements could be taken with a high temperature clip gauge.

7.2.3.3 Test piece preparation

Prior to testing in zinc the test pieces were treated using the same cleaning and fluxing regime as an industrial galvanizer:

- Degrease: 10 min in mildly caustic degreaser at 60-80°C.
- Pickling: 30 min. in HCL, pH =12 at room temperature.
- Rinsing: 1 – 2 min. in no. 1 solution (from a galvanizer) at room temperature.
- Flux: 10 min at 70°C.
- Drying: 30 min at 60 – 70°C.
- Dipping: LMAC test in zinc at 445 – 455°C. The zinc alloy bath was a typical UK composition with 0.9% Pb and 0.3% Sn (Table 17).

7.3 Modelling

7.3.1 Models examined

1. Modelling of small-scale specimens (simulating the loading during the test procedure). This was carried out by the University of Kaiserslautern for the modified CT used by IEHK Aachen, and by CRD&T for the CT with a key-hole notch used at CRD&T.
2. Modelling of large scale structures.

The following structures/details were modelled using ANSYS and SYSWELD software at TUK and using ABAQUS at CRD&T:

- Beam with half cover plate.
- Beam with full cover plate and drilled holes.
- Beam with cope cut.

The following processes were simulated:

- Welding process
- Galvanizing process

Again these processes were modelled using ANSYS and SYSWELD software at TUK and using ABAQUS at CRD&T.

7.3.2 Physical parameters required for modelling

The modelling of thermal processes and the calculation of the resulting stresses and strains requires special input data, especially the temperature dependence, material properties such as expansion coefficient, phase changes and mechanical properties. The required parameters are summarised in Tables 18 and 19 for welding and galvanizing respectively. Some data were generated during the FAMEGA programme.

Tensile tests at various temperatures up to 450°C as well as dilatometry tests were carried out at Corus Swinden Technology Centre [2]. Figure 30 shows the flow stress curves derived from the tensile test data for the Corus grade S460M steel, the changes of yield strength and Young's modulus of the same material with temperature are given in Fig. 31. The variation of thermal strain as a function of

temperature within the temperature range of galvanization is shown in Fig. 32. These data were used in the Corus RD&T FE modelling of the TU Kaiserslautern galvanizing trial No. 1 as described in Sections 7.4 and 8.4 and the mesh sensitivity study in Section 8.3.5.

7.3.3 Kaiserslautern programme (Work Packages 5 and 6)

The laboratory tests conducted by RWTH were simulated using Finite Element techniques (using Ansys software) and the stress limit state respectively. The strain limit state at the point of crack initiation was determined.

To understand the development of stresses and strains during the galvanizing process in real steel structures and components the modelling of large structures was necessary. For this purpose the following three details were chosen:

1. Detail: beam with half cover plate, IPE 550, S460
2. Detail: beam with drill holes, S355, HEB 450, S355
3. Detail: beam with cope cut, S355, IPE 550, and S355

These examples are typical steel structural details in which LMAC during hot dip galvanizing has been reported in the past.

The analysis included the variation of the dipping speed, the dipping angle, the preheat temperature and the composition of the zinc alloy (taken into consideration via the heat transfer coefficient).

The standard parameters were the following:

- Dipping speed: 0.25 m/min
- Dipping angle: 0°
- Preheat temperature: 50°C
- Heat transfer coeff.: 6000 W/m²K (heat transfer from liquid zinc to steel)

Further parameters were:

- Zinc bath temperature: 450°C
- Duration in the bath: 20 min

To cover all effects of the thermal loading during the immersion process volume elements with a three-dimensional thermal conduction capability were used for the thermal analysis.

To investigate the effect of residual stresses coming from fabrication and machining processes before the galvanizing process on the unsteady stress and strain state during the galvanizing process the welding process was simulated in one case (beam with half cover plate).

The standard parameters were the following:

- Welding energy (gross): = 7.54 kJ/s
- Degree of efficiency: m = 0.85
- Welding energy (net):q = 6.41 kJ/s
- Welding velocity: vs = 6 mm/s

7.3.4 Corus RD&T programme (Work Packages 5 and 6)

7.3.4.1 Thermal and mechanical modelling of TU Kaiserslautern galvanizing trial No. 1

The details of the galvanizing process of the TU Kaiserslautern trial No. 1 have been reported in Section 8.3.1.4.2. Figure 33 shows the trial component geometry. Vertical dipping was used in the

orientation as shown in Fig. 33 during the galvanizing trial with a speed of 0.28 m/min. The ambient temperature was 27 °C and the zinc bath temperature was 445°C [9]. The starting position of the galvanization process was assumed to be when the lowest point of the component was 250 mm above the zinc bath surface and the whole procedure took 600 s. The heat transfer coefficient between the zinc and the galvanizing component at the interface was initially assumed to be 1000 W/m^2K [10]. This was similar to the value of 1350 W/m^2K quoted in Reference [5]

A parametric study of the effect of heat transfer coefficient on the prediction of temperature history was carried out on a galvanizing trial conducted by Corus using various values of heat transfer coefficient: 1000, 6000, 10000 and 15000 W/m^2K, in Section 8. It was found that the best agreement between the FE prediction and experimental measurement in terms of temperature history was achieved when the heat transfer coefficient was chosen to be 15000 W/m^2K. This value is in line with what has been recommended and used by TU Kaiserslautern for galvanizing simulation [8-10], and hence has been used for all the modelling work reported here, unless stated otherwise.

The thermal modelling of the TU Kaiserslautern galvanizing trial No. 1 was therefore re-run using the new heat transfer coefficient value of 15000 W/m^2K.

7.3.5 Experimental validation of models

7.3.5.1 Kaiserslautern programme

7.3.5.1.1 Welding process

For the validation of the welding simulation the simple geometry of a butt weld connection of two rectangular steel plates was used and the calculated results (temperature/stresses) were compared with the values taken from the literature [8].

The process parameters were the following:

Steel grade: S355J2G3
Number of weld paths: 1 or 3
Transformation temperatures: AC_1 = 727°C
AC_3 = 867°C
TS = 1440°C (Solidus temperature)
TL = 1505°C (Liquidus temperature)
Welding energy (gross): = 8.40 kJ/s
Degree of efficiency: m = 0.85
Welding energy (net): q = 7.14 kJ/s
Welding velocity: vs. = 6 mm/s

The geometry used for validation purpose is given in Fig. 34.

The accuracy of the thermal analysis has been verified by controlling the temperature field (temperature distribution and maximum temperature) during the process and by comparing the cooling time $t_{8/5}$.

7.3.5.1.2 Galvanizing process

To validate the calculated results of the galvanizing process, especially the temperature development and the deformation behaviour at points with a high cracking potential, a large-scale trial (beam with half cover plate) with special measurement devices was carried out. The geometry and the application of the measurement devices are given in Fig. 35.

The vertical deformation underneath the half cover plate was measured with two displacement transducers positioned at the upper flange of the profile and thus outside the zinc. The transducers were connected with the measurement points via ceramic rods.

The temperature was recorded at the middle and at the quarter height of the web.

The test parameters were:

Pre-treatment: cleaning by sandblast
Pickling: HCl for 1.5 h
Flux: 450 g/l double salt solution
Bath composition: 0.3% Pb + 0.9% Sn + 0.08% Bi
Bath temperature: 443°C
Dipping speed: 0.35 m/min

7.3.5.2 Corus RD&T programme

In order to acquire experimental data to assist FE model development and validation, Corus successfully carried out a galvanizing trial using a channel section of 2 m length and S275 grade. The geometrical dimensions of this channel section are shown in Fig. 36.

During the galvanizing trial the section was dipped vertically into the zinc bath at 440°C and fully immersed within 4 seconds. Temperature and longitudinal strain were measured at two locations as indicated in Fig. 36. FE modelling of this galvanizing trial was subsequently carried out using a half geometry model due to symmetry. The temperature and strain histories at the nodes (N737 web and N803 leg) corresponding to the locations of experiment measurement during the trial were determined and compared with the measured experimental values. The material properties for the same grade of Corus steel were generated in a previous study [11] and were used in the FE simulation.

8. Results

8.1 Full scale trials and simulations (Work Package 3)

8.1.1 Galvanizing test results no.1 and no. 2

The results of these two trials are presented together because of the similarity of the welded joints in each test (see Fig. 12).

After galvanizing and after having received the different sections of both test series in the workshop, visual examinations and dye penetrant tests were carried out, which resulted in the following observations:

- In trials 1 and 2 a beam of steel grade S450J0 (steel J) contained long cracks, clearly visible by eye, without recourse to the dye penetrant test. The cracks were located in the web, 13-15 mm below the cover plate and had lengths of 12 to 72 cm (see Fig. 37). This result showed that these tests accurately reproduced critical industrial conditions.
- Some sections continued much smaller cracks (1 cm) revealed by the dye penetrant test.
- Visual inspection alone may be insufficient to detect small cracks.

Figure 38 shows the appearance of the small cracks described above. In order to reveal such cracks in galvanized welded joints the following technique was devised:

1. A 50 mm wide complete beam section was cut from each end of a beam fitted out with its half cover plate.
2. A tensile test of this section was carried out in the transverse direction (Fig. 39). It should be noted that all the ruptures were located at about 13-15 mm below the cover plate.
3. The crack length was measured on the broken fracture i.e. where the presence of zinc was observed. In some cases the presence of zinc on the fracture face was checked by means of a scanning electron microscope.

The results of the crack length measurements are shown in Tables 20 and 21.

The results of the tensile tests indicated that nearly all the beam samples in grades S275 to S460 contained cracks 4 to 25 mm long, with the exception of steel J. In this case it was not necessary to perform transverse tensile tests, as long cracks were already visible by eye.

These results demonstrate that designs, with half cover plates welded on the end of beams, are very prone to LMAC. By comparing LMAC results from the two galvanizing baths it would appear that the beams galvanized in a zinc bath alloyed with Zn-Sn present a greater sensitivity to cracking than beams galvanized in a more conventional Pb rich bath, irrespective of whether they contained mechanical defects (saw cuts). After galvanizing in the Sn-rich baths longer cracks were observed on the beam side containing the 2 mm deep saw cut.

8.1.2 Results of galvanizing test no. 3

Figure 40 shows a galvanised beam being examined for cracking by the magnetoscopic technique. Also shown is a crack revealed by this technique. The crack lengths revealed by visual or magnetoscopic technique are shown in Table 22.

8.1.3. Results of galvanizing test no. 4

8.1.3.1. Residual stress

Results of residual stress measurements before and after welding are shown in Fig. 7. Results after galvanizing are shown in Fig. 41. As shown in the figures, the measurements of residual stresses were carried out in the web of sections in the zone located below the welded half butt plate. The measurements were made parallel and perpendicularly to the rolling direction on two positions in the web, on the face and on the edge (see Figure 41: point marking).

The results of the residual stress measurements led to the following observations:

- In the as-rolled state compressive residual stresses were measured in most directions and for both steels. The residual stresses have levels of compression corresponding to a maximum of 50% of the values of the yield strength of the respective steels.
- In the welded state, a clear change in the values of residual stresses was observed compared to the values in the as-rolled state. All the measurements show high levels of tensile residual stresses which may approach the yield strength.

The measurements of residual stresses performed on welded joints, with additional thermal or mechanical treatments, resulted in the following observations:

- All processes led to the reduction of tensile residual stresses compared to the welded state. Most of the measurements showed compressive residual stresses in the different directions examined and for both steels.
- A comparison of the various processes used in this study to reduce the levels of residual stresses showed that the mechanical stress relieving process seems to be more effective than thermal stress relieving. Nevertheless it should be pointed out that that the X ray measurements used relate only to the steel surface, due to the limited penetration depth of the X ray beam.

It is possible that thermal stress relieving may influence deeper into the section than the mechanical treatment.

8.1.3.2 Galvanizing test no. 4

After galvanizing the crack lengths measured either by visual or magnetoscopic technique are shown in Table 23. From the analysis of the results the following comments can be made:

- The improvement methods applied for the grade S355ML (steel L) do not show any benefit compared to the results of the galvanizing test no. 2, where these actions were not carried out. The improvement techniques were thus considered ineffective and were not undertaken in future trials.
- Mechanical stress relieving techniques (shot blasting and ultrasonic peening) applied to the grades S275J0 (steel G) and S450J0 (steel J) also do not show any improvement compared to the results of the galvanizing tests no.2, where these actions were not carried out. These techniques were thus considered ineffective and were not undertaken in future trials.
- Thermal stress relieving techniques produced the best results. For both steel grades examined heating at 600°C was more effective than heating at 700°C. For the grade S275J0 (steel G) the extremity heated at 600°C did not crack, while the extremity heated at 700°C produced a small 13 mm long crack. For the grade S450J0 (steel J), which is the most sensitive to LMAC, a very clear improvement was observed, although both extremities did contain cracks (18 mm and 50 mm long). This improvement should be compared with the results of galvanizing test no.2 and the mechanical stress relieving variants, where this steel grade suffered 50 cm long cracks located below the half cover welded plates.

These results show that mechanical stress relieving techniques generated the greatest compressive residual stresses, but produced no improvement in LMAC. The implication is that the techniques only have an impact on the product surface. In contrast thermal stress relieving has a large beneficial effect, which is considered to result from stress relief to a much greater depth.

Thermal stress relieving was thus used for further trials, as the thermal relieving method at 600°C seemed to offer the best answer to reducing LMAC. The next stage involved thermal treatments by heating the critical zone at 600°C with a holding time of 2 minutes, the temperature being controlled by optical pyrometers or by thermal pencils.

8.1.4 Results of galvanizing test no.5

In trial no. 5 only 6 of the 10 tests have been reported (Table 24). Attempts to use a protective coating resulted in uneven coating thickness over large areas of the web under the cover plate, which meant that the results could not be considered as valid.

None of six perfectly galvanized profiles was affected by cracking. This result confirms the beneficial effects of the thermal stress relieving at 600°C followed by a holding time of 2 minutes. As no cracks were detected below the half cover plate, it was difficult to assess the use of a supplementary weld bead under the cover plate.

It should be noted that the profiles of S275J0 and S450J0, which did not have welded half cover plates (and were not heat treated) did not show any cracking after galvanizing. This confirms the decisive role of the welded half cover plates in producing cracks in the web of rolled sections.

8.1.5 Results of galvanizing test no. 6

All beams were visually examined after galvanizing and additionally all beams were checked by the magnetoscopic technique in order to detect non-visible cracks. The results of the examination are given in Tables 27-29 and summarized as follows:

1. Welded half cover plate:

- Side 1 of the beam welded with a compression seam: 7 beams from 10 showed cracking, localised under the ½ cover plate. Crack lengths were in general ~1 cm. Only the beam identified IPE A 600 (grade S450 J0) contained a very long crack of about 1 m.

- Side 2 of the thermally treated beam (600°C with a holding time of 2 minutes);: none of the 9 beams examined contained any cracks. However, one variant contained a small (L = 1.5 cm) crack.

2. Plate welded on the flange:

- None of the 10 beams contained any cracks on either end of the welded plate.

3. Flame-cut flanges (cope cut), without drilling of a preliminary hole:

- Side 1 untreated thermally: 2 beams out of 3 contained 2 mm and 5 mm long cracks.
- Side 2 treated thermally at 600°C with a holding time of 2 minutes: none of the three beams contained any cracks.

4. Flame-cut flanges (cope cut), with drilling of a preliminary hole:

- Side untreated thermally: none of three beams contained any cracks.
- Side treated thermally at 600°C with a holding time of 2 minutes: no beams contained any cracks.

5. Holes, drilled or flame cut in the web:

- None of the 2 beams contained any cracks. These beams, where half a side was thermally treated, contained 24 holes having diameters of 22, 29 and 150 mm.

From this cracking evaluation concerning 15 beams, it was concluded that a thermal treatment of 600°C reduced considerably the sensitivity to LMAC during hot dip galvanizing.

8.1.6 Results of galvanizing tests no. 7 and no. 8

A supplementary galvanizing test was carried out to examine the case of welded half cover plates with and without stress relief annealing. This trial examined the efficiency of annealing at a lower temperature of 550°C and again at 600°C.

For the first test the galvanizing bath was alloyed with tin but without lead and for the second test the zinc bath contained neither lead nor tin (Table 12).

Tests no. 7 and no.8 concerned 10 welded joints of all the steels used in this research (Table 8), where each end of the beam was welded with a half cover plate. The welding was properly performed according to the usual procedure. After welding, one extremity was left in the as-welded condition, whereas the other was thermally treated in the critical cracking zone with a torch at a temperature of 550°C and 600°C respectively for duration of 2 minutes.

The results of magnetoscopic inspection after galvanizing are listed in Tables 30 and 31, and allowed the following observations:

- Test no. 7 confirmed the results obtained on previous galvanizing trials (increased cracking sensitivity for tin alloyed bath). The test also showed the beneficial effect of thermal stress relief carried out with a hand-held torch to avoid or to limit the cracking problem after galvanizing.
- Test no. 8 specifically showed the significant influence of the chemical composition of the galvanizing bath. Cracks were not detected after galvanizing in the critical zones of half cover plate test specimens, either with or without the application of a stress relief annealing. It is to be noted that the bath contained no Pb and Sn elements. This bath chemistry could be very useful for cases where it is necessary to galvanize complex welded joints or designs, where it is impossible to apply any thermal treatment.

Summary and conclusions of full-scale simulations

The performance of eight sets of galvanizing tests on an industrial scale allowed an improved understanding of the effects of processing and metallurgical variables on the cracking during hot dip galvanizing.

Ten sections, in steel grades ranging from S275 to S460, including thermo mechanical, normalised rolled and conventional steels, were used to examine the following cases leading to cracking after galvanizing:

- Half cover plate welded on the web at the end of beams, which constitutes one of the most severe cases in term of constraint and residual tensile stress. In some cases, deliberate defects were introduced for comparison with properly welded plates.
- Flame-cutting of the flange, known as a "cope cut".
- Plate welded on the flange.
- Drilling and oxy-cutting of holes of various diameters in the web.

The tests were carried out by using different processing parameters, namely:

- Classical zinc baths with usual pickling and over-pickling.
- Zinc baths alloyed with tin with or without bismuth (usual pickling).

The test results allowed the identification of some factors leading to the onset of cracking during hot dip galvanizing. A combination of causes generated the cracks on assemblies, which can originate from:

- The high stress level following the design and the fabrication method.
- The steel grade or material susceptibility.
- Galvanizing processes.

Welding and finishing operations such as flame cutting or drilling inevitably generate high tensile residual stress. Actions aimed at reducing the level of residual stress in the critical area prior to galvanizing included:

- Application of thermal stress relieving at temperatures ranging between 550 and 700°C, with and without a holding time of 2 minutes.
- Application of mechanical stress relieving by sand blasting and ultrasonic shot peening.
- Modification of the welding sequence and the welding of additional weld beads under the half cover plates.

Analysis of the test results allowed the following conclusions to be drawn:

- Sections with half cover plates welded on the ends were very sensitive to LMAC and provided a good test model in this research to study the sensitivity to cracking in hot dip galvanizing. Cracks, always filled with zinc, were systematically located in the web at about 15 mm below the half cover plate and their length varied from a few mm to 700 mm following the galvanizing process.
- The steel variant combining a high strength and relatively low toughness level (J_0: Charpy V at 0°C) presented the greatest sensitivity to cracking after galvanization. This section also had a highly sensitive geometry (see below).
- Compact sections appear to be less sensitive to cracking compared with high and slender sections with a weaker moment of inertia.
- The thickness of the cover plate appeared to have no influence on LMAC - a 40 mm thick welded cover plate was no worse than a 25 mm thick plate.
- A mechanical defect, like a saw cut, may increase the sensitivity to cracking. This indicates that it is necessary to carefully perform the preparation of the welded joints prior to galvanization.

- The magnetic particle inspection (magnetoscopic) technique is the most suitable NDT method; visual inspection and the dye penetrant test are insufficiently accurate and do not allow the systematic detection of all cracks.
- Over-pickling did not appear to have any detrimental effect on the structural steels tested.
- There was a clear increase in the values of residual stresses measured on welded sections compared to the as-rolled state. The tensile residual stresses associated with welding approached the yield strength level.
- A thermal stress relieving process prior to galvanizing was carried out using a hand-held torch at 550-600°C and a small holding time. This technique was shown to reduce the residual stresses of welded sections and to considerably reduce or avoid the cracking of metal structures. Mechanical stress relieving using ultrasonic peening was not successful and had only an effect on the product surface, while thermal stress relief acted more deeply.
- By comparing LMAC occurring in different galvanizing baths it was apparent that the beams galvanized in a zinc bath alloyed with tin presented a greater sensitivity to cracking at the beam end (with or without a mechanical defect). A bath containing a minimum amount of (or no) lead (Pb) and tin (Sn) could be very useful in galvanizing complex welded joints or designs, where a thermal stress relief treatment cannot be applied.

8.2 Laboratory tests (Work package 4)

8.2.1 University of Cantabria programme

8.2.1.1 Surface roughness tests

Surface roughness tests were performed in order to determine the effect of pre-galvanizing surface treatments in the generation of surface defects able to promote crack initiation.

Figure 42 shows the surface roughness results for steel J. Surface roughness after 2 hours of pickling increased slightly. In the fluxing stage, surface roughness suffered a sharp increase after 10 minutes of fluxing with $ZnCl_2 \cdot 4NH_4Cl$ salt. Once the sample was washed with water and dried to eliminate the flux salts its surface was examined by SEM. Deposits with high Zn content and low Cl content were observed leading to the conclusion that metallic Zn was deposited also during fluxing. An example of Zn deposits on the steel surface after fluxing is shown in Fig. 43.

8.2.1.2 Hydrogen concentration tests

Hydrogen concentration was measured in order to understand the possible effect of hydrogen embrittlement in the cracking processes during galvanizing.

Hydrogen concentration tests were divided in two groups. The first group of tests was performed on specimens of steels A, B, C and J. The hydrogen content was measured in the following conditions:

- 1.1: As received.
- 1.2: After pickling
- 1.3: After pickling+fluxing with $ZnCl_2 \cdot 4NH_4Cl$ salt.
- 1.4: After pickling+fluxing with $ZnCl_2 \cdot 4NH_4Cl$ salt+galvanising in the Zn-Sn bath.

The results of this group appear in Fig. 44. In this graph, the H content after galvanization (condition 1.4) included the hydrogen trapped in the Zn layer over the steel (η layer, composed of pure Zn). A sharp increase in H content was detected after fluxing, and this increase continued after galvanizing. The results depend on the steel, with steel B showing the highest hydrogen solubility.

The second group of tests was carried out on steel D with hydrogen content measured in the following conditions:

- 2.1: As received.
- 2.2: Pickling
- 2.3: Fluxing with $ZnCl_2 \cdot 4NH_4Cl$ salt.
- 2.4: Fluxing with $ZnCl_2 \cdot 2NH_4Cl$ salt.
- 2.5: Pickling+fluxing with $ZnCl_2 \cdot 4NH_4Cl$ salt.
- 2.6: Pickling+fluxing with $ZnCl_2 \cdot 2NH_4Cl$ salt.
- 2.7:Pickling+fluxing with $ZnCl_2 \cdot 4NH_4Cl$ salt+galvanizing in Zn-Sn bath.
- 2.8: Pickling+fluxing with $ZnCl_2 \cdot 4NH_4Cl$ salt+galvanizing in Zn-Pb bath.
- 2.9: Pickling+fluxing with $ZnCl_2 \cdot 2NH_4Cl$ salt+galvanizing in Zn-Sn bath.
- 2.10: Pickling+fluxing with $ZnCl_2 \cdot 2NH_4Cl$ salt+galvanizing in Zn-Pb bath.
- 2.11: Galvanizing in Zn-Pb bath without pickling and fluxing.

The results of these tests appear in Table 32. Figure 45 shows the results obtained in galvanizing conditions, which do not include [H] in the Zn layer over the steel. It can be seen that, as in the first group of results, the hydrogen content increased during fluxing and galvanizing conditions. Some other results can be highlighted:

1. $ZnCl_2 \cdot 4NH_4Cl$ salt flux introduced generally more H than $ZnCl_2 \cdot 2NH_4Cl$ salt flux.
2. Zn-Sn galvanizing bath introduced more H than Zn-Pb galvanizing bath.
3. Pickling did not have any important effect on the final hydrogen absorption.
4. Originally the Zn baths did not have any hydrogen content, but they finally (as in industrial conditions) accumulated hydrogen from the flux salts on the previous steel specimen. This probably accounts for the appearance of hydrogen in condition 2.11.

8.2.1.3 Fracture tests in liquid Zn

J-integral fracture tests were performed in order to determine toughness changes at each stage of the galvanizing process.

J-integral tests were performed (standard ESIS P-2) with CT specimens of steel J. The experimental conditions were as-received (at 20ºC and 450ºC), and during galvanization in liquid Zn baths (Zn-Sn or Zn-Pb) at 450ºC. Tests during galvanization required the experimental setup shown in Fig. 23(b). The results are shown in Fig. 46. The decrease in the toughness parameter Jc in air at 450ºC is 63% and the decrease in a liquid Zn-Sn bath is 88%; both with reference to room temperature and as-received

conditions. Figure 46 also shows that toughness in a Zn-Sn bath is lower than in a Zn-Pb bath. The CT specimens fractured in liquid Zn in a brittle manner, with low plastic deformation.

Complementary experiments were carried out using slow strain rate tests on round-notched axi-symmetric specimens (Fig. 22) made of steel J. The experimental conditions were as received (at 20ºC and 450ºC), and during galvanization in liquid Zn-Sn bath at 450ºC. The results appear in Fig. 47. A decrease of 24% in maximum load was measured in air at 450ºC and of 68% in liquid Zn compared to the room-temperature as-received conditions. Besides, the fracture in liquid Zn showed very little plastic deformation compared with that obtained in the as-received conditions.

8.2.1.4 SEM examination of Zn layers on samples tested in liquid Zn

The first step in this study was to compare the microstructure of the Zn-Fe layer of industrial pieces galvanized with the two Zn baths. Arcelor Profil Luxembourg delivered galvanized steels L and P to the University of Cantabria. Representative micrographs appear in Figs. 48 and 49. The main difference is the presence of a Sn and Pb rich deposit between traditional δ and ζ layers observed only when the steel was galvanized in the Zn-Sn bath.

Also Sn and Pb deposits were not over the δ layer, but in direct contact with the steel base. Figure 50 shows an example of a point at the beginning of a pre-fatigue crack in a DCB specimen of steel B immersed in a liquid Zn-Sn bath.

The second step was to perform an EDS spectrum of Zn layers on crack tips and notches on specimens tested in liquid Zn. Pre-fatigue cracks and machined notches on DCB specimens of steel B tested were examined by SEM. A concentration effect of Sn was observed at the fatigue pre-cracks of the two DCB specimens made of steel B tested in the Zn-Sn bath (see Fig. 51). The Sn concentration increased with crack length from the surface to the tip, at the time that the crack opening reduced. However, specimens tested in Zn-Pb baths did not show a variation in chemical composition at any point along the crack or notches (see Fig. 52) compared with the composition of the original bath (Table 15).

LMAC occurred during galvanizing in different areas of the tested DCB samples. A crack initiated and grew from a notch on the side of DCB specimen made of steel B which was galvanized in Zn-Sn bath (Fig. 53). The composition of alloy deposited in the crack was richer in Sn at the crack tip than at the start of the crack. Figure 54 shows the crack, (after etching in 5% Nital) generally following ferrite boundaries.

There was also a failure during galvanizing in a CT specimen of steel C in which pre-loading to a value of K_I = 20 MPa $\sqrt{m}$ resulted in crack propagation. The composition of the solidified metal at the crack tip was principally Sn, with some spots of Bi and Pb (Fig. 55) and no presence of Zn.

8.2.2 RWTH Aachen University programme

A LMAC tested specimen is shown in Fig. 56. It is possible to observe a crack running from the bottom of the drilled hole at the end of the notch about 40 mm into the ligament. Taking a closer look at the distribution alongside the thickness direction a V-shaped crack form can be observed. To reveal the fracture surface itself the L-N(T) specimen was broken apart after cooling in liquid nitrogen. A very jagged formation had developed typical of galvanizing cracks.

From the load v displacement testing curve a maximum achievable load (F_{max}) at the moment of crack initiation was obtained. In addition, the load line displacement of the specimen corresponding to that critical load F_{max} can be given. As an example, Fig. 57 shows a typical load-displacement plot from L-N(T) testing, here with material A in alloy a0 and in air at 450°C. Comparing these results gives a clear indication of the detrimental effect of a zinc alloy in terms of reduced critical load F_{max} and maximum load line displacement v_{LL}, F_{max}. In a post-processing step these two factors F_{max} and v_{LL} F_{max} were used to determine the stress and the strain at the notch tip at the onset of cracking by use of an FE analysis, which was performed by TU Kaiserslautern (see Section 8.3.1). Not all performed tests were analysed

by FE. Nevertheless, Tables 33-44 contain relevant data from all the tests performed within this part of the FAMEGA project.

The majority of testing was performed under load control using rising load at different rates to check the influence of straining rates at the notch tip by FE analysis. A few of the later tests, especially with material F, were performed in displacement control, which turned out to be the preferred control mode for a correlation with strain rates.

The test results show a certain scatter, but results are given individually without any statistical evaluation.

While establishing the new test method, the first series of tests with material A with alloy a0, used the L-N(T) specimen with notches of 1 mm and 3 mm radius. These results are given in the relevant figures. For all further testing the variant with 3 mm was used. As to be expected, the higher stress concentration due to the smaller radius leads to lower failure loads in L-N(T) specimen testing.

8.2.2.1 Influence of zinc alloy on cracking

LMAC results at different loading rates are given in Figs. 58 - 63 respectively. Displacement rates in Figs 64 and 65 indicate the overall detrimental effect from the attack of zinc alloy a0 and a2. Tests performed using alloy a1 resulted in much higher values of failure load F_{max} and the corresponding displacement v_{LL},F_{max}. Comparing the results from testing in alloy a0 and a2 only a slight difference can be seen. Nevertheless, tests performed in alloy a2 clearly gave the poorest values. In the tests using material A, no cracking could be observed in alloy a1. For material B, only slow loading rates lead to cracking. Within the tests performed with material F cracking was observed in alloy a2 only. In contrast, the series with material C lead to cracking regardless of the zinc alloy and loading rate, but still achieving the highest values for F_{max} as well as v_{LL}, F_{max} in alloy a1. Overall it was found that decreasing the loading rate and respective displacement rate resulted in lower F_{max} values.

Looking at the figures giving the displacements v_{LL},F_{max} it can be seen that the values seem to run through a minimum depending on the loading/displacement-rates and the individual zinc alloy. This supports the idea of a strain rate controlled mechanism with a critical range.

The results show that maximum load and load-line displacement at the notch mouth of the L-N(T) specimen, i.e. the mechanical resistance of the material in terms of critical stressing and straining at the notch tip, is significantly influenced by the surrounding liquid zinc alloy and its composition. Regardless of the material, the results are clearly leading to the same conclusion for each individual zinc alloy investigated. There also appear to be a time effect as tests performed with the slowest rates (allowing for extended attack of the zinc alloy) lead to the lowest critical values.

8.2.2.2 Influence of material grade on cracking

The influence of the material grade on LMAC susceptibility can only be assessed by taking the thickness dependence of the L-N(T) specimens into account. As the materials for specimen machining are extracted at full thickness from the web of different I-beam profiles, the thickness varies depending on the delivered profile type. When comparing the cracking susceptibility of the material, the determined values from the testing need to be related to the particular web thickness b. For comparing F_{max} these values also need to be related to the strength. This was simply done by dividing with the upper yield R_{eH} leading to a unit in mm.

Again material A had the best resistance towards cracking, displaying the highest values of displacement at F_{max}. Comparing the results from testing in a0 and a2 shows that the distribution of the results from the tests in these two different alloys is quite similar. Although testing in alloy a0 resulted in slightly higher values and hence verifies the conclusion from the previous section that a2 was the most detrimental of the three investigated zinc alloys. In Figs 70 and 71, the values of F_{max} and displacement appear to go through a minimum at a specific loading rate, suggesting that LMAC is most

severe at a critical loading rate as described in Section 8.2.2.1. There are insufficient data to draw the same conclusion from Figs. 72 and 73 or to assess the influence of material grade on LMAC. Regardless of the scatter the tests in a1 gave the highest critical values as seen in the displacement values.

8.2.2.3 Testing results

All the results from L-N(T) testing are given in Tables 33-44 with the relevant values achieved.

8.2.3 Corus RD&T programme

8.2.3.1 LMAC testing with tensile test pieces

In the CRD&T test programme only one zinc alloy bath was used with 0.9% Pb and 0.3% Sn (Table 17). Engineering fracture stress was determined on tensile test pieces (Fig. 28(a)) for steels A, B and C. Test pieces were either machined or the profile cut out using flame-cutting. Various strain rates were used.

The failure stresses were compared to tensile curves obtained at 450°C for steels B and A in Figs. 74 and 75 respectively. There was a fairly wide scatter of results. Within one steel grade failure stresses varied by up to 25%, but failure strains varied by an order of magnitude due to the flat nature of the tensile curves. The lowest values of failure stress were just above the yield stress, while the highest values were close to the tensile strength. However, unlike a tensile test curve there was always a very abrupt brittle failure at the failure stress, with greatly reduced strain to fracture and no necking.

The results of all three steels in the machined and flame cut condition are shown in Fig. 76. It is clear that surface finish in terms of machining and flame cutting had no effect on the results. Steel type had some influence with the lowest strength steel (steel A, S355JR) giving the lowest failure stresses. No beneficial influence of toughness was observed with steels B and C showing similar results.

The influence of strain rate is shown in Fig. 77. For each steel grade there is considerable scatter, but there is a clear move to lower failure stresses as the strain rate is reduced.

8.2.3.2 LMAC tests on keyhole test pieces

Keyhole test specimens (Fig. 29(c)) have the advantage that the grips do not enter the zinc bath and the clip gauge can directly measure load line displacement in the test piece. They also have a greater constraint. The tests were carried out shortly after the samples had been fully immersed into the zinc bath using different crosshead rates. The measured load vs. clip gauge displacement curves are given in Fig. 78. The maximum loads and their corresponding clip gauge displacements obtained from the experiments (as derived from Fig. A1) are given in Table 45.

A quasi-static FE simulation (without the effect of strain rate) of the compact tensile test has been carried out based on the geometry of this modified compact tensile specimen. In order to simulate the thermal effect of the zinc bath, the FE simulation was conducted using the flow stress data for the Corus S460M steel at 450°C (scaled down by 20% to achieve a good fit between the FE and experiment in terms of the load vs. clip gauge curves). The FE prediction of the load vs. clip gauge displacement curve is plotted in Fig. 78, together with the experimental measurements.

Fig. 79 shows the FE prediction of the through-thickness average stress and strain vs. clip gauge displacement curves evaluated at the bottom of the round notch (location A, Fig. 79).

The transverse stress and strain distributions in the surface of the modified compact tensile specimen predicted by the FE simulation at different clip gauge displacements are given in Fig. 80.

According to Table 45, for all the submerged key hole CT tests, the clip gauge displacement at the maximum load (indicating crack initiation or failure) falls between 0.76 mm (minimum) and 1.63 mm (maximum), the corresponding (failure) strain values in the transverse direction at the bottom of the notch can therefore be derived from Fig. 79 to be 3.0% to 8.3% respectively. This compares with tensile results from the same steel, which ranged from 1.9%-8.5% true strain for the same steel (steel B, S460ML). This indicates a fairly good correlation between uniaxial tensile tests and round notch CT tests.

8.2.3.3 LMAC tests using fracture mechanics

The results of the compact tension tests are shown in Table 46. There appears to be no particular influence of crosshead rate. It is suspected that the scatter of results is primarily a function of the ability to wet the fatigue pre-crack with zinc alloy.

The threshold stress intensity for LMAC and the threshold stress (Section 8.2.3.1) have been used to construct a level 2 Failure Analysis Diagram (FAD) [14] using the commercial software Crackwise 4. In this it was assumed that a long surface crack (i.e. across the full edge of the web) was growing from the edge of a beam down the web, which was assumed to be 10 mm thick. This type of analysis is usually applied to fracture but has been modified in this case to examine the influence of initial defect sizes on LMAC. The FAD itself (Fig. 81(a)) shows that small cracks are governed by the threshold stress. As the cracks grow longer they approach the fracture-controlled portion when they are about 20 mm deep. Between ~ 2 mm and 20 mm LMAC is on the intermediate zone where both stress and stress intensity terms influence the crack growth. Figure 81(b) shows that defects up to ~ 2 m have no effect on the threshold stress. Hence small cracks associated with welding, grinding or burning should have little effect (ignoring any influence of residual stress).

8.2.3.4 LMAC tests using short crack fracture mechanics

The objective of this was to determine whether a level 2 FAD approach is applicable to LMAC or whether there are two distinct criteria; namely threshold stress and stress intensity. The results are shown in Fig. 82 and strongly suggest that a level 2 FAD is applicable. This means that the calculation based on a level 2 FAD in Fig. 81(b) is applicable and the change from LMAC controlled by threshold stress to stress intensity occurs at about 2 mm crack depth for the S460ML examined.

8.3 Modelling (Work Packages 5 and 6)

8.3.1 Kaiserlautern programme

8.3.1.1 Welding process

The accuracy of the thermal analysis was proved by controlling the temperature field (temperature distribution and maximum temperature) during the welding process and by comparing the cooling time $t_{8/5}$. Figure 83 shows the temperature distribution at t = 40 s. The effect of the moving the heat source can be seen clearly by means of the isotherms. The molten area with temperatures above the melting point (T > 1505°C) is small and limited to the local vicinity of the heat source.

The control of the cooling rate in terms of the $t_{8/5}$-time shows a calculated value of 13 seconds (see Fig. 84) vs. 15 seconds given by the literature [5]. Controlling the residual stress state after the welding process has proved the accuracy of the structural analysis.

The stress distributions in both longitudinal and transverse direction of the weld taken from the literature are shown in Fig. 85. From the structural analysis the following stress states were obtained.

- Longitudinal stress state (Fig. 86)
- Transverse stress state (Fig. 87)

All results show good accuracy.

8.3.1.2 Galvanizing trial

The results of the trial are as follows:

- The development of the temperature and the deformation were recorded over the trial time.
- On both sides of the specimen large cracks with a length of 450 mm occurred, Fig. 88.
- The temperature development and the corresponding deformations can be simulated with high accuracy, Fig. 89 and Fig. 90.
- The comparison of the measured and the simulated deformation clearly show the point of crack initiation during the immersion of the profile, Fig. 90.

8.3.1.3 Modelling of RWTH Aachen University Small Scale Tests

The geometry of the RWTH small-scale test specimen was modelled and the loading procedure was recalculated. Figure 91 shows the recorded load-displacement-development and the corresponding calculated plastic strain development for a modified CT-specimen (S460, Sn-alloyed zinc bath). The comparison between the recorded and the calculated loading curve shows a very good agreement.

The stress and strain state at the point of crack initiation, which is clearly defined by reaching the maximum load with a subsequent quick drop off, the von-Mises-stress and the plastic equivalent strain at the bottom of the drilled hole (= notch tip = point of highest loading) were analysed.

In Fig. 91 the calculated plastic strain development correlating to the loading curve is given. The limit equivalent strain at the maximum test load is indicated.

In Fig. 92 the limit state (corresponding to the results presented in Fig. 91) in terms of von Mises stress state and the plastic equivalent strain in the vicinity of the notch tip are given respectively.

In the above way the results from the RWTH test programme were recalculated for the stress and strain limit state, which analysed the effects of:

- The zinc bath composition
- The material properties
- The loading velocity

The results are summarized in Figs. 93 and 94.

8.3.1.4 Modelling of downstream processes

8.3.1.4.1 Welding process

The fillet welding of a half cover plate at the end of a beam was simulated with variations of the welding velocity, the welding direction and the number of welding runs. The results of the analysis using the standard parameters are given below.

The width of the heat affected zone, with a maximum bainite percentage of 87% and a martensite percentage of 33%, is limited to 1 – 3 mm, depending on the chosen welding parameters. This analysis shows that the welding process does not affect the microstructure at the point of crack initiation, which is about 5 – 10 mm underneath the end of the half cover plate.

The distribution and the quantity of the residual stresses are influenced by the state of metallurgical phases. The changes of the microstructural phases from ferrite to bainite or martensite are accompanied by a higher yield strength, which may result in the development of higher stresses.

The residual stress state in the longitudinal direction of the weld seam is presented in Fig. 95 and the von Mises-equivalent stress in Fig. 96. In the heat affected zone with high bainite and martensite very high stresses occur. In the region underneath the end plate the maximum stress in the longitudinal weld seam direction is about 370 MPa, which is lower than the yield stress, hence no plasticity occurs.

8.3.1.4.2 Galvanizing process

The galvanizing process for three structures was simulated with variation of the dipping speed, the dipping angle, the preheat temperature and the zinc bath composition. The results of the analysis using the standard parameters are as follows:

8.3.1.4.2.1 Beam with half cover plate

The results of the process simulation are shown in Fig. 97 and can be summarized as follows:

- During the dipping process very high stresses and strains occur below the half cover plate.
- The critical point of maximum loading is about 3 mm below the end of the cover plate.
- The stress development during immersion is characterized by a double change of sign from compression to tension and back to compression with stress values up to the yield strength.
- The minimal compressive stress occurs when the beam is half dipped in, the maximum tensile stress occurs when the beam is just completely dipped in.
- The strain rate that develops during the dipping process might be critical to activate the mechanism of liquid metal induced embrittlement.
- Below the cover plate a local area of plasticity with strains up to 10% is formed.

8.3.1.4.2.2 Beam with full cover plate and drilled holes

The results of the process simulation are shown in Fig. 98 and can be summarized as follows:

- During the dipping process very high stresses and strains occur at the edges of the holes.
- The stress development during immersion is characterized by a double change of sign from tension to compression and back to tension with stress values up to 260 MPa after full immersion.
- The strain rate that develops during the dipping process might be critical to activate the mechanism of liquid metal induced embrittlement.
- At the edge of a hole two local areas of plasticity with strains up to 2.5% form in the 45° direction.

8.3.1.4.2.3 Beam with cope cut

The results of the process simulation are shown in Fig. 99 and can be summarized as follows:

- During the dipping process very high stresses and strains occur in the corner arc of the cope cut.
- The stress development during immersion is characterized by a double change of sign from compression to tension and back to compression with stress values up to 400 MPa.
- The strain rate that develops during the dipping process might be critical to activate the mechanism of liquid metal induced embrittlement.
- In the corner arc of the cope cut an area of plasticity is formed with strains up to 10%.

8.3.1.4.2.4 Summary

The results of the galvanizing simulation can be summarized as follows:

1. In contrast to previous assumptions of a constant or quasi constant stress and strain state during the galvanizing process the computations above show that a strongly unsteady behaviour is present, which can be described primarily by the strains (due to non elastic deformations).
2. Fabrication details like stiffness changes or drilled holes are defined points with high potential for deformation concentration.
3. Local areas of plasticity were formed with remaining strains in a range of 2 – 10% depending on the specific fabrication detailing.
4. The development of temperatures and the coincident stresses/strains strongly depends on parameters chosen in the galvanizing process.

8.3.2 Corus RD&T programme

8.3.2.1 Mechanical modelling of galvanizing

8.3.2.1.1 Upright (horizontal) dipping

Using the temperature history predicted by the thermal modelling analysis of the galvanizing process described in the previous section, the mechanical modelling of the half-cover plate component was carried out (namely in the upright dipping orientation to be differentiated from the additional analyses conducted under the 45-degrees and upside-down dipping orientations). The material properties data used in this modelling analysis was those of Corus grade S460S as given in Section 7.3.

Figures 105 and 106 show the FE prediction of temperature and longitudinal stress development sequences of the half-cover plate component during the galvanizing simulation. It can be seen from Fig. 105 that as the component is being immersed into the zinc bath there is a compressive stress zone along each of the long edges just above the zinc bath level, which is followed by a high tensile stress zone immediately below the zinc bath level, Fig. 105(b). This longitudinal stress distribution pattern is maintained during the entire immersion process, although it is somewhat complicated near the two punch hole areas, except that when the zinc bath level just passes the end of the attached half plate, Fig. 106(a), the tensile stress level is significantly increased near the long edge just below the end of the attached half plate, Fig. 106(b). As the full-scale tests have shown this area is particularly susceptible to LMAC during galvanizing. It is believed that it is the sudden change in geometry and hence the local structural rigidity that causes the significant increase in the longitudinal tensile stress, which in turn results in the cracking.

Because the full-scale tests reported cracking 10-15 mm from the weld toe of the half-cover plate, the local temperature and stress was evaluated at a node (N14) located at the corner of the long edge, 13 mm below the end of the attached half plate, and compared with that of another node further down (N642). The results and the locations of the evaluation are presented in Fig. 107.

It can be seen from Fig. 107 that during the dipping process as nodes N642 and N14 approached the zinc bath level, compressive stress rapidly built up in each of these local areas. The compressive stresses reached virtually the same maximum value (-511 MPa at N642 and -532 MPa at N14) at the time when the corresponding node was immersed into the zinc bath. After that the stress built up in the opposite direction, i.e. rapidly turning into a tensile stress as the local areas were heated up by the molten zinc. The maximum value of this tensile stress was attained when each of the corresponding areas attained the zinc bath temperature of 445°C. However, there was a big difference (about 32%) between the maximum tensile stress values attained at nodes N14 (369 MPa) and N642 (251 MPa).

The compressive stresses experienced at nodes N642 and N14, with the maximum values being -511 MPa and -532 MPa respectively (compared to the room temperature yield strength of 593 MPa for the Corus grade S460M steel), are not considered to be detrimental and should not cause any

mechanical (strain) damage to the local material. However, the tensile stress history experienced by the material near N14 with a maximum value of 369 MPa reached the yield strength of the material (376 MPa for the Corus grade S460M steel at 450°C), resulted in some localised strain damage at node N14 (0.7% plastic strain) as shown in Fig. 108. Some strain damage due to galvanizing was also observed in Fig. 108 near the edges of the two punched holes at node N1255 (0.5% plastic strain) and node N1273 (0.4% plastic strain). Therefore these areas have been identified by the FE simulation as being susceptible to LMAC in this component. This is predominantly associated with the sudden change of geometry.

It has to be stated that according to the FE prediction shown in Fig. 107, the local material at node N14 and N642 experience a cyclic straining/stressing during the galvanizing process. If the material had yielded during the compression phase of the stress cycle, the yielding point of the material during the tension phase of the stress cycle would have been reduced significantly due to the Bauschinger effect [14] consequently the possibility of cracking would have been increased.

8.3.2.1.2 45-degrees and upside-down dipping

The galvanizing simulation was also carried out on two additional dipping orientations; namely the 45-degree and upside-down orientation, with all other conditions being kept the same as in the simulation of the upright dipping operation. The typical temperature and longitudinal stress distributions predicted are shown respectively in Figs. 109 and 110.

The FE predictions of the local temperature and stress histories at nodes N14 and N642 during galvanizing of the half-cover plate in the 45-degrees and upside-down dipping orientation are given in Figs. 111 and 112 respectively. Judging by the maximum tensile stress experienced by the material at node N14 among all the three dipping orientations (compare Figs. 107, 111 and 112), it can be argued that the worst case is the 45-degrees dipping orientation, since it has the highest maximum tensile stress at node N14 (440 MPa, Fig. 111). Whereas for the upright and upside-down dipping orientations the maximum tensile stresses experienced by node N14 are relatively low (respectively 369, Fig. 107 and 381 MPa, Fig. 112). This is confirmed by the FE prediction of the longitudinal strain histories at node N14 under the three dipping orientations, as shown in Fig. 113, where the maximum strain is also found under the 45-degree dipping orientation.

8.3.2.1.3 Effect of weld residual stress

In order to investigate the influence of the weld induced residual stresses on LMAC the welding process of the fillet weld was simulated prior to the galvanizing modelling in the upright orientation, as described in the previous section. Due to the half geometry model used in the galvanizing modelling analysis it had to be assumed that the welding process used was also symmetrical, i.e. the two weld beads (one on each side of the symmetry plane) were laid down simultaneously in the same direction. The welding process parameters used for the FE simulation were chosen in such way that a fully fused weld was achieved after welding. Since the material properties data for S460M steel was only available up to 450°C, a different set of data of a similar material, S355 grade steel, generated from another RFCS project [11] was used as an alternative in order to cover the full welding and galvanizing temperature range.

Figure 114 shows the temperature distribution of the component during welding predicted by the FE simulation and the HAZ (heat affected zone) index contours after welding are shown in Fig. 115, showing the extent of the weld fusion zone (contour value = 1.0). The distributions of the longitudinal residual stress and generalised plastic strain induced by the welding as predicted by the FE simulation are given in Figs. 116 and 117 respectively.

Figure 118 shows the FE prediction of local temperature and stress history at nodes N14 and N642 during galvanizing of the half-cover plate with consideration of the weld induced residual stress and strain (dipping in upright orientation). The peak tensile stress predicted at node N14 was 413 MPa in this case, exceeding the yield strength of this material (382.5 MPa for the S335 steel at 450°C).

The FE predictions, using the material properties of the S355 grade steel, of the local stress histories at nodes N14 and N642 during galvanizing of the half-cover plate with and without consideration of the weld residual stress and strain are given in Fig. 119. It is clearly shown by the FE results that the introduction of welding residual stress has caused an increase in the tensile stress experienced by node N14 during galvanizing. Residual stress from welding, however has no influence on the stress history seen by node N642.

8.3.2.1.4 Thermal and mechanical modelling of Corus galvanizing trial

Figures 120 and 121 show the FE prediction of temperature and longitudinal stress development sequences of the channel section during the galvanizing simulation. The temperature and stress contours are plotted on distorted shapes exaggerated by 10 times, showing the dynamic response of the channel section to the thermal shock during the rather fast dipping operation. This type of curving distortion during dipping is attributed to the non-uniform heating between the legs (heating relatively slowly due thicker gauge) and the web (heating relatively quickly due to thinner gauge) of the channel section (Figs. 120(a) and 121(a)). The development of the compressive longitudinal stress in the surface of the section during dipping (Figs. 120(b) and 121(b)) is due to the through thickness temperature non-homogeneity as well as the bending distortion.

Figures 122 and 123 shows the comparison of temperature history between the FE calculation and experiment. A compatible heating rate from the FE simulation was achieved only when using an artificially large heat transfer coefficient of 15000 W/m^2K. It is shown both by the FE calculation and experiment that the leg is heating up slower than the web. The discrepancy between the FE calculation and experiment towards the later stage of the heating process is believed to be a result of zinc solidification and re-melting (melting point of zinc: 419°C), which was not sufficiently considered by the FE simulation.

The comparison of the longitudinal strain histories between the FE prediction and experiment at the corresponding locations is given in Fig. 123. It is clearly seen that although the FE simulation gives a similar strain history pattern at both the leg and web locations, it has underestimated the maximum compressive strain by more than 2 times. A number of factors could have potentially contributed to the large discrepancy between the FE prediction and experiment:

- Dipping process parameters.
- Material properties data used.
- Difference in locations between FE evaluation and measurement.
- Accuracy of measurement.
- Lack of consideration of metallurgical and fluid dynamic effect in heat transfer modelling.
- Effect of mesh density.

The mesh density effect is briefly investigated in the next section.

8.3.2.1.5 Investigation of FE mesh effect on galvanizing modelling

During the galvanizing process, depending on the dipping speed, orientation and the amount of preheat, the material is subjected to a very high surface thermal shock. This may generate significant thermal stress and strain gradients near the surface for the material being immersed into the zinc bath. Therefore it is envisaged that the density of the FE mesh used in the galvanizing simulation would influence the accuracy of the results.

The current investigation into the FE mesh effect on galvanizing modelling involves three quarter geometry FE models of three identical square bars (10 x 10 x 100 mm), as shown in Fig. 124. The only difference is that they were meshed with finite elements of three different densities: coarse, medium and fine, as indicated. It was assumed that the dipping took place in the vertical orientation and the bars were fully immersed in the zinc bath of 450°C in 2 seconds, i.e. with a dipping speed of 50 mm/s. The

material properties data used was that of the Corus S460M grade steel, as presented in Section 2, and the value of the heat transfer coefficient chosen for this study was 10000 W/m^2K.

Figure 125 shows the temperature and longitudinal stress distributions of the steel bar predicted by the FE simulation using FE meshes of different mesh densities. The corresponding temperature and longitudinal strain histories predicted at the face centre nodes of each FE model (as indicated in Fig. 124) are presented in Figs. 126 and 127 respectively. It can be seen that while mesh density had little influence on temperature prediction (see Figs. 125(a) and 126), it greatly affected the FE results in the prediction of the longitudinal stress (Fig. 126(b)) and strain (Fig. 127). It can be seen from Fig. 127 that the difference between the maximum compressive strains predicted by coarse mesh model and the fine mesh model at their respective face centre nodes is nearly 6 times.

Concluding remarks

Through this modelling exercise and the results presented in this report, it has been shown that:

- A rigorous technique of material properties characterisation has been developed for generation of material properties data for FE modelling analysis of galvanizing.
- Advanced FE modelling capabilities for galvanizing process simulation have been established through the current programme of work, with the possibility of allowing weld induced residual stresses and strains to be included.
- The current work has shown that the galvanizing dipping orientation has an effect on the stress and strain history near the galvanizing cracking susceptible zone, and hence influences the cracking susceptibility.
- It has been demonstrated that using FE simulation the galvanizing cracking susceptible zones of a structure can be identified in relation to galvanizing process parameters, which would provide valuable information for the galvanizing practitioners
- It has also been shown that weld residual stress has a detrimental effect on galvanizing cracking.
- It has been recognised that the values chosen for the heat transfer coefficient were artificially high. In the meantime, it has been demonstrated that the discrepancies between the FE prediction and experimental measurements in terms of temperature and strain history during galvanizing are largely attributed to the fact that the metallurgical and fluid dynamic effect was not sufficiently considered in the heat transfer modelling, and possibly the density of the FE meshes employed might not be high enough, particularly near the surface. It is therefore felt that further research in these areas, post FAMEGA, may be still needed.

9. Discussion

9.1 Materials

In this project different materials have been tested in air in the as received conditions at 20ºC and 450ºC, the usual galvanization temperature. All materials suffered a decrease of strength and toughness in air at 450ºC compared to room temperature. The average loss in mechanical properties was 24%, but in some cases values exceeded 30%. Steel J, which was the most susceptible to LMAC in full-scale tests (Section 8.1), had the lowest Charpy energy, but the reductions in tensile and impact properties were similar to other steels. After galvanizing, tensile and impact properties recovered, becoming similar to the non-galvanized material.

We can therefore conclude that the material during galvanization is more susceptible to cracking processes associated with the presence of external stresses, but only when it is immersed.

LMAC always occurred at stresses higher than yield stress. There was always a certain amount of scatter in the stress for LMAC, which was dependent on strain rate. Due to the flat nature of the 450°C tensile curves after yielding, small differences of LMAC fracture stress resulted in large differences in failure strain e.g. a 25% difference in fracture stress resulted in an order of magnitude difference in strain. Tests on tensile test pieces suggested lower threshold stresses for lower strength steels.

Embrittlement is produced when steel is tested in liquid Zn. In fracture mechanics tests toughness measured in terms of stress intensity was reduced up to a factor of two, but more like a factor of 7 when expressed as J-integral. The effect is greater when the Zn bath is rich in Sn. Fracture is produced with little or no plastic deformation, which is in good agreement with other studies.

The highest strength lowest toughness material showed the greatest propensity for failure in full-scale tests. However, laboratory tests at UC failed to show an unusual susceptibility of this steel to LMAC. The implication is that the particular susceptibility of this beam is due to its slender geometry, rather than material properties.

Within the laboratory programme there was no evidence indicating that cracking susceptibility can be related to strength. From the two best performing steels tested at RWTH Aachen University, one was of the lowest and one of the highest strength used in the LMAC tests. Steel grades with higher Charpy-V toughness had better resistance to LMAC. However, the steel with the lowest Charpy toughness was not the worst in LMAC tests. It would appear that increased toughness can beneficial and improve the resistance against LMAC.

The material showing the lowest resistance against cracking in the RWTH Aachen University programme had the highest impurity content. In particular the steel contained a large number of manganese sulphides. These are probably associated with attack where intrusions ~ 100-200 µm can sometimes be observed in unstressed samples. Supporting this hypothesis, the material with the second highest manganese sulphides content was the second poorest performing while the steel with the lowest impurity content had the best resistance against LMAC here. Globular inclusions didn't appear to have a major influence. Although this was a relatively small study it would appear that clean steels with a low content of elongated manganese sulphides are to be preferred for decreasing the cracking susceptibility during galvanizing.

9.2 Galvanizing

9.2.1 Pretreatment: Pickling and fluxing

Surface roughness and hydrogen concentration do not increase significantly after pickling in inhibited HCl. However surface roughness and hydrogen concentration increase sharply after fluxing. A salt bath containing $ZnCl_2 \cdot 4NH_4Cl$(500 g/l) was, at the same molar concentration, more aggressive than $ZnCl_2 \cdot 2NH_4Cl$ salt (360 g/l).

These differences in roughness and hydrogen concentration after fluxing could be due to the "activation" reactions that happen between flux salts and steel prior to galvanizing. SEM examination revealed steel surface attack and presence of metallic Zn deposits, which are reaction products from fluxing. The roughness increase was evidence of a deleterious effect in the quality of the surface. Those defects could act as micro-notches and, as a consequence, increase sensitivity to LMAC, although there is no direct evidence for this.

9.2.2 Galvanizing

Hydrogen content after galvanizing was extremely high for the ferritic-pearlitic steels tested. It appeared that hydrogen was accumulated in the steel base-Zn layer boundary, especially in the micro cracks of Zn-Fe compound layers, but this would need more research. There was no evidence of hydrogen embrittlement in the structural steels examined in FAMEGA. Other research has shown hydrogen embrittlement in galvanized steels of 830 MPa minimum yield stress, but only in the presence of manufacturing defects [10].

SEM analysis of Zn layers on steel after galvanizing in Zn-Sn baths was performed. In every Zn layer analysed, a rich Sn-Pb layer are placed between δ and ζ classical layers of Zn-Pb galvanizing baths. It

appears that Sn is not widespread among the Zn-Fe compounds, but it is concentrated constantly at a little distance from the steel base.

9.3 Geometry

A distinction should be made between structural notches such as stiffness changes (e.g. welds) or holes, and micro-notches such as surface hardness, surface roughness or cold forming. Stiffness changes and holes have been examined during the FAMEGA programme and are considered to be one of the most important factors to cause LMAC. The full-scale tests (with and without half cover plates and holes), modelling and the validation tests carried out at TUKL and CRD&T showed the importance of geometry. When simple sections were galvanized the measured and modelled stresses were relatively low and elastic. This was reflected in their LMAC susceptibility and no LMAC was observed on sections without welds or holes. In contrast the half-cover plate geometry cracked in full-scale tests and in-situ measurements using displacement transducers and modelling showed that stresses well above yield were developed in the region where cracking was observed in full-scale tests (in the web 10-15 mm beneath the half cover plate weld). High stresses have been modelled at drilled holes, but no cracks were observed in full-scale tests with holes.

In the case of structural notches stress peaks occur that increase crack sensitivity. These notches can be avoided by reasonable detailing and designing of the steel structure. In particular the thickness ratio of joined plates could be limited depending on the zinc alloy or the process parameters such as dipping speed.

The influence of micro-notches has not been examined in the FAMEGA programme. Micro-notches often act as points of crack initiation that increase the probability of subsequent crack propagation. The FAD analysis, which combines tensile data and fracture mechanics data, suggested that micro cracks less than 1 mm should have little influence for the steels tested (Fig. 81(b)). To avoid a significant damage to the microstructure a good fabrication quality should be provided. Grinding may be required on critical details. Punching of holes should be avoided totally. After drilling of holes the edges should be treated by a chamfer cone. The literature suggests that flame cut edges reduce the stress for LMAC and should be controlled in view of avoidance of roughness and martensite hardness. This was not proved in the FAMEGA programme and no real difference could be determined between machined and flame cut test pieces (Fig. 76).

9.4 Strain rate

Laboratory tests at CRD&T have shown lower threshold stress values for LMAC at lower strain rates, although all values are above the yield stress of the steel at 450°C. The influence of loading rate on round notched samples studied at RWTH Aachen University (Figs. 59-63 and 65-71) suggested the lowest threshold stress values were produced at critical rate i.e. at too slow a rate the threshold stress increased possibly due to the steel surface layer being alloyed with zinc with no further access to the liquid zinc alloy. For practical purposes when galvanizing thin sections the dipping speed is the factor with the most impact on the stresses and strain rates (Fig. 100). An increase in dipping speed can be beneficial in lowering the maximum stress and strain rate close to the half cover plate.

9.5 Residual stress

Residual stress measurements on as-rolled and straightened sections showed very low transverse residual stresses (Figs. 3 and 4). A series of sections collected from various European manufacturers also showed relatively low residual stress, with a maximum of 50% of yield (Fig. 7). In contrast, residual stress measurements associated with welds and on half plate test sections showed residual stresses close to yield either in the weld or adjacent to the weld (Fig. 5 and 7).

The influence of residual stress has been shown by full-scale tests and modelling. The effect of heat treatment on the half-cover plate geometry was examined in several full-scale tests. Residual stress measurements showed a reduction in tensile residual stress in the critical area beneath the half cover

plate and this was reflected in the reduction or complete absence of cracking in full-scale tests on heat treated beams (Tables 20, 21 and 26). Modelling of the half cover plate geometry with and without residual stress in shown in Fig. 119. The residual stress has almost no influence on the peak stress and the time to reach the peak stress. However, it has a considerable influence on increasing the time at high stress. Without residual stresses the peak stresses above yield last only for a few seconds, while with residual stresses a beam would spend a longer time above yield producing the appropriate stress conditions for LMAC to occur.

9.6 Dipping angle

The effect of dipping angle was modelled for a beam with half cover plate at TUKL and RD&T. The TUKL model showed that changing the angle up to 30° resulted in a lower maximum strain (Fig. 101). In the specific position 13mm below the half cover plate, the CRD&T model showed that dipping at 45° results in a slightly higher peak stress, but this peak stress lasted a matter of seconds (Fig. 111). In contrast a horizontal dip produced a marginally lower peak stress (but above the yield stress) for a much longer period. The implication is that horizontally dipped beams with a half cover plate will be more prone to LMAC.

For very long or large beams the angle is often limited to 0° - 30° due to the limited bath depth, which is often ~ 2.5 m.

9.7 Bath composition

Bath composition, particularly those containing Sn, has several effects, which are detrimental to LMAC, notably:

- Chemical attack.
- Influence on melting temperature.
- Thermal effect, notably on heat transfer coefficient.

Sn is a low melting point metal (220ºC), which forms eutectics with Zn and Pb, and is very reactive with steel [25]. Hence Sn can penetrate and concentrate easily in notches, defects, pre-existing cracks and even grain boundaries, remaining liquid for a longer time, and creating some secondary cracks (~100-200 µm, but sometimes longer) which arrest if there is no external stress applied, as demonstrated in test results and SEM examinations of Section 8.2.1.4. High concentrations of Sn have been found at the tips of cracks and in one instance UC showed almost 100% Sn with no zinc.

9.7.1 Effect of bath composition on the stress/strain magnitude

In Fig. 102 different temperature curves, from small-scale tests, show that different zinc alloys have a different heating behaviour. In particular an increase of the alloying elements Sn and Bi in combination with Pb lead to a significant increase of the heating velocity. The mathematical simulation of these tests by FEM allowed the derivation of the effective heat transfer coefficient and thus simulates the effect of different zinc bath compositions. Alternatively the effective heat transfer coefficient for a specific zinc alloy can be obtained by a validation test, such as the one performed by CRD&T (Section 8.3.2.1.4).

The development of the temperature and the vertical stresses and strains underneath the half end plate are given in Fig. 103. It is clear that the heating of the construction is accelerated when using a zinc bath that contains Sn and Bi. Due to the higher temperature differences over the height of the component the maximum stresses and strains increase.

9.7.2 Effect of bath composition on the material resistance

As a result from the L-N(T) testing the zinc alloy mainly containing lead was shown to be less critical. The alloy clearly having the most detrimental effect contained lead, tin and a small amount of bismuth.

Only little improvement could be reached in using an alloy mainly containing tin and bismuth. The data obtained within the FAMEGA project is insufficient to enable a final recommendation concerning the zinc bath composition itself. As a first conclusion, an elevated content of tin could be regarded as responsible for increasing cracking susceptibility during galvanizing and therefore should be reduced.

9.8 Preheating

Preheating reduced the temperature differences before and after heating. It therefore resulted in a significant reduction of the stress gradient across the section as well as across the thickness. Using Finite Element simulations a linear dependence between the preheating temperature and the occurring stresses and respective strains was verified (TUKL), see Fig. 104.

10. Conclusions

1. Measurements of web residual stress showed low transverse values, with longitudinal values up to 50% of yield. In contrast welding processes resulted in tensile residual stresses close to yield.
2. Full-scale tests, predominantly on beams with a half-cover plate, were successful at producing LMAC during galvanizing. Joint stiffness and residual stress are important and these parameters have been modelled (see below). Techniques to reduce LMAC showed that thermal stress relief with a hand-held torch was highly effective while sand blasting, ultrasonic peening and additional weld beads proved ineffective with compressive stresses confined to surface layers.
3. Small scale laboratory tests showed that LMAC occurs above the yield stress, but there is a drastic loss of ductility of steel under mechanical and corrosive loading which can manifest itself as a lower strain in tensile or round notch tests, or as reduced J integral or stress intensity in fracture mechanics based tests. Critical strains for LMAC were reduced in Zn-Sn baths and by lower steel toughness.
4. Fluxing was shown to produce high hydrogen levels at the steel-zinc interface, but this was not considered to influence cracking in the structural steels examined.
5. EDA studies showed a high the concentration of Sn at the crack tips of specimens tested in Zn-Sn baths.
6. A high presence of inclusions, poor welds, fluxing with excess of NH_4Cl, etc. reduce surface quality and may create small defects which make the liquid metal penetration easier, especially for liquid Sn.
7. Combined tensile and facture mechanics data showed that a level 2 FAD approach could be used for LMAC. For cracks > 2 mm deep LMAC was controlled by the intermediate zone of the FAD i.e. both threshold stress and stress intensity. For cracks <2 mm LMAC was controlled only by the threshold stress for the S460ML steel investigated. This fully justified the use of a threshold stress or strain in the modelling work.
8. The simulation of realistic steel structures created an understanding for the transient character of the stress/strain state during the galvanizing process. The development of high stresses or strains for a sufficiently long period of time is the basis to define an ultimate limit state for LMAC.
9. The combination of data obtained from laboratory scale tests and modelling simulation allowed the classification of multiple effects and influences contributing to LMAC initiation.
   Factors considered to have a large detrimental effect included:
   - Stiffness of joint combined with residual stress – the geometry produced a high stress concentration, while the residual stress caused the stress/strain to remain high for a longer period of time.
   - The zinc bath composition – Sn-rich baths influenced the concentration of Sn at the steel interface and increased corrosivity. In addition Sn additions had a large influence on heating rate by increasing the heat transfer coefficient.
   - Dipping speed - this controlled both the maximum strain and the strain rate, with a reasonable correlation with laboratory tests. Higher dipping speeds could be used to prevent LMAC in critical situations.

   Factors considered as having a secondary detrimental effect included:

- The base material - strength of the base material (S355 and S450/460 grades) appeared to be relatively small. There was some influence of toughness with lower critical strains associated with lower toughness steels.
- Preheating - modelling showed a linear effect of preheating. In practice preheating is not widely practiced and may be little more than a drying operation. If it involves suspending above the zinc bath it is not well controlled.
- Dipping angle - the influence on strain was relatively small

11. Exploitation and impact of the research results

Technical and economic potential for the use of the results.

The basic relations between the multiple effects that contribute to the cracking phenomenon were clarified for some specific structural details and three zinc alloys (covering the range from a conventional Pb-alloyed zinc bath to a high alloyed Pb-Sn –zinc composition).

Specific measures have been derived to avoid cracks during the galvanizing process.

The cracking potential of further constructions and zinc alloys may be determined in the future and further measures could be recommended.

The results of this project will lead to a more controlled and safe galvanizing process, counteract the current uncertainty due to recent damage cases and establish or even increase the market share.

11.1 Guidelines for the Avoidance of LMAC During Hot Dip Galvanizing of Steel Structural Components

(These are a draft and condensed version of the Guidelines, which were produced for dissemination and a wide circulation throughout Europe. These guidelines contain further appendices for explanation of the most important basics that a ready must know. The appendices are not part of this report as they are already covered in the various chapters of the report.)

Scope

This guideline has been prepared in the course of the European Research Project named FAMEGA[1] funded in the frame of the RESEARCH FUND FOR COAL and STEEL (RFCS) during 2003 and 2007. Detailed results of the research will be published by RFCS under the title of the project within one year after Finalisation of the project in 2/2007. Further details can be obtained from any of the participating project partners.

This guideline is intended to summarise in a practical way recommendations for crack free galvanising from the findings made during the FAMEGA project. Background knowledge as far as necessary to understand the recommendations is provided in the Appendices, deeper background may be found in the relevant publications. Some of the most relevant ones are listed in the Bibliography.

Members of the project group have agreed that such a recommendation as given here has not the character of a standard or any guideline because this lies far behind the responsibility of the group, but shall provide additional knowledge in a short and precise manner to the actual discussion. Through this the group expects far deeper diffusion of new results into the European community than by the full final report, which serves as a source to this guideline.

Important note: This guideline is not a standard, it is not an official document and the authors exclude any responsibility for subsequent application of this paper by third people.

---

[1] FAMEGA – Failure Mechansim during Galvanising, RFCS contract, FRS-CR-03014, 9/2003 – 2/2007, to be published in 2008 by RFCS

Introduction

Galvanizing is an extremely reliable, cost effective and aesthetically pleasing solution for the corrosion protection of steelwork. In recent years there have been increasing reports of cracking, of liquid metal assisted cracking (LMAC) in galvanized steelwork. This has been attributed to the use of higher strength steels, in increasingly complex shapes and designs that for both aesthetic and economic reasons often incorporate welds rather than bolted connections. Such Cracks formed during galvanizing can be extremely difficult to detect by visual inspection methods and the consequences of structural failure, either during erection or in service may be severe. Galvanising cracks approaching a metre in length have been observed in extreme cases and the implications of these on structural integrity are obvious. In the case of fatigue loaded structures, even small galvanising cracks of only a few mm length, however, provide ideal sites for continued growth by fatigue and the design lives may be reduced considerably by the effective by-passing of the usual fatigue crack initiation phase. Indeed, it could be argued that, because they are more likely to remain undetected by normal post-galvanising inspection, smaller cracks pose the greater risk, to fatigue loaded structures. Risk of structural failure must be reduced to acceptable levels, particularly where public safety is an issue, and the possibility of steel structures going into service whilst containing pre-existing cracks cannot be allowed. To achieve this it is necessary to understand the circumstances under which the cracks are initiated during the galvanizing process and provide recommendations that shall to help to avoid these failures.

Cracking of steel products during galvanising is not a new phenomenon and several research projects, both in Europe and the rest of the world have investigated the problem. However an increase of the cracking occurrence was reported during the last years concomittant with the introduction of new galvanizing bath alloyed with either tin and/or bismuth. Examples from a number of independent sources have been cited in products supplied to national, European and American specifications by different steel makers. These outbreaks are rare and were often confined to the higher strength grades ($\geq$ S355) in the form of structural sections, plates, long hollow sections/tubes etc. that had undergone some form of downstream fabrication process. The cracks, which in extreme cases can extend to hundreds of mm in length, tend to initiate in the vicinity of fabrication details such as welds, cut edges and drilled or punched holes.

The mechanism, the ruling effects and the interactive dependencies that cause failure were not known or fully understood when FAMEGA started and attempts by researchers to reproduce the phenomenon using both large and small scale simulations had not been completely successful. It was claimed, however, that the factors contributing to the problem were:

- Steel strength and toughness.
- Steel microstructure and cleanliness.
- Residual stresses arising from manufacturing of e.g. steel profiles and from fabrication processes.
- Localised stress concentrations, hard zones and microscopic defects as a result of machining, welding, hole punching, bending etc. during fabrication processes.
- Variations during preparation for galvanising (cleaning, pickling, preheat), e.g. hydrogen embrittlement.
- Variations in the dipping practice such as dipping angle and speed giving rise to adverse thermal stresses.
- The zinc bath composition.

Basically, it was known that high tensile stresses must be present for LMAC, but in addition there had to be a mechanism of liquid corrosive agression on the metal surface leading to crack initiation and subsequent crack growth. To understand the development of stresses during dipping Finite Element (FE) modelling techniques were employed after all boundary conditions and parameters were known. The chemical potential was more difficult to assess as phase transformations between metal layer and zinc alloy must be known and defined in terms of temperature and time. This required thermodynamic simulations which were beyond the scope of the FAMEGA project. Nevertheless, findings with respect to chemical crack potential were found on a phenomenological base and could serve for a first engineering hypthesis of the crack mechanism.

Two new test types were developed by the project partners and results from these tests in liquid zinc were added to the knowledge gained. The tests create a situation which reflects the factors found to be most important for LMAC:

1. Stresses causing local plasticity.
2. Strain rate reflecting different dipping speeds.
3. Notched specimen simulating local stress triaxility.
4. Different surfaces of the notch reflecting the surface quality.

Using Energy dispersive X-ray analysis (EDX) it was found that the concentration of the elements on the site of measurement were quite different from the concentration in the zinc alloy. In the subsidiary cracks and in the tip of the main crack alloying elements such as tin (Sn), Lead (Pb) or Bismuth (Bi) were enriched, whereas in the main crack the microstructural phases typical of a galvanized layer were observed

Recommendations

Liquid metal assisted cracking (LMAC) does not have a single root cause. It is a consequence of a combination of effects with higher or lower strengths of impact, which have a conjoint action.

This should always be kept in mind when reading the following recommendations, which are given in relation to:

1. Material choice
2. Design of the structure
3. Fabrication
4. Galvanizing process

Material choice

This part covers only steels used in welded constructions. Other steels or metals may be affected in a similar way, but were not subject of the underlying research project and aim.

Category	Description	Reference
Mechanical properties	It may be expected that the sensitivity increases with the level of the steel strength (S235 to S460 and higher) and decreases with the level of toughness (JR, J0, J2, K2, M/N to ML/NL). The requirements for the mechanical properties are applicable at specific locations. These locations are specified in the relevant standard or agreed at order. Products with variable thickness normally exhibit higher strength and lower toughness at the thinnest locations. However, safe behaviour may be obtained in galvanizing with steel grades up to S460.	FAMEGA Literature
Micro structure	It may be expected that the sensitivity increases for steels with higher inclusion contents and coarse grain sizes.	FAMEGA
Ageing	For components submitted to cold deformation during fabrication, grades with ageing resistance should be preferred. In particular for cold deformed elements in grade >= S355, only ageing resistant steels with an improved notch resistance should be selected (J2 or better following EN 10025-2 or fine grain steels following EN 10025-3 or EN 10025-4.	GERMAN Guidelines
Secondary stresses	Secondary stresses result from production of sheet, plates and sections. They can contribute to the effect of LMAC. Their effect was not quantified. Such stresses cannot be avoided but should be minimized.	FAMEGA
Hydrogen	For quenched and tempered (QT) steel with yield strength higher than S500 hydrogen embrittlement due to long pickling treatment is more likely to occur.	Literature

Design of the structure

The design stands right at the beginning of the construction. Some important decisions are taken here by the designer, which should also refer to the avoidance of LMAC during subsequent galvanising.

Category	Description	Reference
Geometry	Avoid or reduce constructional details which lead to high remote or local secondary stresses, especially during the galvanizing process due to high temperature differences.	FAMEGA national guidelines
	Avoid geometrical details that have high geometrical restraints.	National guidelines
	Closed profiles are difficult to dip because they initially float. Cut outs shall be planned to avoid this.	National guidelines
	Limit the thickness ratio between to steel members to $t_1/t_2 < 2.5$ to avoid or at least minimize restraint effects due to a different heating up behaviour.	National guidelines
	Prefer symmetrical sections. For asymmetrical elements, weld seams should be placed near the neutral axis of the piece, or symmetrically balanced on both sides of the neutral axis with simultaneous execution.	Empirical knowledge
	Members with high webs are more sensitive because of the thermal gradient during dipping causing high stresses.	FAMEGA

Fabrication

To enable their use in structures, the individual components are generally subjected to various finishing operations before galvanizing. These processes may include: drilling, flame cutting, coping, cambering, straightening, cold sawing, bending and of course welding. More caution should be used for certain processes addressed in the following.

Category	Description	Reference
Cold deformation	Excessive local cold deformation as may result from punching devices used for pre bending of girders clearly raise the risk of LMAC.	GERMAN guide
	Normal cold deformation can be performed, ideally in a smooth and continuous procedure, e.g. three point rolling better than three point bending.	GERMAN guide
Cutting (cold and warm) and Drilling	Cutting affects the surface structure of the component. The more severe the local defect the higher the risk of LMAC. Using sharp drills, avoiding punching and grinding of surface may lower this risk. The effect of thermal cutting was not checked but local hardening from high thermal gradients could have negative effects.	FAMEGA National guidelines
Welding	Welding causes residual stresses. Some LMAC cracks occur along the HAZ starting from the surface and going through the base material. It is very likely that residual stresses perpendicular to the HAZ contribute to the cracking process. In these circumstances stress relief would appear to be ideal to reduce LMAC, but it has not been proved that this is always required. A careful low restraint weld design should help reduce such stresses.	National guidelines
	Steel hardness before and after fabrication should be limited to 340 HV.	Empirical knowledge

Galvanizing process

The galvanizing process stands at the end of the chain and consists of more than just dipping in liquid zinc alloy. Preparatory steps may also contribute to the problem and must be taken into account.
From the point of galvanizing it is evident that quality control must be performed in every step using personnel who are qualified for the job and for the detection of possible failure and for the assessment of the risk of cracking of any component during each step in the process.

Category	Description	Reference
Bath composition	Alloying elements such as Sn and Bi were found to have a major effect on LMAC. Pb contributes too but only in conjunction with Sn and Bi or at very long times. Therefore the reduction of Sn and Bi to values below 0.15 is recommended until full understanding is available from further research.	FAMEGA and national research
Category	Description	Reference
Bath Composition	Pb may stay in the bath up to the full dissolubility.	FAMEGA and national research

Sand Blasting	No effects were observed.	FAMEGA
Pickling	Long time pickling is not good, do not over pickle, use inhibitors and replenish solutions regularly.	Empirical knowledge
Fluxing	The effect of flux was not fully studied. However it has effects on the heat transfer, the development of the zinc layer and the adsorption of additional Hydrogen in the subsurface area.	Empirical knowledge FAMEGA

Dipping	Use a high dipping speed and a large dipping angle.	FAMEGA
	Avoid double dipping.	Empirical Knowledge
	Bath composition shall be known and be measured regularly.	FAMEGA
	High preheating and drying temperatures are positive.	Empirical Knowledge
Quality Control	Control of construction elements directly after galvanisation (100% visual; NDT of critical parts).	FAMEGA
	Immediate corrective actions if defects are detected.	FAMEGA
	Carry out a galvanising test in the case of elements with complex geometry.	FAMEGA

Bibliography

1. "Liquid metal embrittlement cracking by molten zinc in structural steel HAZ", Yoneo Kiruta, Takao Araki, Masafumi Yoneda, Kei Uchikawa: Technology reports of the Osaka university, (1986), Vol. 36, No. 1828, p65.

2. Elboujdaini, M, Tyson, W R and Pouskouldi, G: 'ZM-396: Control of Cracking During Galvanized Structurals', MTL 93-9(CF), CANMET, Metals Technology Laboratories, International Lead Zinc Organisation Inc., March 1993.

3. Elboujdaini, M and Tyson, W R: 'ZM-396: Control of Cracking During Galvanised Structurals: Final Report Phase 2', MTL 93-51(CF), CANMET, Metals Technology Laboratories, International Lead Zinc Organisation Inc., December 1993.

4. Elboujdaini, M and Tyson, W R: 'ZM-396: Control of Cracking During Galvanised Structurals: Final Report Phase 3', MTL 95-5(CF), CANMET, Metals Technology Laboratories, International Lead Zinc Organisation Inc., April 1995.

5. Elboujdaini, M, Tyson, W R and Shen, G: 'ZM-396: Control of Cracking During Galvanised Structurals: Final Report Phase 4b', MTL 96-14(CF), CANMET, Metals Technology Laboratories, International Lead Zinc Organisation Inc., May 1996.

6. Elboujdaini, M, Tyson, W R, Shen, G and Ray, G: 'ZM-396: Control of Cracking During Galvanised Structurals: Final Report Phase 4b', MTL 97-18(CF), CANMET, Metals Technology Laboratories, International Lead Zinc Organisation Inc., April 1997.

7. "Cope cracking in structural steel after galvanizing": Thomas Langill, Tom Schafly: Modern steel construction, October 1995, p40.

8. "Update on galvanized beam cope cracking", Structural shapes producers council, Technical committee meeting 8 November 2000.

9. "Rissbildung beim feuerverzinken von feinkornbaustählen", "Cracking of fine grained structural steels related to hot-dip galvanizing", K Menzel, W Beul, Werkstoff und korrosion 46, 1995, p39.

10. "Influence of hot dip galvanizing on the properties of HSLA structural steels", Richard Kreski: Processing of Microstructure and properties of HSLA steesl, ed. By A J DeArdo, the minerals, metals and materials society, 1988.

11. Cresdee, R B, Edwards, W J, Thomas, P J and Viss, G F: 'Analysis of Beam Distortion During Hot Dip Galvanising', Materials Science and Technology, Volume 9, February 1993.

12. Guidance Note – Hot Dip Galvanizing (D02) No.8.03, 'Guidance Notes on Best Practice In Steel Bridge Construction', SCI P185, Steel Bridge Group, 7 January 2002.

12. List of Tables and Figures

Tables

Table 1 Factors contributing to liquid metal assisted cracking [1,5]
Table 2 Summary of planned and accomplished tasks
Table 3 Steel sections for testing
Table 4 Chemical compositions of steels
Table 5 Summary of web properties (lab tests)
Table 6 Mechanical properties before and after galvanizing
Table 7 Summary of tensile properties of steels used in full-scale tests (flange properties)
Table 8 Sections for full-scale galvanizing test program
Table 9 Variations in galvanizing process in four European Countries
Table 10 Details for welding half cover plate for full-scale tests
Table 11 Results of metallographic examinations of steels M, L, N
Table 12 Summary of full-scale test variables
Table 13 Test variants for full scale galvanizing test no. 4.
Table 14 Test matrix of the University of Cantabria programme
Table 15 Composition of the baths used at UC for the tests in liquid Zn
Table 16 Zinc alloys used for testing at RWTH Aachen University
Table 17 Zinc alloy used for testing at Corus RD&T
Table 18 Parameters required for modelling the welding process
Table 19 Parameters required for modelling the galvanizing process
Table 20 Full scale galvanizing test no. 1 – fracture examination after transverse tensile test
Table 21 Full scale galvanizing test no. 2 – fracture examination after transverse tensile test
Table 22 Full scale galvanizing test no. 3 – fracture examination by magnetoscopic technique
Table 23 Results of test no. 4 – Zn-Sn bath, magnetoscopic fracture examination
Table 24 Results of the test no. 5, checking below the cover plates. Fracture examination by magnetoscopic technique
Table 25 Results of test no. 5, control of the plate welded on beam flange. Fracture examination by magnetoscopic technique
Table 26 Galvanizing test no. 6, section with half cover plate. Magnetoscopic fracture examination
Table 27 Galvanizing test no. 6, 10 mm plate welded on beam flange. Magnetoscopic fracture examination
Table 28 Galvanizing test no. 6, cope cut. Magnetoscopic fracture examination
Table 29 Galvanizing test no. 6, drilled holes in the web. Magnetoscopic fracture examination
Table 30 Results of galvanizing tests no. 7, sections with half cover plates. Magnetoscopic fracture examination
Table 31 Results of galvanizing tests no. 8, sections with half cover plates. Magnetoscopic fracture examination
Table 32 Results of hydrogen concentration tests for steel code D. Values in ppm.
Table 33 RWTH Aachen University LMAC results. Test results material A, alloy a0
Table 34 Test results material B, alloy a0
Table 35 Test results material C, alloy a0
Table 36 Test results material F, alloy a0
Table 37 Test results material A, alloy a1
Table 38 Test results material B, alloy a1
Table 39 Test results material C, alloy a1
Table 40 Test results material F, alloy a1
Table 41 Test results material A, alloy a2
Table 42 Test results material B, alloy a2
Table 43 Test results material C, alloy a2
Table 44 Test results material F, alloy a2

Table 45 Maximum loads and corresponding clip gauge displacements from LMAC tests on CT test pieces with key hole notch
Table 46 CRD&T LMAC tests using compact tension (fracture mechanics) tests

Figures

Fig. 1 The requirements for liquid metal assisted cracking [1, 5]
Fig. 2 Typical microstructures
Fig. 3 FE predicted residual stress profile for IPE220 section.
Fig. 4(a-c) Measurements of residual stress in section using 3 MA meter (a) after cooling, (b) after lifting, (c) after straightening
Fig. 5 Residual stress across a submerged arc weld measured using X-ray techniques
Fig. 6 Sonats X-ray equipment for the measurement of residual stress.
Fig. 7 X-ray measurement of residual stresses before (base metal) and after welding.
Fig. 8 Schematic of process route for galvanizing
Fig. 9 Assembly design for full-scale tests
Fig. 10 Position of the macrographic section and HV10 hardness measurements
Fig. 11 Full-scale tests carried out on 10 off 2 m lengths of half cover plate sections
Fig. 12 Geometry of sections for galvanizing tests no. 1 and no. 2
Fig. 13 Deliberate defect introduced by saw cut 10 mm below half cover plate.
Fig. 14 Assemblies for full scale galvanizing test no. 3
Fig. 15 Assembly for full scale galvanizing test no. 4
Fig. 16 Weld bead added in critical area below welded half cover plate
Fig. 17 Thermal stress relieving with hand held torch
Fig. 18 Full scale Galvanizing test no. 5
Fig. 19 SEM picture showing pits in web section after pickling
Fig. 20 Assembly designs for full scale galvanizing test no. 6
Fig. 21 Experimental equipment used for [H] concentration tests at the University of Cantabria.
Fig. 22 Test pieces used for LMAC test at the University of Cantabria
Fig. 23(a and b) University of Cantabria LMAC testing (a) Bolt loaded WOL (b) LMAC test facility.
Fig. 24 Schematic of the UC experimental equipment for (a) slow strain rate tests and (b) toughness tests
Fig. 25 Modified CT Specimen (dimensions in mm) used for laboratory LMAC tests at the RWTH Aachen University
Fig. 26 RWTH Aachen University LMAC test set-up
Fig. 27 Schematic of RWTH Aachen University (UA) LMAC test using modified compact tension (DCB) test piece
Fig. 28 Test pieces used in laboratory LMAC testing at Corus RD&T
Fig. 29 Corus RD&T LMAC test facility
Fig. 30 Flow stress curves for steel C (grade S460M) at various temperatures used for modelling galvanizing.
Fig. 31 Change in yield strength and Young's modulus with temperature for steel C (grade S460M).
Fig. 32 Variation of thermal strain with temperature for steel Grade S460M steel
Fig. 33 Schematic of component used in Corus model of galvanizing trial No. 1 conducted by TU Kaiserslautern (TUKL) [2].
Fig. 34 Geometry used for validation of the welding process model at TUKL
Fig. 35 TUKL validation Trial No. 3 - Geometry and application of measurement devices
Fig. 36 Geometry of the channel section used in a galvanizing trial carried out by Corus for model development and validation (nodes highlighted in red are locations where temperature and longitudinal strain histories were monitored both in the FE simulation and experiment. *70 in reality).
Fig. 37 Full-scale test. LMAC in Section of IPE 600A S450J0 (Steel J) – Rolling process : as rolled
Fig. 38 Metallographic examination of small cracks

Fig. 39 Transverse tensile test used on full-scale tests
Fig. 40 Full-scale galvanizing test no. 3. Crack detection by magnetoscopic (magnetic particle inspection) technique
Fig. 41 Measurements of residual stresses, X ray technique
Fig. 42 Surface roughness tests for steel grade J.
Fig. 43 Deposits on the surface of steel grade J after fluxing.
Fig. 44 Hydrogen concentration test results for different steel grades. H content after galvanizing includes hydrogen in the Zn layer over the steel.
Fig. 45 Hydrogen concentration test results on steel grade J for different pre-galvanizing and galvanizing processes. H content after galvanizing does not include H in upper Zn layer.
Fig. 46 Results of J tests on CT specimens made of steel grade J.
Fig. 47 Slow strain rate test results on specimens made of steel grade J.
Fig. 48 Microstructure of a Zn layer obtained with a Zn bath rich in Sn, and an EDS spectrum on a point rich in Sn and Pb (steel grade P).
Fig. 49 Microstructure of a Zn layer. Chemical composition from the steel base to the surface of the Zn layer (Steel grade L).
Fig. 50 Concentration of Sn and Pb on the steel base in a DCB specimen of steel grade B.
Fig. 51 Sn concentration effect on a pre-fatigue crack of a DCB specimen made of steel B
Fig. 52 Sn concentration effect on a crack produced by embrittlement in the notch marked as R1 in the DCB specimen of steel B.
Fig. 53 Sn, Bi and Pb concentration effect in a CT specimen of steel grade C tested in liquid Zn.
Fig. 54 Detail of the failure during galvanizing of Fig. 52, etched with Nital 5%.
Fig. 55 Sn, Bi and Pb concentration on CT test piece after testing in liquid zinc. Steel C.
Fig. 56 Crack and fracture surface appearance after testing
Fig. 57 Typical example for load-displacement plot from L-N(T) testing
Fig. 58 Maximum load values in different loading rates, material A
Fig. 59 Displacement at maximum load in different loading rates, material A
Fig. 60 Maximum load values in different loading rates, material B
Fig.61 Displacement at maximum load in different loading rates, material B
Fig. 62 Maximum load values in different loading rates, material C
Fig. 63 Displacement at maximum load in different loading rates, material C
Fig. 64 Maximum load values in different displacement rates, material F
Fig. 65 Displacement at maximum load in different displacement rates, material F
Fig. 66 Maximum loading values achieved for testing performed in alloy a0 divided by L-N(T) thickness b and upper yield R_{eH}
Fig. 67 Displacement values achieved corresponding to F_{max} divided by L-N(T) thickness b for testing performed in alloy a0
Fig. 68 Maximum loading values achieved for testing performed in alloy a1 divided by L-N(T) thickness b and upper yield R_{eH}
Fig. 69 Displacement values achieved corresponding to F_{max} divided by L-N(T) thickness b for testing performed in alloy a1
Fig. 70 Maximum loading values achieved for testing performed in alloy a2 divided by L-N(T) thickness b and upper yield R_{eH}
Fig. 71 Displacement values achieved corresponding to F_{max} divided by L-N(T) thickness b for testing performed in alloy a2
Fig. 72 Maximum loading values achieved for testing performed in alloy a0 divided by L-N(T) thickness b and upper yield R_{eH} (for material F from flange testing)
Fig. 73 Displacement values achieved corresponding to F_{max} divided by L-N(T) thickness b for testing performed in alloy a0
Fig. 74 CRD&T LMAC test results showing max stress compared to tensile results at 450°C
Fig. 75 CRD&T LMAC tensile test results showing max stress compared to tensile curves at 450°C
Fig. 76 CRD&T LMAC test results for machined and flame cut tensile test pieces
Fig. 77 Effect of strain rate on LMAC failure stress

Fig. 78	Mises stress v strain for LMAC tests on keyhole test pieces
Fig. 79	Keyhole results
Fig. 80	Comparison of tensile and key-hole LMAC tests
Fig. 81(a and b)	Influence of crack size on LMAC (a) FAD diagram for LMAC tests incorporating threshold stress and stress integrity (b) Dependence of critical stress on defect depth
Fig. 82	Results of short crack tests
Fig. 83	Temperature field during the welding process of a butt weld connection of two plates
Fig. 84	Cooling curves in the middle of the weld
Fig. 85(a and b)	Qualitative distribution of longitudinal (a) and transversal stresses (b) in a butt weld connection after the welding process [8]
Fig. 86(a and b)	Longitudinal stresses σ_y: (a) longitudinal cut, (b) lateral cut
Fig. 87(a and b)	Longitudinal stresses σ_y: (a) longitudinal cut, (b) lateral cut
Fig. 88	Cracked section after TUKL validation trial
Fig. 89	Displacement and Temperature Development during the dipping process
Fig. 90	Displacement and Temperature Development in the Time Range of Immersion
Fig. 91	Recorded and recalculated Load-Displacement-Development and calculated strain behaviour
Fig. 92	stress and strain limit state at the point of crack initiation
Fig. 93	Calculated limit strain in dependence of the bath composition and the material
Fig. 94	Calculated limit strain in dependence of the loading velocity and the material
Fig. 95	Residual stress state in longitudinal direction (σ_y)
Fig. 96	Residual von Mises stress
Fig. 97	Galvanizing Process Simulation of a Beam with Half Cover Plate – Results
Fig. 98	Galvanizing Process Simulation of a Beam with Full Cover Plate and Drilled Holes- Results
Fig 99	Galvanizing Process Simulation of a Beam with Cope Cut- Results
Fig. 100	Effect of the dipping speed on the maximum strain and strain rate
Fig. 101	Effect of dipping angle on the strain development
Fig. 102	Effect of Zinc Alloy Composition on the Heating Behaviour – Small Scale Test Results
Fig. 103	Effect of Different Heat Transfer Coefficients on the Strain and Temperature Development During Immersion in the Zinc Smelter
Fig. 104	Effect of Preheat Temperature on Strain and Strain rate During Immersion in the Zinc Smelter
Fig.105(a and b)	Temperature (a) and longitudinal (S22) stress (b) development contours of the half-cover plate component during galvanizing (at 30 s) predicted by ABAQUS FE simulation (CRD&T).
Fig.106(a and b)	Temperature (a) and longitudinal (S22) stress (b) development contours of the half-cover plate component during galvanizing (at 69.5 s) predicted by the FE simulation.
Fig. 107	Local temperature and stress history at nodes N14 and N642 during galvanizing of the half-cover plate predicted by the FE simulation (upright dipping).
Fig. 108	Generalised plastic strain distribution of the half-cover plate after full immersion in the zinc bath predicted by the FE simulation, showing localised strain damage primarily in three areas (near nodes N14, N1255 and N1273).
Fig.109(a and b)	Temperature (a) and longitudinal (S22) stress (b) development contours of the half-cover plate component during galvanizing (at 165 s, 45-degrees dipping) predicted by the FE simulation.
Fig.110(a and b)	Temperature (a) and longitudinal (S22) stress (b) development contours of the half-cover plate component during galvanizing (at 70 s, upside-down dipping) predicted by the FE simulation.
Fig. 111	Local temperature and stress history at nodes N14 and N642 during galvanizing of the half-cover plate predicted by the FE simulation (45-degrees dipping).
Fig. 112	Local temperature and stress history at nodes N14 and N642 during galvanizing of the half-cover plate predicted by the FE simulation (upside-down dipping).
Fig. 113	FE prediction of strain history at node N14 with different dipping orientations.
Fig. 114	FE prediction of temperature distribution during fillet welding.

Fig. 115 FE prediction of HAZ index contours after fillet welding (contour value = 1.0: weld metal; contour value between 0.5 and 1.0: HAZ; contour value less than 0.5: parent material).
Fig. 116 FE prediction of longitudinal residual stress (S22) distribution after fillet welding.
Fig. 117 FE prediction of generalised plastic strain distribution after fillet welding.
Fig. 118 Local temperature and stress history at nodes N14 and N642 during galvanizing of the half-cover plate predicted by the FE simulation including the effect of weld induced residual stress and strain (upright dipping).
Fig. 119 Local stress history at nodes N14 and N642 during galvanizing of the half-cover plate predicted by the FE simulation with (*) and without the effect of weld induced residual stress and strain (upright dipping).
Fig. 120(a and b) FE prediction of temperature (a) and longitudinal stress (S33) (b) distributions at 2.87 s of dipping during the channel section galvanizing process simulation (distorted geometry exaggerated by 10 times).
Fig. 121(a and b) FE prediction of temperature (a) and longitudinal stress (S33) (b) distributions at 5.81 s of dipping during the galvanizing process simulation (distorted geometry exaggerated by 10 times).
Fig. 122 Comparison of temperature history between FE prediction and experiment.
Fig. 123 Comparison of longitudinal strain history between FE prediction and experiment.
Fig. 124 Identical model geometry and different mesh density used in the FE mesh sensitivity study (face centre nodes are used for temperature and longitudinal strain history comparison).
Fig. 125(a and b) FE prediction of temperature (a) and longitudinal stress (S33) (b) distributions at 1.72 s of dipping during the galvanizing process simulation (mesh density increases from left to right).
Fig. 126 FE prediction of temperature history at face centre nodes showing no effect of mesh density used in the FE simulation.
Fig. 127 FE prediction of strain history at face centre nodes showing the significant effect of mesh density used in the FE simulation.

13. References

1. Kinstler, T J: "Current knowledge of the cracking of steels during galvanizing – A synthesis of the available technical literature and collective experience for the American Institute of Steel Construction".

2. Weigand, H: "The effects of hot dip galvanizing on the mechanical properties of steel sections" Proc 6th Hot Dip galvanizing Conf., Interlaken, 1961, pp69-77.

3. McDonald, R D: "Steel embrittlement problems associated with hot dip galvanizing – causes, mechanisms, and selected references", Materials performance, Jan. 1975, pp31-37.

4. Kinstler, T J: "The mechanical properties of galvanized structural steels and their weldments" Fifth Int. Symposium on Corrosion in the pulp and paper industry", Vancouver, Canada, 1986, Vol. 3, pp251-259.

5. Kinstler, T J: "Current knowledge of the cracking of steels during galvanizing – a synthesis of the available technical literature and collective experience", EGGA Conf, 2006.

6. Cook, T H: “Composition, Testing, and Control of Hot-Dip Galvanizing Flux” In “Metal Finishing”. July-August 2003, Vol. 101, issues 7-8. pp22-35.

7. “ESIS Procedure for Determining the Fracture Behaviour of Materials. ESIS PS-92”. European Structural Integrity Society. Delft, The Netherlands, 1992.

8. Rudd, W J et al: "Failure mechanisms during galvanizing", Technical report no. 4, Contract no. RFS-CR-03021. Ref Source no. 114839, Corus Research, Development & Technology, Swinden Technology Centre, September 2005.

9. Rudd, W J et al: "Failure mechanisms during galvanizing", Technical report no. 5, Contract no. RFS-CR-03021. Ref Source no. 120268, Corus Research, Development & Technology, Swinden Technology Centre, March 2006.

10. Brogan, J, Rudd W J and Webster, S E, "A study of hydrogen embrittlement in Macalloy prestressing steel", Swinden Laboratories, British Steel Technical report EM/RSC/S10954/1/89/E, 8 Aug 1989.

11. Thompson, A et al: Improving the competitiveness of the European steel fabrication industry using synchronised tandem wire welding technology (SYNFAB), RFS-CR-03049, Technical report No. 3, Corus Research, Development, Swinden Technology Centre, March 2005.

12. Wen, S W, Church, S and Parker, S V: Proc. 14th Int. Conf. On “Computer technology in welding and manufacturing”, Sheffield Hallam University, UK, June 2004, TWI.

13. 6. ABAQUS: http://www.abaqus.com.

14. British Standard, BS 7910: 2005 "Guide to methods for assessing the acceptability of flaws in metallic structures".

15. Richter, F: Physikalische Eigenschaften von Stählen und ihre Temperatur-abhängigkeit, Polynome und graphische Darstellungen, Stahleisen-Sonderberichte, Heft 10, Verlag Stahleisen mbH, Düsseldorf, 1983.

16. Richter, F: Die wichtigsten physikalischen Eigenschaften von 52 Eisenwerkstoffe. Stahleisen-Sonderberichte, Heft 8, Verlag Stahleisen mbH, Düsseldorf, 1973.

17. Peil, U and Wichers, M: Schweißen unter Betriebsbeanspruchungen – Werkstoffkennwerte für einen S355J2G3 unter Temperaturen bis 1200°C, Stahlbau 73 (2004), H. 6, S. pp400-416.

18. Peil, U and Wichers, M: Schweißen unter Betriebsbeanspruchungen – Werkstoffkennwerte für einen S355J2G3, Stahlbau 74 (2005), H.4, S. pp249–257.

19. Radaj, D: Wärmewirkungen des Schweißens, Temperaturfeld, Eigenspannungen, Verzug. Springer-Verlag, Berlin, 1988.

20. N.N.: SYSTUS 2004 Analysis Reference Manual; Heat Transfer Reference Manual; Man-Machine Interface Commands; Geometry/Meshing Reference Manual, Paris: ESI Software, 2003.

21. N.N.: How to get Material Properties for a Welding and Heat Treatment Simulation with SYSWELD. Paris: ESI Software, 2003.

22. Dilthey, U: Schweißtechnische Fertigungsverfahren Band 2 Verhalten der Werkstoffe beim Schweißen. Düsseldorf: VDI-Verlag, 1995.

23. Hasselmann, U: Flüssigmetallinduzierte Rissbildung bei der Feuerverzinkung hochfester HV-Schrauben großer Abmessungen infolge thermisch bedingter Zugeigenspannungen, Dissertation am Institut für Werkstofftechnik der TU Darmstadt, 1997.

24. Pankert, R and Gilles, M: Umicore Zinc alloy & chemicals/Research, private communication.

25. Clegg, R E and Jones, D R H: ‘Liquid metal embrittlement of tensile specimens of EN19 by tin’, Engineering Failure Analysis, 2003, Vol. 10 pp119-130.

Tables

Table 1: Factors contributing to liquid metal assisted cracking [1,5]

Stress	Material susceptibility	Liquid metal
• Stress concentration due to geometry (especially welds) • Residual stress due to ▪ straightening ▪ thermal cutting ▪ welding ▪ cold work (shearing, punching, bending) • Thermal stress due to dipping (affected by angle and speed) • Reduced thermal stress due to preheat	• Strength/hardness (>250-290 VHN) • Hydrogen cracking during pickling/fluxing of high strength steels • Flux containing Fe> 10 g/l	• Pb: increases incidence and severity to cracking • Ni: no affect • Sn and Bi > 0.2% increases crack size • Sn >0.3% increases crack size

Table 2: Summary of planned and accomplished tasks

Work Package	Task	Description	Acc.	Comment
1	1.1	Procure steels	√	16 steels in total
	1.2	Chemical analysis + mechanical properties	√	Mechanical properties greatly extended for modelling. In WP 5/6
2	2.1	Review product manufacturing	√	Residual stress measurements made for full-scale tests and on some Corus products
	2.2	Review customer fabrication	√X	Residual stress measurements carried out for full-scale tests and at CRD&T. Confidentiality issues with fabricators
	2.3	Review galvanizing procedures	√	Reviewed for UK, Germany, Luxembourg and Spain
3	3.1	Fabrication	√	Half cover plates, saw cuts, holes in full-scale tests
	3.2	Full scale tests	√	80 full-scale tests were carried out against 50 suggested in the proposal
	3.3	Evaluation inspection	√	
4	4.1	Fracture toughness	√	
	4.2	LMAC tests	√	
	4.3	Critical parameters for LMAC	√	
	4.4	Susceptibility: steels, zinc bath	√	
5	5.1	Galvanizing trials on pre-stressed test pieces	X	WOL test pieces did not suffer LMAC
	5.2	Modelling of welding	√	Limited amount of modelling
	5.3	Guidance on optimum welding	X	
6	6.1	Effect fabrication on residual stress	√	Original concepts overtaken with modelling which was much more than re-distribution of residual stress
	6.2	Effect galvanizing on residual stress	√	
	6.3	Correlation small and large scale tests	√	
	6.4	Transfer small to large scale	√	Full scale tests used to validation modelling
7	7.1	Co-ordination project	√	Regular meetings
	7.2.	Interpretation and assimilation of results into Guidance Document	√	UK and German documents written during FAMEGA project. Guidance concentrated on additional findings from project

Table 3: Steel sections for testing

Code	Rolling process	Dimensions tw x tf x h	Grade	Type of test	Lab.
A	AR	11.1 x 17.3 x 607.6	S355JR	Lab	UC + UA + CRD&T
B	CR	14.1 x 23.6 x 620.2	S460ML	Lab.	UC + CRD&T
C	CR	11.8 x19.7x 612.4	S460M	Lab.	UC + CRD&T
D	AR	13.1 x 22.1 x 617.2	S235J0	Lab	UC + UA
E	AR	10.2 x 16 x 500	S355J2	Lab	UA
F	CR	11.1 x 17.2 x 550	S460N	Lab	UA
G	CR	12 x 19 x 600	275J0	FS	
H	CR	12 x 19 x 600	355J0	FS and Lab.	UC
I	CR	11.5 x 17 x 753	S420N	FS	
J	CR	9.8 x 17.5 x 597	S450J0	FS and Lab	UC
K	QST	12 x 19 x 600	S420M	FS	
L	QST	11.9 x 19.6 x 612	355ML	FS	
M	CR	12.9 x 12.9 x 346.4	460N	FS	
N	QST	15.6 x 15.6 x 351.9	S460	FS	
O	QST	14.4 x 21x 762	S460	FS	
P	QST	12 x 19 x 600	460ML	FS	

UC = University Cantabria, UA = University Aachen, CRD&T = Corus Research and Development
AR = As rolled, CR = Controlled rolled, QST = Quenched and self tempered
FS = Full-scale test (Arcelor Profil Luxembourg), Lab. = Laboratory test
t_w web thickness, t_f = flange thickness, h = height

Table 4: Chemical compositions of steels

Code	Grade	C	Mn	Si	P	S	Nb	V	Ni	Cr	Cu	Al	Sn	N	CEV
A	S355JR	0.11	1.42	0.23	0.019	0.020	0.334	0.0015	0.02	0.03	0.018	0.035	<0.02	0.008	0.36
B	S460ML	0.11	1.43	0.36	0.017	0.003		0.086	0.35		0.223	0.041	<0.02	0.0151	0.408
C	S460M	0.11	1.45	0.35	0.013	0.015		0.087	0.36		0.284	0.047	<0.02	0.0175	0.418
D	S235JR	0.11	1.36	0.21	0.019	0.016	0.037	0.001	0.02	0.02		0.031	0.001	0.0061	0.337
E	S355	0.10	1.47	0.21	0.009	0.006	0.015	0.056	0.05	0.03	0.06	0.029			
F	S460	0.10	1.6	0.26	0.015	0.003	0.023	0.112	0.04	0.02	0.06	0.033			
G	S275J0	0.089	0.64	1.80	0.02	0.019	0.001	0.001	0.13	0.10	0.25			0.0085	0.258
H	S355J0	0.147	0.55	1.80	0.02	0.022	0.001	-	0.13	0.10	0.25			0.0085	0.301
I	S420N	0.092	1.34	1.80	0.02	0.015	0.019	0.054	0.13	0.10	0.25			0.0085	0.364
J	S450J0	0.13	1.18	1.80	0.02	0.015	0.005	0.002	0.13	0.10	0.25			0.0085	0.393
K	S420M	0.091	1.11	1.80	0.02	0.019	0.010	0.019	0.13	0.10	0.25			0.0085	0.344
L	S355ML	0.10	1.10	1.80	0.02	0.005	0.008	0.002	0.13	0.10	0.25	0.011		0.0085	0.334
M	S460N	0.14	1.48	1.80	0.02	0.018	0.019	0.070	0.13	0.10	0.25			0.0085	0.456
N	S460	0.13	1.31	1.80	0.02	0.014	0.018	0.002	0.13	0.10	0.25			0.0085	0.405
O	S460	0.137	1.35	1.80	0.02	0.022	0.016	0.002	0.13	0.10	0.25			0.0085	0.405
P	S460ML	0.091	1.38	1.80	0.02	0.003	0.010	0.014	0.13	0.10	0.25	0.014		0.0085	0.377

Table 5: Summary of web properties (lab tests)

Code	Grade	Tested by	Temp. (°C)	Upper yield (MPa)	0.2% proof stress (MPa)	Tensile strength (MPa)	Elongation (%)	Charpy E (J)
A	S355JR	CRDT + UC+ UA	RT	454.3	435	538	26.7	101
A	S355JR	CRDT + UC +UA	450		279	441	30.7	88
B	S460ML	CRDT + UC	RT	604.7	569	682	20.0	184
B	S460ML	CRDT + UC	450		411	492	21.7	138
C	S460M	CRDT + UC	RT	556.7	534	650	21.7	99
C	S460M	CRDT + UC	450		366	482	24.3	72
D	S235JR	UC	RT					197
D	S235JR	UC	450					124
E	S355	UA	RT	497		545	26.6	
E	S355	UA	RT	472		549	29.6	
F	S460	UA	RT	631		715	21.1	
F	S460	UA	RT	618		683	18.5	
J	S450J0	UC	RT		607	699	13.7	35
J	S450J0	UC	450		481	584	11.1	27
	S460N	UC						
	S460N	UC						

Table 6: Mechanical properties before and after galvanizing

Steel	Condition	$\sigma_{y0.2}$ (MPa)	σ_R (MPa)	Elongation (%)	Charpy energy (J)
M	Galvanized	512	648	22.7	146
	As received	545	616	20.8	130
L	Galvanized	441	519	24.6	46
	As received	459	544	20.2	41

Table 7:Summary of tensile properties of steels used in full-scale tests (flange properties)

Section	Grade	Tensile properties of the flange in longitudinal direction		
		R_e (MPa)	R_m (MPa)	A5d (%)
IPE 600	S275 J0	318	452	38.8
IPE 600	S355 J0	430	527	27.6
IPE 750	S420 N	459	531	30.7
IPE A 600	S450 J0	465	566	29.0
IPE 600	S420 M	491	582	26.3
W 24 x 9 x 84	S355 ML	388	492	33.5
HP 356 x 109	S460 N	540	645	29.6
HP 356 x 133	S460	543	653	24.3
W 30 x 10 x 116	S460	578	679	24.2
IPE 600	S460 ML	542	633	24.3

Table 8: Sections for full-scale galvanizing test program

	Section tw x tf x h (mm)	Grade
IPE 600	12 x 19 x 600	S275 J0
IPE 600	12 x 19 x 600	S355 J0
1P 750	11.5 x 17 x 753	S420 N
IPE A 600	9.8 x 17.5 x 597	S450 J0
IPE 600	12 x 19 x 600	S420 M
W 24 x 9 x 84	11.9 x 19.6 x 612	S355 ML
HP 356 x 109	12.9 x 12.9 x 346.4	S460 N
HP 356 x 109	15.6 x 15.6 x 351.9	S460
W 30 x 10 x 116	14.4 x 21.6 x 762	S460
W 30 x 10 x 116	12 x 19 x 600	S460 ML

tw = web thickness; tf = flange thickness; h = height

Table 9: Variations in galvanizing process in four European Countries

Country	Dipping speed (m/min)		Preheat (°C)		Temperature of bath (°C)	Composition range	
	Range	Most used	Range	Most used*	Range	Sn	Pb
Germany	0.3 - 8	0.8	RT-100	40-50	440 - 445	0.3-1.2	0.3-1.2
Luxembourg	0.4 - 8	1.0	RT-100	40	445 - 450	0-1.2	0.3-1.2
Spain	0 - 10	1.5	RT-150	120	440 - 460	0-0.2	0.9-1.3
UK	0 -10	0 -1.5	RT-140	50-70	445 - 455	0-0.3	0.6-1.2

* No preheat is most common; this refers to where preheat is used

Table 10: Details for welding half cover plate for full scale tests

N°run	Positioning of the section during welding of the half cover plate	t(s)	l(cm)	E (kJ/cm)
1	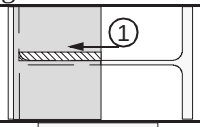	29	66	21.3
2	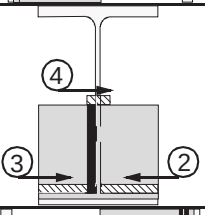	9.5	24	23.6
3		9.5	25	24.6
4		1.2	/	/
5	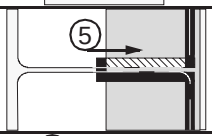	29	66	21.3
6	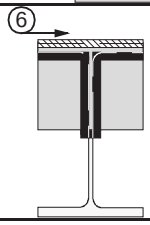	20	39	18.3

Welding voltage U = 30, 2 volts
Welding current I= 310 amperes

Table 11: Results of metallographic examinations of steels M, L, N

Welded joint D

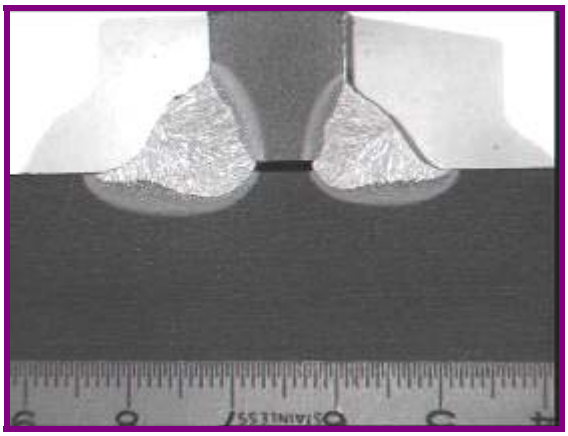

Hardness HV10 , after run 1 :

Web : BM= 206, 210, 210
HAZ= 260, 289, 283
WM= 245, 245, 289
Plate : HAZ= 297, 260, 245
BM= 186, 179, 177

Hardness HV10 , after run 5 :

Web : BM= 205, 206, 206
HAZ= 242, 258, 306
WM= 232, 232, 219
Plate : HAZ= 283, 262, 221
BM= 169, 166, 167

Welded joint F

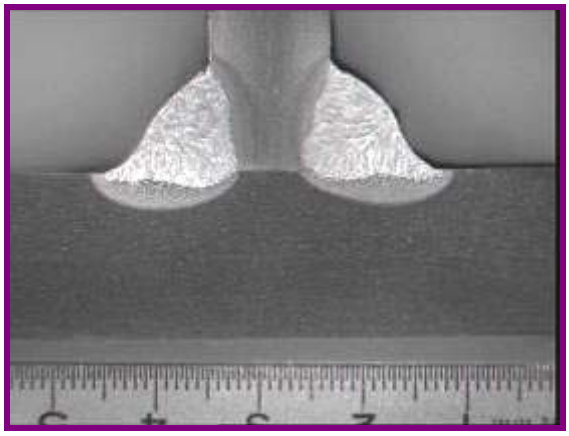

Hardness HV10 , after run 1 :

Web : BM= 168, 172, 177
HAZ= 172, 210, 222
WM= 221, 227, 224
Plate : HAZ= 254, 339, 212
BM= 178, 173, 173

Hardness HV10 , after run 5 :

Web: BM= 182, 178, 176
HAZ= 181, 196, 213
WM= 218, 218, 222
Plate : HAZ= 254, 343, 230
BM= 175, 171, 165

Welded joint I

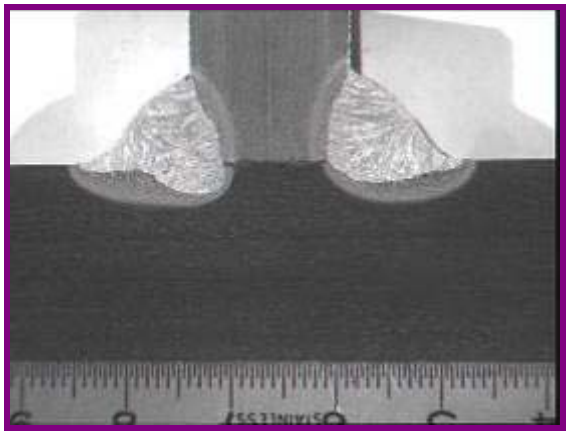

Hardness HV10 , after run 1 :

Web : BM= 219, 222, 225
HAZ= 219, 283, 272
WM= 230, 235, 232
Plate : HAZ= 266, 353, 242
BM= 181, 176, 175

Hardness HV10 , after run 5 :

Web : BM= 222, 219, 227
HAZ= 219, 262, 264
WM= 238, 227, 236
Plate : HAZ= 309, 344, 228
BM= 167, 166, 166

Table 12: Summary of full-scale test variables

Test no.	Treatment prior to galvanizing	Galvanizing treatment	Zinc alloys		
			lead	tin	bismuth
1	Overpickling	Zinc	X	-	-
2	Usual pickling	Zinc/Tin	X	X	X
3	Usual pickling	Zinc	X	-	-
4	Usual pickling	Zinc/Tin	X	X	X
5	Usual pickling	Zinc/Tin	X	X	-
6	Usual pickling	Zinc/Tin	X	X	-
7	Usual pickling	Zinc/Tin	-	X	X
8	Usual pickling	Zinc	-	-	X

Table 13: Test variants for full scale galvanizing test no. 4

Section Web thickness tw (mm)	Grade	Welded joint	Preparation methods for sections welded with a 25 mm half cover plate	Residual stress measure-ment
IPE 600 tw12	S275 J0	A	Thermal stress relieving at 600°C (t = 3 min)	X
			Thermal stress relieving at 700°C (t = 3 min)	X
		B	Stress relieving by shot blasting (steel balls, Stressonic, SONATS)	X
			Stress relieving by sand blasting SA3 (Klein Lux) (t = 1 min)	X
IPE A 600 tw 9.8	S450 J0	A	Thermal stress relieving at 650°C (t = 3 min)	X
			Thermal stress relieving at 700°C (t = 3 mi.)	X
		B	Stress relieving by shot blasting (steel balls, Stressonic, SONATS)	X
			Stress relieving by sand blasting SA3 (Klein Lux) (t = 1 min)	X
W 24 x 9 x 84 tw 11.9	S355 ML	A	Welding of half butt plate with modified welding sequence (+2 rotary movements)	
			Welding of 2 additional weld beads in critical area (L = 100 mm)	

Table 14: Test matrix of the University of Cantabria programme

Test conditions / Tests performed	As received		Pre-galvanizing		In Zn-bath (450ºC)		Galvanised (R.T.)
	20°C	450ºC	Pickling	Fluxing	Zn-Pb	Zn-Sn	Service dry
Chemical	X						
Tensile	X	X					X
Slow strain rate	X	X			X	X	
Toughness	X	X			X	X	X
Crack Characterisation					X	X	
Fractography	X	X			X	X	X
Microstructure	X	X	X	X	X	X	X
Surface roughness	X		X	X	X	X	
[H]	X	X	X	X	X	X	X

Table 15: Composition of the baths used at UC for the tests in liquid Zn

Bath	Zn	Pb	Sn	Bi	Fe	Al	Cd	Cu
Zn-Pb	98.99	0.89	0.065	---	0.02	0.0012	0.0012	0.033
Zn-Sn	97.41	1.30	1.12	0.097	0.026	0.0004	0.0012	0.049

Table 16: Zinc alloys used for testing at RWTH Aachen University

Alloy	Pb	Sn	Bi	Al,	Ni	Fe
a0	---	1,2	0.10	0.005	0.05	0.03
a1	0.7	---	---	0.005	---	0.03
a2	1	1	0.05	0.005	0.05	0.03

Table 17: Zinc alloy used for testing at Corus RD&T

Bath	Pb	Sn	Al	Ni	Fe	Cu
Zn-Pb	0.90	0.29	0.0038	0.07	0.018	0.011

Table 18: Parameters required for modelling the welding process

Parameter	Ansys		Sysweld		Abaqus	
	requ.	ref.	requ.	ref.	requ.	ref.
Physical property						
Density					x	Corus data
Thermal material properties						
Thermal conductivity	x	[15], [16]	x	[20], [21]	x	Corus data
Coefficient of thermal expansion	x		x		x	
Specific heat capacity	x		x		x	
Metallurgical material properties						
			x	[20-22]	x	
Mechanical material properties						
Yield strength	x	[17], [18]	x	[20], [21]	x	Corus data
Tensile strength	x		x		x	
E-Modulus	x		x		x	
Heat input						
Welding energy			x	[20], [21]	x	Corus data
Convection (heat transfer coefficient)	x	[5]			x	

Table 19: Parameters required for modelling the galvanizing process

Parameter	Ansys		Sysweld		Abaqus	
	used	source	used	source	used	source
Physical property						
Density					x	Corus data
Thermal material properties						
Thermal conductivity	x	[15], [16]	x	[20], [21]	x	Corus data
Coefficient of thermal expansion	x		x		x	
Specific heat capacity	x		x		x	
Metallurgical material properties						
Mechanical material properties						
Yield strength	x	[17], [18]	x	[20], [21]	x	true stress-strain from FAMEGA
Tensile strength	x		x		x	
E-Modulus	x		x		x	
Thermal loading (heat transfer)						
Convection (heat transfer coefficient)	x	[23], [24]	x	[23], [24]	x	Backfitted to temp. curve FAMEGA
radiation	negl.		x	[20], [21]	-	Ignored

Table 20: Full scale galvanizing test no. 1 – fracture examination after transverse tensile test

Section tw (mm)	Grade	End with cover plate properly welded	Poorly executed weld + mechanical defects
IPE 600 tw 12	S275 J0	Crack L = 0.5 cm	Crack L = 0.5 cm
IPE 600 tw 12	S355 J0	Crack L = 0.4 cm	Crack L = 0.5 cm
IPE 750 tw 11.5	S420 N	Crack L = 1.2 cm	Crack L = 0.5 cm
IPE A 600 tw 9.8	S450 J0	Crack L = 12 cm	Crack L = 22 cm
IPE 600 tw 12	S420 M	Crack L = 1.1 cm	Crack L = 0.8 cm
W 24 x 9 x 84 tw 11.9	S355 ML	Crack L = 0.6 cm	Crack L = 0.7 cm
HP 356 x 109 tw 12.8	S460 N	Crack L = 1.0 cm	Crack L = 0.5 cm
HP 356 x 133 tw 15.6	S460	No detected crack	Crack L = 0.5 cm
W 30 x 10 x 116 tw 14.4	S460	Crack L = 1.0 cm	Crack L = 0.5 cm
IPE 600 tw 12	S460 ML	Crack L = 0.8 cm	Crack L = 2.0 cm

tw = web thickness; $\sum L = 6.6$ cm + 12 cm; $\sum L = 6.5$ cm + 22 cm

Table 21: Full scale galvanizing test no. 2 – fracture examination after transverse tensile test

Section tw (mm)	Grade	Properly welded cover plate	Poorly executed weld + mechanical defects
IPE 600 tw 12	S275 J0	Crack L = 0.6 cm	Crack L = 0.8 cm
IPE 600 tw 12	S355 J0	Crack L = 1.4 cm	Crack L = 1.0 cm
IPE 750 tw 11.5	S420 N	Crack L = 1.0 cm	Crack L = 1.5 cm
IPE A 600 tw 9.8	S450 J0	Crack L = 66 cm	Crack L = 72 cm
IPE 600 tw 12	S420 M	Crack L = 0.8 cm	Crack L = 1.4 cm
W 24 x 9 x 84 tw 11.9	S355 ML	Crack L = 0.7 cm	Crack L = 1.1 cm
HP 356 x 109 tw 12.8	S460 N	Crack L = 1.0 cm	Crack L = 0.8 cm
HP 356 x 133 tw 15.6	S460	Crack L = 1.2 cm	Crack L = 1.4 cm
W 30 x 10 x 116 tw 14.4	S460	Crack L = 0.8 cm	Crack L = 1.7 cm
IPE 600 tw 12	S460 ML	Crack L = 2.0 cm	Crack L = 2.5 cm

tw = web thickness; $\sum L = 9.5$ cm + 66 cm; $\sum L = 12.2$ cm + 72 cm

Table 22: Full scale galvanizing test no. 3 – fracture examination by magnetoscopic technique

Section tw (mm)	Grade	End with cover plate properly welded 25 mm thick plate	End with cover plate properly welded 40 mm thick plate
IPE 600 tw 12	S275 J0	Crack L = 1.0 cm	Crack L = 1.8 cm
IPE 600 tw 12	S355 J0	Crack L = 1.5 cm	Crack L = 1.0 cm
IPE 750 tw 11.5	S420 N	Crack L = 1.0 cm	Crack L = 1.0 cm
IPE A 600 tw 9.8	S450 J0	Crack L = 30 cm	Crack L = 27 cm
IPE 600 tw 12	S420 M	Crack L = 0.8 cm	Crack L = 2.0 cm
W 24 x 9 x 84 tw 11.9	S355 ML	Crack L = 1.0 cm	Crack L = 0.5 cm
HP 356 x 109 tw 12.8	S460 N	Crack L = 0.6 cm	No detected crack
HP 356 x 133 tw 15.6	S460	No detected crack	No detected crack
W 30 x 10 x 116 tw 14.4	S460	Crack L = 1.5 cm	Crack L = 2.0 cm
IPE 600 tw 12	S460 ML	Crack L = 2.0 cm	Crack L = 3.5 cm

tw = web thickness; $\sum L = 9.4$ cm + 30 cm; $\sum L = 11.8$ cm + 27 cm

tw = web thickness

Table 23: Results of test no. 4 – Zn-Sn bath, magnetoscopic fracture examination

Section tw (mm)	Grade	Preparation methods for sections welded with a 25 mm half butt plate	Surface state (crack = web cracking)
IPE 600 tw 12	S275 J0 G	Thermal stress relieving at 600°C (t = 3 min)	/
		Thermal stress relieving at 700°C (t = 3 min)	Crack L = 1.3 cm
		Stress relieving by shot blasting (steel balls, Stressonic, SONATS)	Crack L = 1.0 cm
		Stress relieving by sand blasting SA3 (Klein Lux) (t = 1 min)	Crack L = 1.0 cm
IPE A 600 tw 9.8	S450 J0 J	Thermal stress relieving at 650°C (t = 3 min)	Crack L = 1.8 cm
		Thermal stress relieving at 700°C (t = 3 min)	Crack L = 5.0 cm
		Stress relieving by shot blasting (steel balls, Stressonic, SONATS)	Crack L = 43 cm
		Stress relieving by sand blasting SA3 (Klein Lux) (t = 1 min)	Crack L = 60 cm
W 24 x 9 x 84 tw 11.9	S355 ML L	Welding of half butt plate with modified welding sequence (+2 rotary movements)	Crack L = 0.5 cm
		Welding of 2 additional weld beads in critical area (L = 100 mm)	Crack L = 1.5 cm

Table 24: Results of the test no. 5, checking below the cover plates. Fracture examination by magnetoscopic technique

Section tw (mm)	Grade	Cover plate with small weld seam Thermal relieving at 600°C	Cover plate without weld seam Thermal relieving at 600°C
IPE 600 tw 12	S275 J0	No detected crack	no cover plate - no detected crack
IPE A 600 tw 9.8	S450 J0	No detected crack	no cover plate - no detected crack
IPE 600 tw 12	S420 M	No detected crack	No detected crack
HP356x109 tw 12.8	S460 N	No detected crack	No detected crack
HP356x133 tw 15.6	S460	No detected crack	No detected crack
IPE 600 tw 12	S460 ML	No detected crack	No detected crack

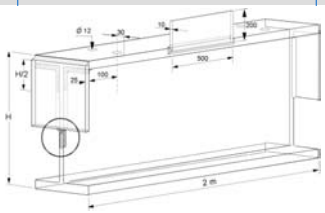

Table 25: Results of test no. 5, control of the plate welded on beam flange
Fracture examination by magnetoscopic technique

Section tw (mm)	Grade	500 x 200 x 10 mm plate welded on beam flange
IPE 600 tw 12	S275 J0	No detected crack
IPE 600 tw 12	S355 J0	No detected crack
IPE 750 tw 11.5	S420 N	No detected crack
IPE A 600 tw 9.8	S450 J0	No detected crack
IPE 600 tw 12	S420 M	No detected crack
W24x9x84 tw 11.9	S355 ML	No detected crack
HP356x109 tw 12.8	S460 N	No detected crack
HP356x133 tw 15.6	S460	No detected crack
W30x10x116 tw 14.4	S460	No detected crack
IPE 600 tw 12	S460 ML	No detected crack

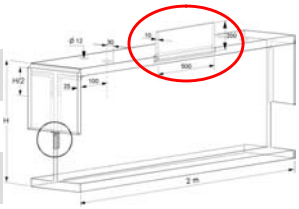

Table 26: Galvanizing test no. 6, section with half cover plate.
Magnetoscopic fracture examination

Section tw (mm)	Grade	End with cover plate properly welded + 50 mm weld seam	End with cover plate properly welded + thermal relieving at 600 °C, 2 minutes
IPE 600 tw 12	S275 J0	No detected crack	No detected crack
IPE 600 tw 12	S355 J0	Crack L = 0,2 cm under plate, 1 side	No detected crack
IPE 750 tw 11.5	S420 N	Crack L = 1,0 cm under plate	No detected crack
IPE A 600 tw 9.8	S450 J0	Crack L = 99 cm under weld seam	No detected crack
IPE 600 tw 12	S420 M	Crack L = 1,0 cm under plate	No detected crack
W24x9x84 tw 11.9	S355 ML	No detected crack	Crack L = 1,5 cm on 1 side
HP356x109 tw 12.8	S460 N	No detected crack	No detected crack
HP356x133 tw 15.6	S460	Crack L = 1,0 cm under plate	No detected crack
W30x10x116 tw 14.4	S460	Crack L = 1,0 cm under plate	No detected crack
IPE 600 tw 12	S460 ML	Crack L = 1,0 cm 5 mm under plate	No detected crack

ΣL = 5,2cm + 99cm

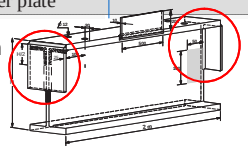

ΣL = 1,5cm + 0cm

Table 27: Galvanizing test no. 6, 10 mm plate welded on beam flange
Magnetoscopic fracture examination

Section tw (mm)	Grade	Plate side 1	Plate side 2
IPE 600 tw 12	S275 J0	No detected crack	No detected crack
IPE 600 tw 12	S355 J0	No detected crack	No detected crack
IPE 750 tw 11.5	S420 N	No detected crack	No detected crack
IPE A 600 tw 9.8	S450 J0	No detected crack	No detected crack
IPE 600 tw 12	S420 M	No detected crack	No detected crack
W24x9x84 tw 11.9	S355 ML	No detected crack	No detected crack
HP356x109 tw 12.8	S460 N	No detected crack	No detected crack
HP356x133 tw 15.6	S460	No detected crack	No detected crack
W30x10x116 tw 14.4	S460	No detected crack	No detected crack
IPE 600 tw 12	S460 ML	No detected crack	No detected crack

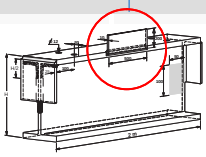

Table 28: Galvanising test no. 6, cope cut
Magnetoscopic fracture examination

Section tw (mm)	Grade	Section side with thermal relieving	Section side without thermal relieving
Upper flanges: oxycutting performed without previously drilled hole			
IPE 600 tw 12	S355 J0	No detected crack	Crack L = 2 mm
HP 356x109 tw 12.8	S460 N	No detected crack	Crack L = 5 mm 1 side
IPE 356x133 tw 15.6	S460	No detected crack	No detected crack
Lower flanges: oxycutting performed with previously drilled holes			
IPE 600 tw 12	S355 J0	No detected crack	No detected crack
HP 356x109 tw 12.8	S460 N	No detected crack	No detected crack
IPE 356x133 tw 15.6	S460	No detected crack	No detected crack

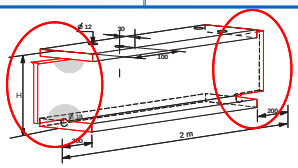

Table 29: Galvanising test no. 6, drilled holes in the web
Magnetoscopic fracture examination

Section tw (mm)	Grade	Web side with thermal relieving	Web side without thermal relieving
Drill hole diameter: 29 mm			
IPE 750 tw 11.5	S420 N	No detected crack	No detected crack
IPE 600 tw 12	S460 ML	No detected crack	No detected crack
Drill hole diameter: 22 mm			
IPE 750 tw 11.5	S420 N	No detected crack	No detected crack
IPE 600 tw 12	S460 ML	No detected crack	No detected crack
Oxycut hole diameter: 150 mm			
IPE 750 tw 11.5	S420 N	No detected crack	No detected crack
IPE 600 tw 12	S460 ML	No detected crack	No detected crack

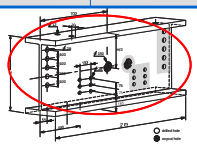

Table 30: Results of galvanising tests no. 7, sections with half cover plates
Magnetoscopic fracture examination

Variant 7

Section tw (mm)	Grade	End with cover plate properly welded without thermal relieving	End with cover plate properly welded + thermal relieving at 600 °C, 2 minutes
IPE 600 tw 12	S275 J0	Crack on both web sides: 5 and 10 mm	No detected crack
IPE 600 tw 12	S355 J0	Crack on 1 web side: 5 mm	No detected crack
IPE 750 tw 11.5	S420 N	Crack on 1 web side: 15 mm	No detected crack
IPE A 600 tw 9.8	S450 J0	Crack on both web sides: 250 mm	No detected crack
IPE 600 tw 12	S420 M	Crack on both web sides: 5 mm	Crack on both web sides: 6 and 10 mm
W24x9x84 tw 11.9	S355 ML	No detected crack	No detected crack
HP356x109 tw 12.8	S460 N	Crack on both web sides: 10 mm	No detected crack
HP356x133 tw 15.6	S460	Crack on 1 web side: 15 mm	No detected crack
W30x10x116 tw 14.4	S460	Crack on 1 web side: 10 mm	Crack on both web sides: 1x10, 2x15 mm
IPE 600 tw 12	S460 ML	Crack on both web sides: 5 and 10 mm	No detected crack

ΣL = 8,0cm + 25cm

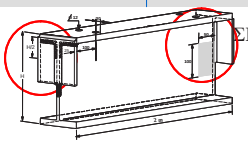

ΣL = 2,5cm + 0cm

Table 31: Results of galvanising tests no. 8, sections with half cover plates
Magnetoscopic fracture examination

Variant 8

Section tw (mm)	Grade	End with cover plate properly welded without thermal relieving	End with cover plate properly welded + thermal relieving at 550 °C, 2 minutes
IPE 600 tw 12	S275 J0	No detected crack	No detected crack
IPE 600 tw 12	S355 J0	No detected crack	No detected crack
IPE 750 tw 11.5	S420 N	No detected crack	No detected crack
IPE A 600 tw 9.8	S450 J0	No detected crack	No detected crack
IPE 600 tw 12	S420 M	No detected crack	No detected crack
W24x9x84 tw 11.9	S355 ML	No detected crack	No detected crack
HP356x109 tw 12.8	S460 N	No detected crack	No detected crack
HP356x133 tw 15.6	S460	No detected crack	No detected crack
W30x10x116 tw 14.4	S460	No detected crack	No detected crack
IPE 600 tw 12	S460 ML	No detected crack	No detected crack

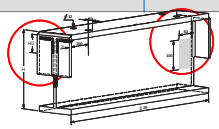

Table 32: Results of hydrogen concentration tests for steel code D. Values in ppm.

Specimen number / Conditions	1	2	3	4	5	6	Mean
Condition 2.1	1.37	0.99	---	0.90	0.86	0.77	1.0
Condition 2.2	1.45	1.33	---	1.88	2.20	1.20	1.6
Condition 2.3	5.72	5.49	6.38	4.63	---	5.86	5.6
Condition 2.4	3.38	4.03	---	3.69	---	3.66	3.7
Condition 2.5	3.32	3.62	3.80	3.78	3.63	3.83	3.7
Condition 2.6	3.27	4.21	3.78	3.73	3.58	3.91	3.7
Condition 2.7	6.70	8.42	5.30	---	5.35	7.06	6.6
Condition 2.8	6.72	5.94	5.88	7.01	5.71	4.69	6.0
Condition 2.9	3.67	4.50	---	5.26	4.30	4.76	4.5
Condition 2.10	5.99	4.91	5.02	---	---	---	5.3
Condition 2.11	4.66	4.07	4.79	4.84	4.58	---	4.5

Condition list:

- 2.1: As received.
- 2.2: Pickling
- 2.3: Fluxing with $ZnCl_2 \cdot 4NH_4Cl$ salt.
- 2.4: Fluxing with $ZnCl_2 \cdot 2NH_4Cl$ salt.
- 2.5: Pickling+fluxing with $ZnCl_2 \cdot 4NH_4Cl$ salt.
- 2.6: Pickling+fluxing with $ZnCl_2 \cdot 2NH_4Cl$ salt.
- 2.7:Pickling+fluxing with $ZnCl_2 \cdot 4NH_4Cl$ salt+galvanizing with Zn-Sn bath.
- 2.8: Pickling+fluxing with $ZnCl_2 \cdot 4NH_4Cl$ salt+galvanizing with Zn-Pb bath.
- 2.9: Pickling+fluxing with $ZnCl_2 \cdot 2NH_4Cl$ salt+galvanizing with Zn-Sn bath.
- 2.10: Pickling+fluxing with $ZnCl_2 \cdot 2NH_4Cl$ salt+galvanizing with Zn-Pb bath.
- 2.11: Galvanizing with Zn-Pb bath without pickling or fluxing.

Table 33: RWTH Aachen University LMAC results. Test results material A, alloy a0

material **A** , alloy **a0**, webthickness b=10.8 mm								
name	cracktip radius	control		maximum force		displacement		crack initiation
-	(mm)	Load F(t) (kN/s)	displacement v_{LL}(t) (mm/s)	F_{max} (kN)	$F_{max}/(b*R_{eH})$ (mm)	$v_{LL,Fmax}$ (mm)	$v_{LL,Fmax}/b$ (mm/cm)	-
1	1	0.25	-	15.2	2.58	5.8	5.37	y
2	1	constant	-	15.1	2.56	5.9	5.46	y
3	1	0.25	-	14	2.37	6.2	5.74	y
4	1	0.25	-	13.6	2.31	5	4.63	y
5	1	constant	-	12.5	2.12	4.5	4.17	y
6	1	incremental	-	14.7	2.49	6.3	5.83	n
7	1	1	-	16.8	2.85	7.9	7.31	y
8	1	1	-	17.2	2.92	8.6	7.96	y
9	1	0.25	-	12.4	2.10	6	5.56	y
1	3	0.25	-	14.6	2.48	9.1	8.43	y
2	3	0.25	-	14.9	2.53	9.2	8.52	y
3	3	0.1	-	15.6	2.64	9.4	8.70	y
4	3	0.1	-	16.6	2.82	12.4	11.48	y
5	3	1	-	15.1	2.56	8.5	7.87	y
6	3	1	-	17	2.88	15.9	14.72	y
7	3	10	-	21.1	3.58	13.1	12.13	n
8	3	0.25	-	15.6	2.64	8.8	8.15	y
9	3	0.25	-	15	2.54	9.2	8.52	y
10	3	0.25	-	16.5	2.80	10.5	9.72	y
11	3	0.1	-	16.5	2.80	11.5	10.65	y
12	3	1	-	16.7	2.83	9.5	8.80	y
26 w	3	-	0.05	18.24	3.09	11.56	10.70	y
27 w	3	-	0.05: incremental	17.30	2.93	11.64	10.78	y
28 w	3	-	0.05; incremental	19.22	3.26	14.04	13.00	y
29 w	3	-	0.05	17.26	2.93	11.56	10.70	y
30 w	3	-	0.05	20.33	3.45	9.77	9.05	y
31 w	3	-	0.05	17.42	2.95	11.70	10.83	y
32 w	3	-	0.05	18.55	3.14	10.92	10.11	y
33 w	3	-	0.01	17.20	2.92	10.66	9.87	y
34 w	3	-	0.05; stopped	16.48	2.79	11.31	10.47	y
35 w	3	-	0.05; stopped	16.57	2.81	12.19	11.29	y
36 w	3	-	0.1	17.48	2.97	8.45	7.82	y
37 w	3	-	0.1	16.30	2.76	8.63	7.99	y
38 w	3	-	0.1	17.42	2.95	12.35	11.44	y
39 w	3	-	0.1	18.92	3.21	11.88	11.00	y
40 w	3	-	0.1	17.95	3.04	9.59	8.88	y

Table 34: Testing results material B, alloy a0

material **B** , alloy **a0**, web thickness b=11.2 mm								
name	cracktip radius	control		maximum force		displacement		crack initiation
-	(mm)	Load F(t) (kN/s)	displacement $v_{LL}(t)$ (mm/s)	F_{max} (kN)	$F_{max}/(b*R_{eH})$ (mm)	$v_{LL,Fmax}$ (mm)	$v_{LL,Fmax}/b$ (mm/cm)	-
1	3	0.25	-	14.6	2.58	9.1	8.13	y
2	3	0.25	-	14.9	2.63	9.2	8.21	y
3	3	0.1	-	15.6	2.76	9.4	8.39	y
4	3	0.1	-	16.6	2.93	12.4	11.07	y
5	3	1	-	15.1	2.67	8.5	7.59	y
6	3	1	-	17	3.01	15.9	14.20	y
8	3	0.25	-	15.6	2.76	8.8	7.86	y
9	3	0.25	-	15	2.65	9.2	8.21	y
10	3	0.25	-	16.5	2.92	10.5	9.38	y
11	3	0.1	-	16.5	2.92	11.5	10.27	y
12	3	1	-	16.7	2.95	9.5	8.48	y

Table 35: Testing results material C, alloy a0

material **C** , alloy **a0**, webthickness b=9.8 mm								
name	cracktip radius	control		maximum force		displacement		crack initiation
-	(mm)	Load F(t) (kN/s)	displacement $v_{LL}(t)$ (mm/s)	F_{max} (kN)	$F_{max}/(b*R_{eH})$ (mm)	$v_{LL,Fmax}$ (mm)	$v_{LL,Fmax}/b$ (mm/cm)	-
1	3	0.25	-	13.5	2.46	7.7	7.86	y
2	3	0.25	-	13.1	2.39	7.3	7.45	y
3	3	0.25	-	14	2.55	8	8.16	y
4	3	0.1	-	13.3	2.42	7.8	7.96	y
5	3	0.1	-	13.8	2.51	8.1	8.27	y
6	3	0.5	-	13.7	2.50	7.9	8.06	y
7	3	0.5	-	13.2	2.41	6.9	7.04	y
8	3	0.025	-	14.3	2.61	10.8	11.02	y

Table 36: Testing results material F, alloy a0

material **F** , alloy **a0**, webthickness b=12.8 mm								
name	cracktip radius	control		maximum force		displacement		crack initiation
-	(mm)	Load F(t) (kN/s)	displacement $v_{LL}(t)$ (mm/s)	F_{max} (kN)	$F_{max}/(b*R_{eH})$ (mm)	$v_{LL,Fmax}$ (mm)	$v_{LL,Fmax}/b$ (mm/cm)	-
01	3	-	0.050	14.6	3.09	18.37	14.35	n
02	3	-	0.025	15	3.19	18.10	14.14	n
03	3	-	0.025	15.1	3.21	18.21	14.23	n
04	3	-	0.250	16.2	3.44	18.73	14.63	n
05	3	-	0.010	14.7	3.13	18.91	14.78	n
06	3	-	0.010	15.6	3.30	17.98	14.04	n
07	3	-	0.025; 450°C air	13.8	2.93	18.80	14.69	n

Table 37: Testing results material A, alloy a1

material **A** , alloy **a1**, webthickness b=10.8 mm								
name	cracktip radius	control		maximum force		displacement		crack initiation
-	(mm)	Load F(t) (kN/s)	displacement $v_{LL}(t)$ (mm/s)	F_{max} (kN)	$F_{max}/(b*R_{eH})$ (mm)	$v_{LL,Fmax}$ (mm)	$v_{LL,Fmax}/b$ (mm/cm)	-
14	3	0.25	-	22.1	3.75	27.4	25.37	n
15	3	0.1	-	21.6	3.66	27.3	25.28	n
16	3	0.5	-	22.22	3.77	26.8	24.81	n
13	3	0.25	-	21.3	3.61	27.2	25.19	n

Table 38: Testing results material B, alloy a1

material **B** , alloy **a1**, webthickness b=11.2 mm								
name	cracktip radius	control		maximum force		displacement		crack initiation
-	(mm)	Load F(t) (kN/s)	displacement $v_{LL}(t)$ (mm/s)	F_{max} (kN)	$F_{max}/(b*R_{eH})$ (mm)	$v_{LL,Fmax}$ (mm)	$v_{LL,Fmax}/b$ (mm/cm)	-
28	3	0.1	-	17.26	3.05	24.47	21.85	y
29	3	0.1	-	18.24	3.23	18.25	16.29	y
30	3	0.25	-	19.02	3.36	26.93	24.04	n
31	3	0.25	-	18.29	3.23	26.39	23.56	n
32	3	0.5	-	19.44	3.44	26.88	24.00	n
33	3	0.5	-	19.97	3.53	27.14	24.23	n
34	3	0.025	-	13.90	2.46	12.7	11.34	y
35	3	0.025	-	16.86	2.98	20	17.86	y
36	3	0.025	-	15.06	2.66	18.08	16.14	y
37	3	-	0.05	14.03	2.48	15.13	13.51	y
38	3	-	0.05	16.27	2.88	13.93	12.44	y
39	3	-	cycle	13.98	2.47	13.54	12.09	y
40	3	-	cycle	14.73	2.60	14.1	12.59	y

Table 39: Testing results material C, alloy a1

material **C** , alloy **a1**, webthickness b=9.8 mm								
name	cracktip radius	control		maximum force		displacement		crack initiation
-	(mm)	Load F(t) (kN/s)	displacement $v_{LL}(t)$ (mm/s)	F_{max} (kN)	$F_{max}/(b*R_{eH})$ (mm)	$v_{LL,Fmax}$ (mm)	$v_{LL,Fmax}/b$ (mm/cm)	-
1	3	0.25	-	15.3	2.79	13.6	13.88	y
2	3	0.25	-	16	2.92	12.7	12.96	y
3	3	0.25	-	16.2	2.95	13.8	14.08	y
4	3	0.1	-	14.9	2.71	11.7	11.94	y
5	3	0.1	-	14.9	2.71	11.7	11.94	y
6	3	0.5	-	18.2	3.32	27.1	27.65	n
7	3	0.5	-	17	3.10	15.8	16.12	y
8	3	0.025	-	14.4	2.62	11	11.22	y

Table 40: Testing results material F, alloy a1

material **F** , alloy **a1**, webthickness b=12.8 mm								
name	cracktip radius	control		maximum force		displacement		crack initiation
-	(mm)	Load F(t) (kN/s)	displacement $v_{LL}(t)$ (mm/s)	F_{max} (kN)	$F_{max}/(b*R_{eH})$ (mm)	$v_{LL,Fmax}$ (mm)	$v_{LL,Fmax}/b$ (mm/cm)	-
2	3	-	0.050	15.41	3.27	18.27	14.27	n
3	3	-	0.025	16.21	3.44	18.40	14.38	n
4	3	-	0.025	15.28	3.24	18.87	14.74	n

Table 41: Testing results material A, alloy a2

material **A** , alloy **a2**, web thickness b=10.8 mm								
name	cracktip radius	control		maximum force		displacement		crack initiation
-	(mm)	Load F(t) (kN/s)	displacement $v_{LL}(t)$ (mm/s)	F_{max} (kN)	$F_{max}/(b*R_{eH})$ (mm)	$v_{LL,Fmax}$ (mm)	$v_{LL,Fmax}/b$ (mm/cm)	-
17	3	0.25	-	16.7	2.83	8.3	7.69	y
18	3	0.25	-	15.5	2.63	8.2	7.59	y
19	3	0.25	-	17.8	3.02	8.9	8.24	y
20	3	0.5	-	16.4	2.78	9.1	8.43	y
21	3	0.5	-	16.8	2.85	7.8	7.22	y
22	3	0.1	-	18.2	3.09	9.7	8.98	y
23	3	0.1	-	17.5	2.97	9.5	8.80	y
24	3	0.025	-	18	3.05	10.3	9.54	y

Table 42: Testing results material B, alloy a2

material **B** , alloy **a2**, web thickness b=11,2 mm								
name	cracktip radius	control		maximum force		displacement		crack initiation
-	(mm)	Load F(t) (kN/s)	displacement $v_{LL}(t)$ (mm/s)	F_{max} (kN)	$F_{max}/(b*R_{eH})$ (mm)	$v_{LL,Fmax}$ (mm)	$v_{LL,Fmax}/b$ (mm/cm)	-
23	3	0.025	-	14.5	2.57	8.7	7.77	y
18	3	0.1	-	14.1	2.49	7.2	6.43	y
19	3	0.1	-	14.4	2.55	7.8	6.96	y
25	3	0.1	-	14.6	2.57	8	7.14	y
13	3	0.25	-	12.8	2.26	7.1	6.34	y
14	3	0.25	-	13.7	2.43	7	6.25	y
15	3	0.25	-	14.4	2.55	6.9	6.16	y
20	3	0.25	-	12.4	2.19	7.6	6.79	y, T
21	3	0.25	-	13.6	2.40	7.7	6.88	y, T
22	3	0.25	-	12.9	2.28	7.9	7.05	y, T
24	3	0.25	-	14.2	2.50	6.7	5.98	y
26	3	0.5	-	14.3	2.53	7.1	6.34	y
27	3	0.75	-	16.1	2.84	11	9.82	y
16	3	1.0	-	15.4	2.71	7.9	7.05	y

*) T= crack transverse

Table 43: Testing results material C, alloy a2

material **C** , alloy **a2**, web thickness b=9.8 mm								
name	cracktip radius	control		maximum force		displacement		crack initiation
-	(mm)	Load F(t) (kN/s)	displacement $v_{LL}(t)$ (mm/s)	F_{max} (kN)	$F_{max}/(b*R_{eH})$ (mm)	$v_{LL,Fmax}$ (mm)	$v_{LL,Fmax}/b$ (mm/cm)	-
9	3	0.25	-	12.9	2.35	8.2	8.37	y
12	3	0.25	-	12.5	2.28	6.3	6.43	y
13	3	0.25	-	11.6	2.11	5.9	6.02	y
10	3	0.1	-	13.2	2.41	7.2	7.35	y
11	3	0.1	-	12.7	2.31	6.9	7.04	y
14	3	0.25	-	12.8	2.33	6.5	6.63	y
15	3	0.5	-	12	2.19	6.6	6.73	y
16	3	0.5	-	12.1	2.21	6.3	6.43	y
17	3	0.75	-	12.2	2.22	6.5	6.63	y

Table 44: Testing results material F, alloy a2

material **F** , alloy **a2**, web thickness b=12.8 mm								
name	cracktip radius	control		maximum force		displacement		crack initiation
-	(mm)	Load F(t) (kN/s)	displacement $v_{LL}(t)$ (mm/s)	F_{max} (kN)	$F_{max}/(b*R_{eH})$ (mm)	$v_{LL,Fmax}$ (mm)	$v_{LL,Fmax}/b$ (mm/cm)	-
1	3	-	0.250	14.88	3.16	9.99	7.80	y
2	3	-	0.050	14.13	3.00	14.22	11.11	y
3	3	-	0.050	15.00	3.18	11.53	9.01	y
4	3	-	0.050	14.15	3.00	16.6	12.97	y
5	3	-	0.050	14.45	3.07	14.04	10.97	n
6	3	-	0.250	15.07	3.20	13.41	10.48	y, T
7	3	-	0.250	14.90	3.16	11.63	9.09	y
8	3	-	0.250	14.91	3.17	11.58	9.05	y
9	3	-	0.500	15.14	3.21	10.99	8.59	y, T
10	3	-	0.500	15.70	3.33	11.02	8.61	y
11	3	-	0.500	15.65	3.32	12.24	9.56	y
12	3	-	0.050	15.44	3.28	18.72	14.63	n

*) T= crack transverse

Table 45: Maximum loads and corresponding clip gauge displacements from LMAC tests on CT test pieces with key hole notch

Cross head speed, mm/s	0.005	0.0075	0.01	0.012	0.015	0.02	0.025	0.05
Max. load, kN	8.896	8.257	9.144	9.142	8.902	9.144	8.496	8.438
Clip gauge displacement at max. load, mm	1.4609	1.4347	1.2632	1.2424	1.632	1.1748	0.7571	1.0936

Table 46: CRD&T LMAC tests using compact tension (fracture mechanics) tests

Code	Steel type	Cross head rate (mm/s)	K_{max}
B	S460ML	0.05	61.2
		0.015	50.6
		0.01	71.4
		0.01	58.6
A	S355JR	0.05	53.8
		0.02	58.4
		0.01	57.1
		0.0075	57.4
		0.005	53.3

FIGURES

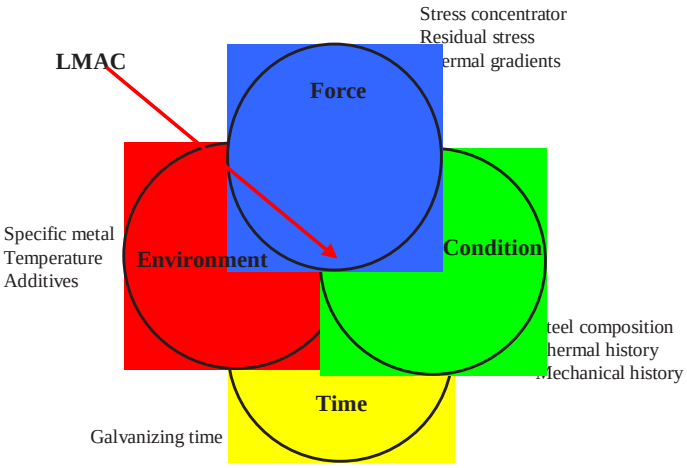

Fig. 1: The requirements for liquid metal assisted cracking [1,5]

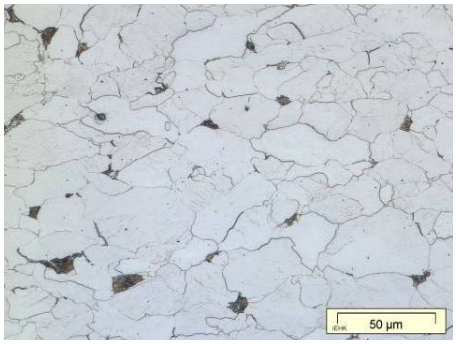

(a) S235JR (as rolled)

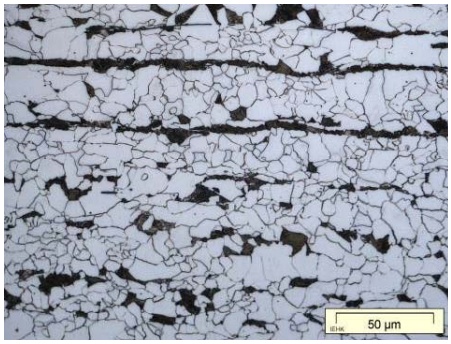

(b) S355JR (as rolled)

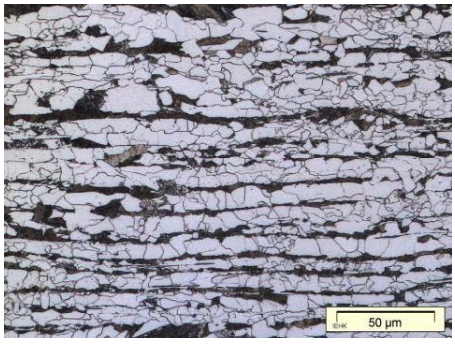

(c) S460N (controlled rolled)

Fig. 2(a-c): Typical microstructures

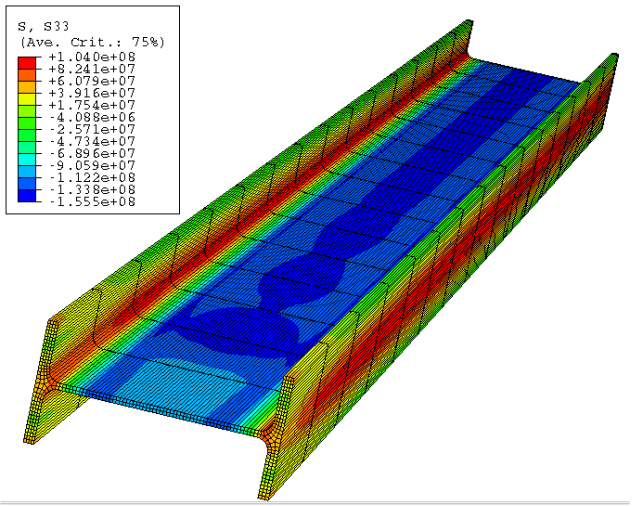

Fig. 3: FE predicted residual stress profile for IPE220 section.

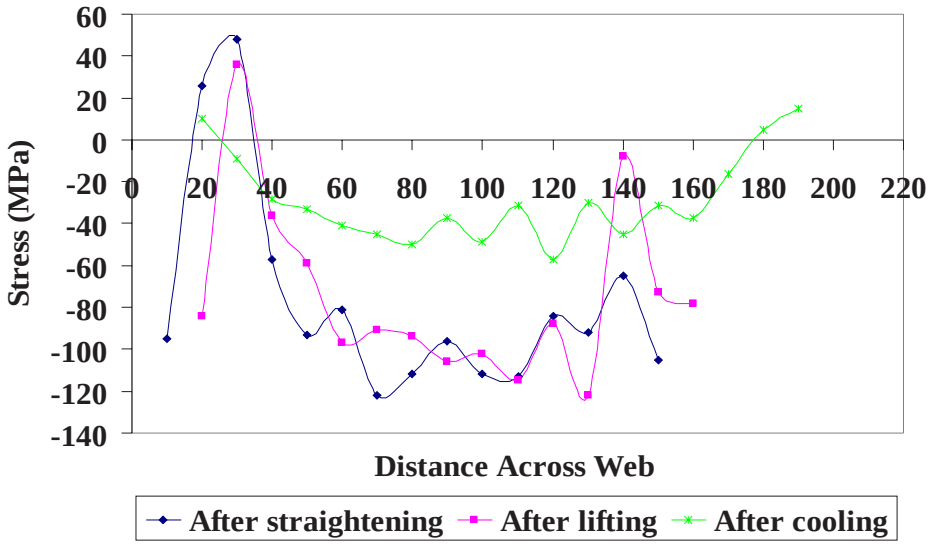

Fig. 4: Measurements of residual stress in section using 3 MA meter (a) after cooling, (b) after lifting, (c) after straightening

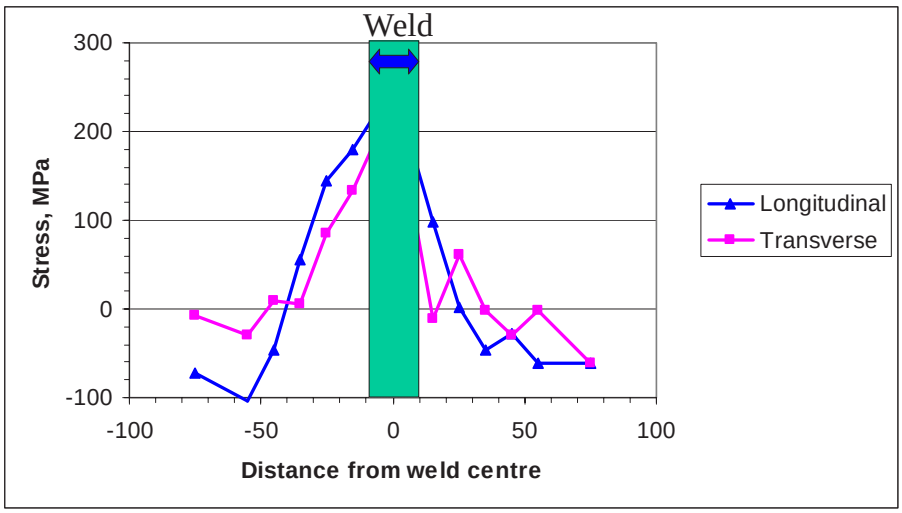

Fig. 5: Residual stress across a submerged arc weld measured using X-ray techniques

Fig. 6: Sonats X-ray equipment for the measurement of residual stress.

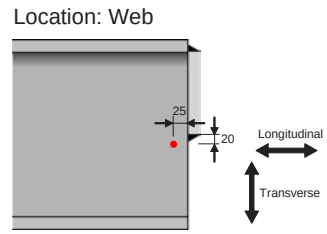

Before welding (MPa)

	S 275 J0	S 450 J0
Web L	-93	- 278
Web T	-6	- 80
Edge L	-104	
Edge T	110	

After welding (MPa)

	S 275 J0	S 450 J0
Web L	351/263/305	395/309/17(?)
Web T	205/215/204	156/126/190
Edge L	468/276/238	286/370/253
Edge T	233/248/241	129/127/187

+ : tension
- : compression

Fig. 7: X-ray measurement of residual stresses before (base metal) and after welding.

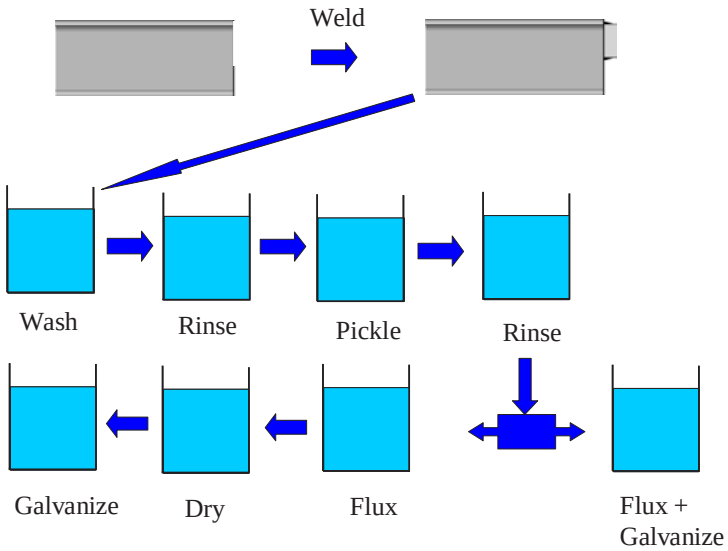

Fig. 8: Schematic of process route for galvanizing

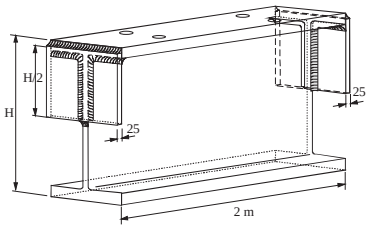

Fig. 9: Assembly design for full-scale tests

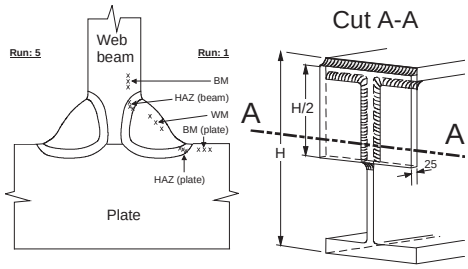

Fig. 10: Position of the macrographic section hardness measurements

Fig. 11: Full scale tests carried out on 10 off 2 m lengths of half cover plate sections

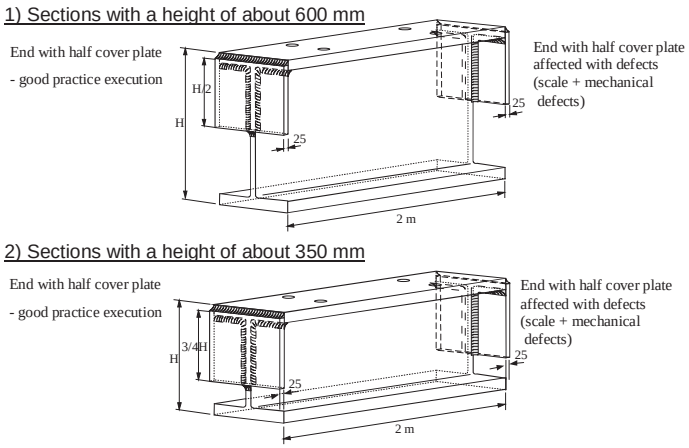

Fig. 12: Geometry of sections for galvanizing tests no. 1 and no. 2

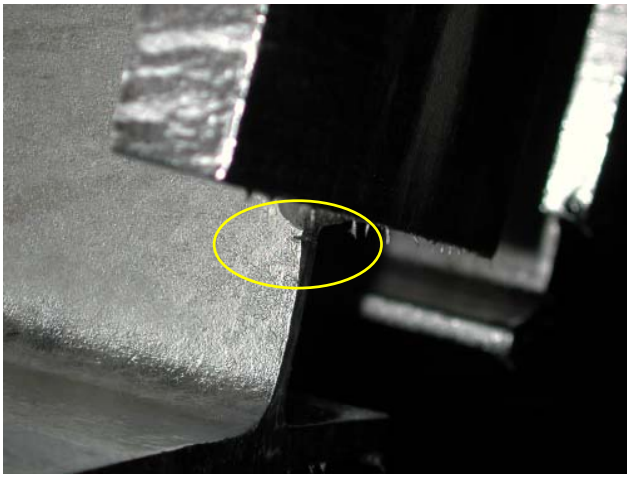

Fig. 13: Deliberate defect introduced by saw cut 10 mm below half cover plate

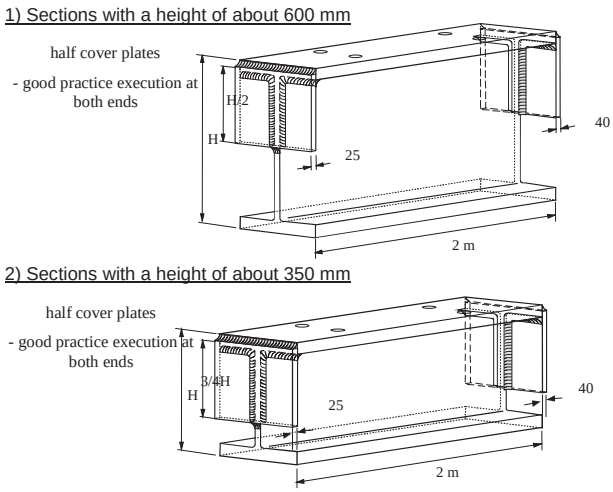

Fig. 14: Assemblies for full scale galvanizing test no. 3

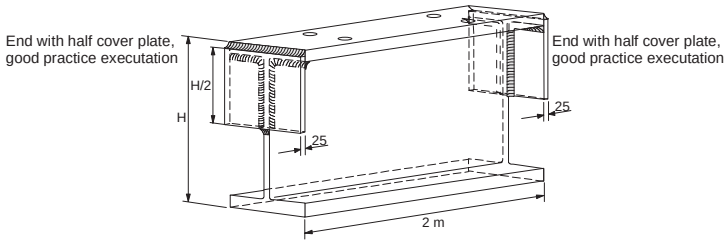

Fig. 15: Assembly for full scale galvanizing test no. 4

Fig. 16: Weld bead added in critical area below welded half cover plate

Fig. 17: Thermal stress relieving with hand held torch

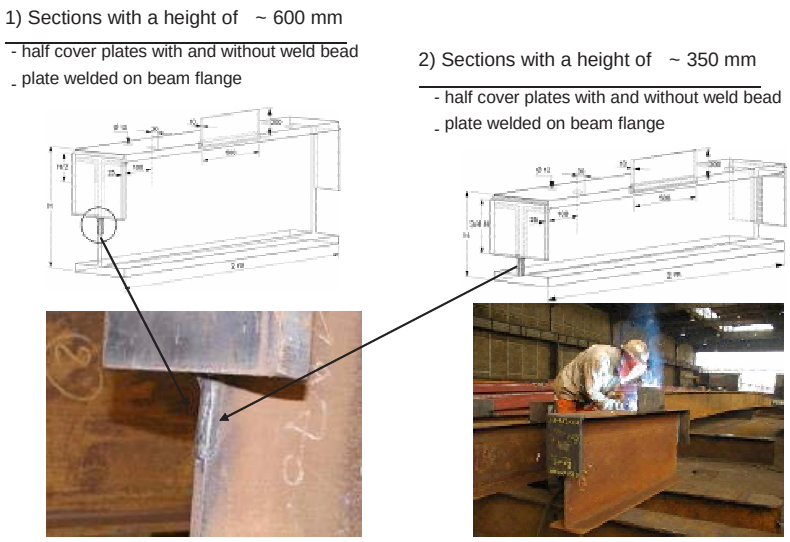

Fig. 18: Full scale Galvanizing test no. 5

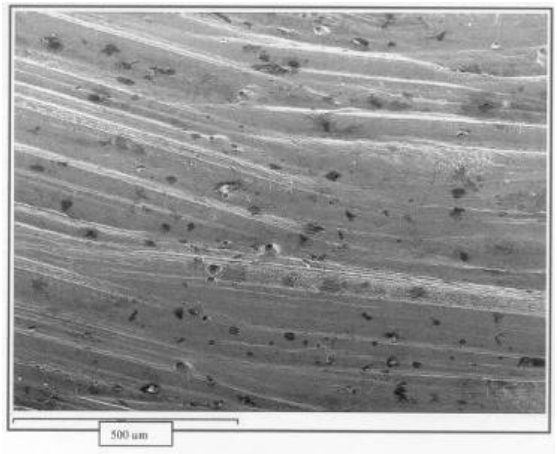

Fig. 19: SEM picture showing pits in web section after pickling

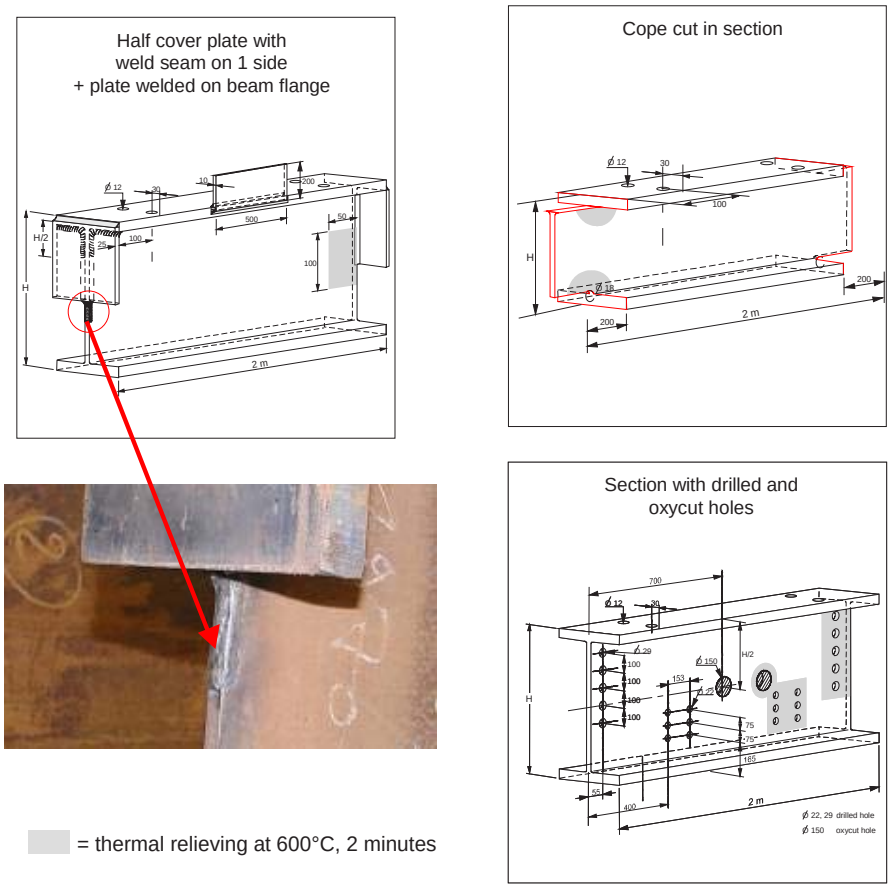

Fig. 20: Assembly designs for full scale galvanising test no. 6

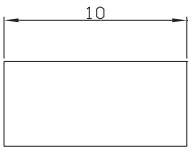

Fig. 21: Experimental equipment used for [H] concentration tests at the University of Cantabria.

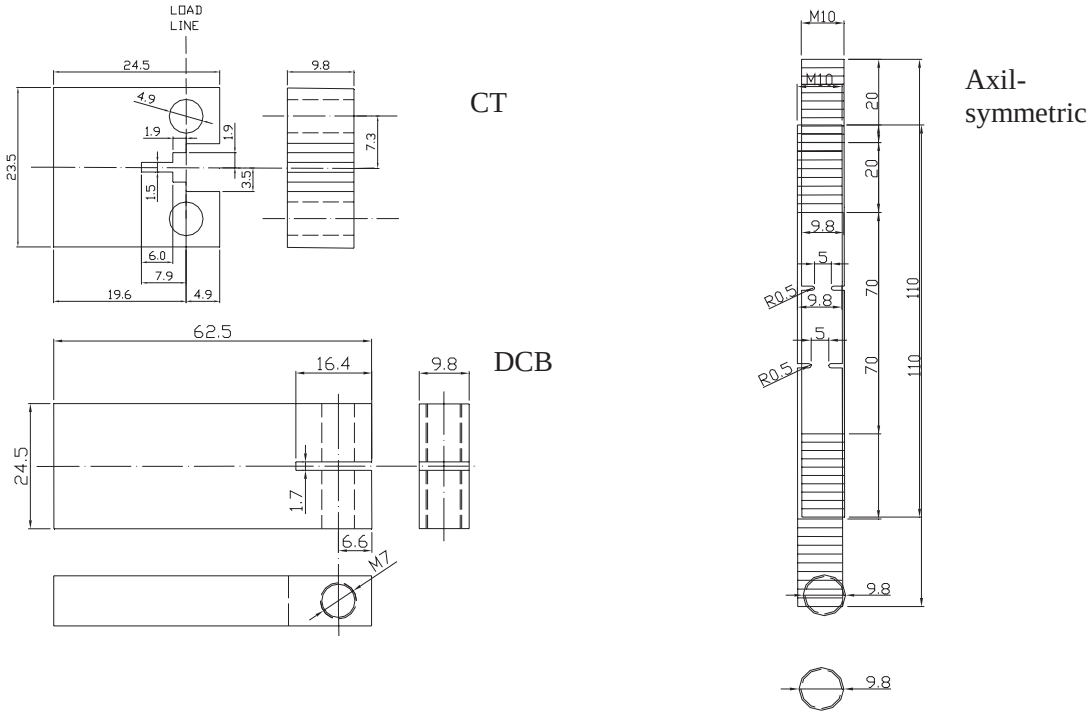

Fig. 22: Test pieces used for LMAC test at the University of Cantabria

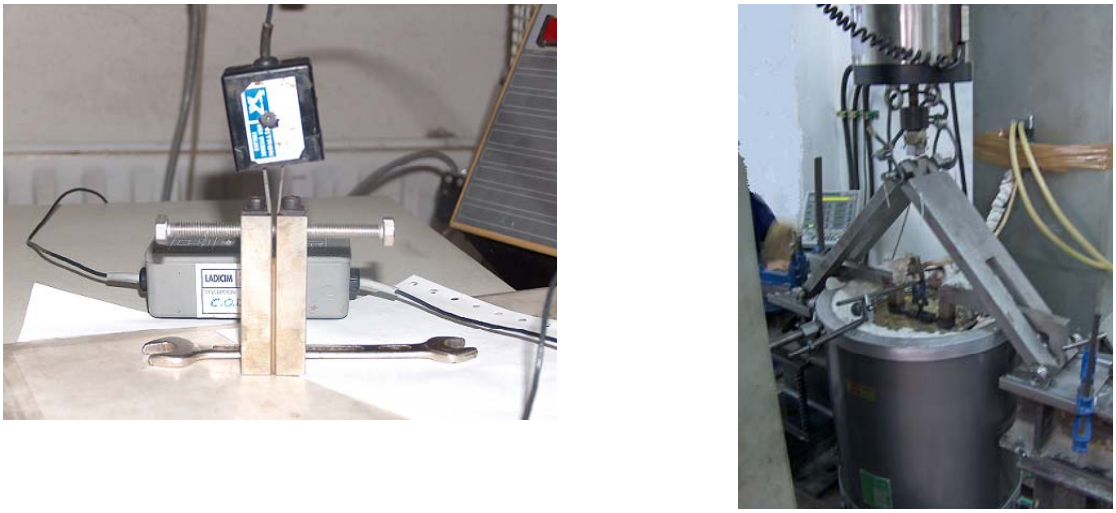

(a) DCB specimen (b) LMAC test

Fig. 23(a and b): University of Cantabria LMAC testing (a) Bolt loaded WOL (b) LMAC test facility

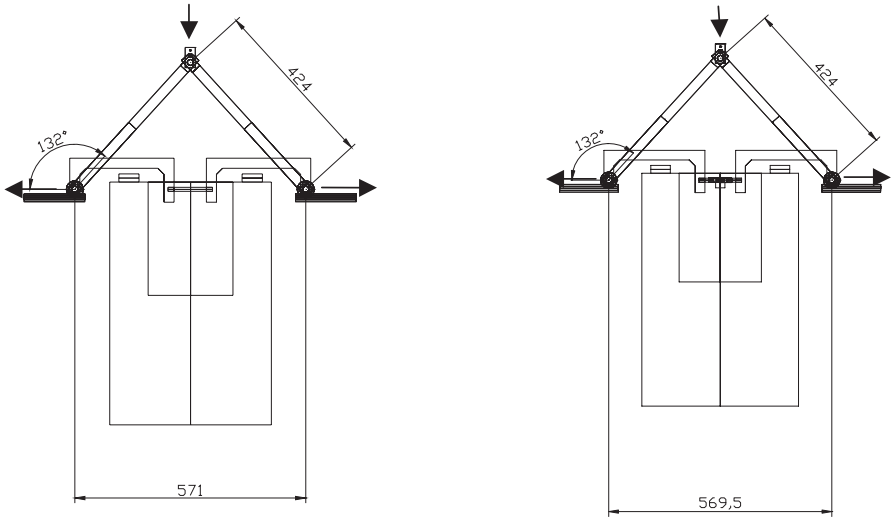

(a) Slow strain rate test on tensile test piece

(b) Toughness test

Fig. 24(a and b): Schematic of the UC experimental equipment for (a) slow strain rate tests and (b) toughness tests

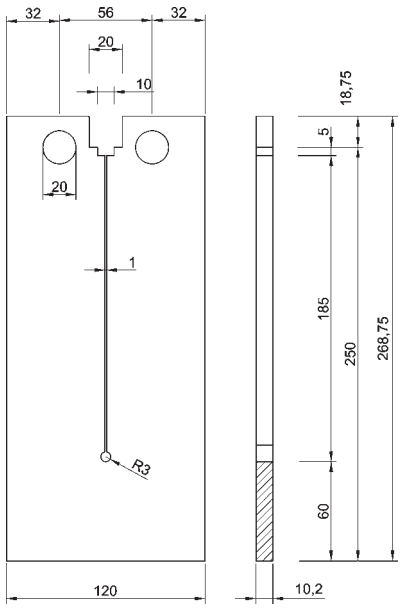

Fig. 25: Modified CT Specimen (dimensions in mm) used for laboratory LMAC tests at RWTH Aachen University

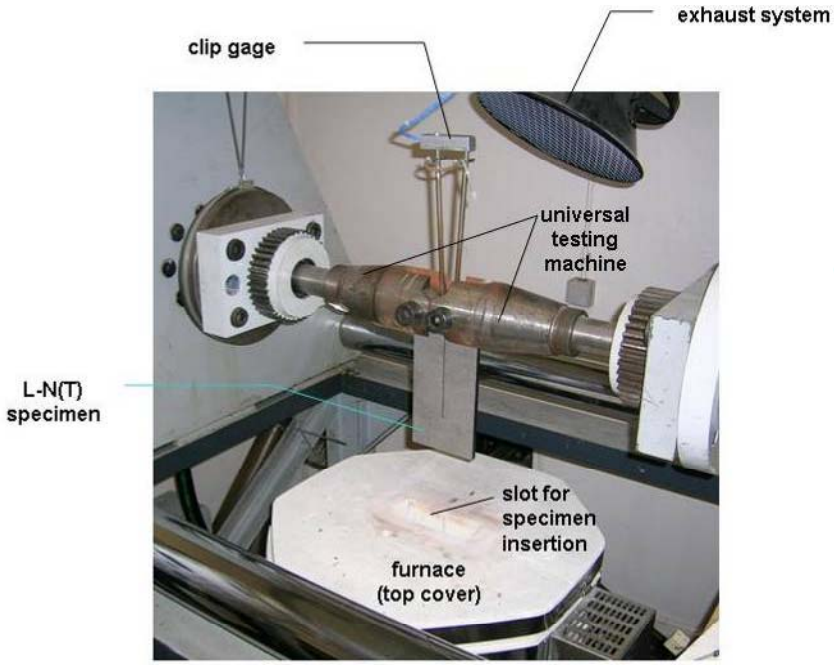

Fig. 26: RWTH Aachen University LMAC test set-up

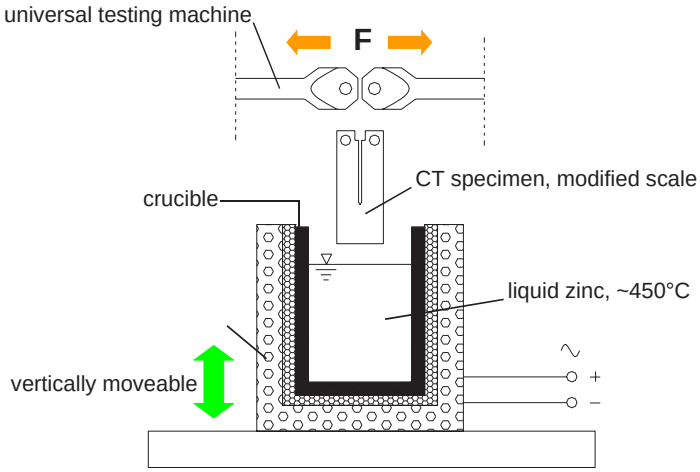

Fig. 27: Schematic of RWTH Aachen University (UA) LMAC test using modified compact tension (DCB) test piece

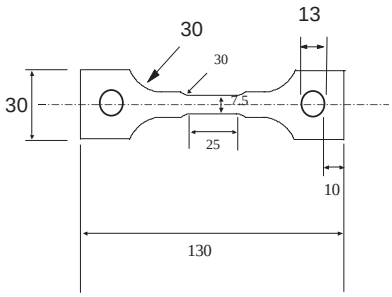

(a) Tensile test piece

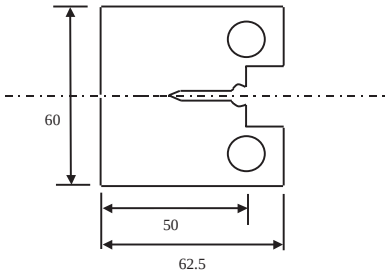

(b) Compact tension test piece

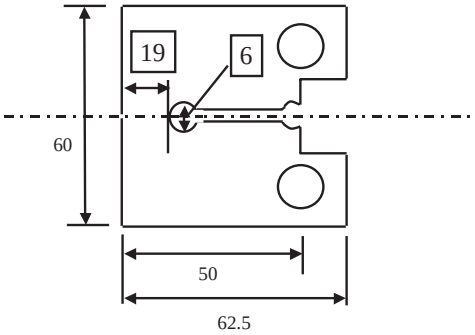

(c) key hole test piece

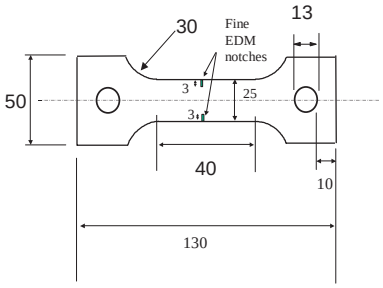

(d) Short crack test piece

Fig. 28(a-d): Test pieces used in laboratory LMAC testing at Corus RD&T

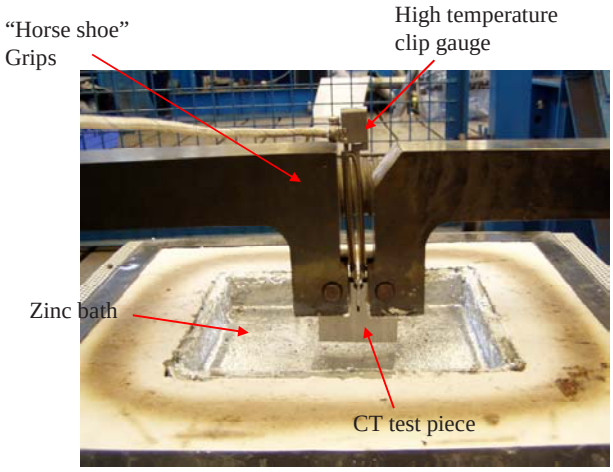

Fig. 29: Corus RD&T LMAC test facility

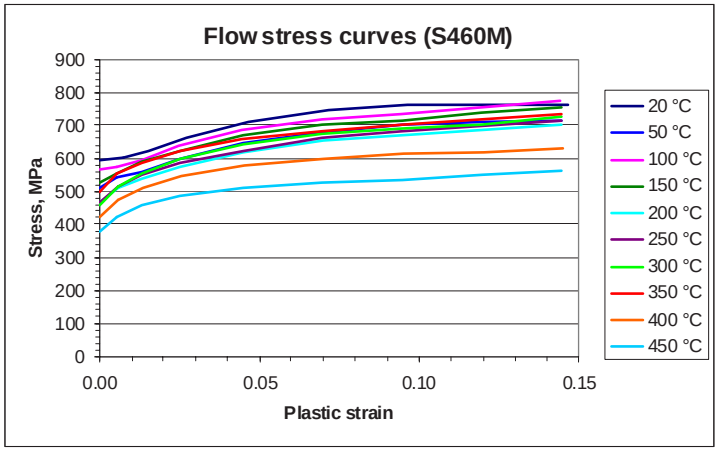

Fig. 30: Flow stress curves for S460M steel at various temperatures used for modelling galvanizing

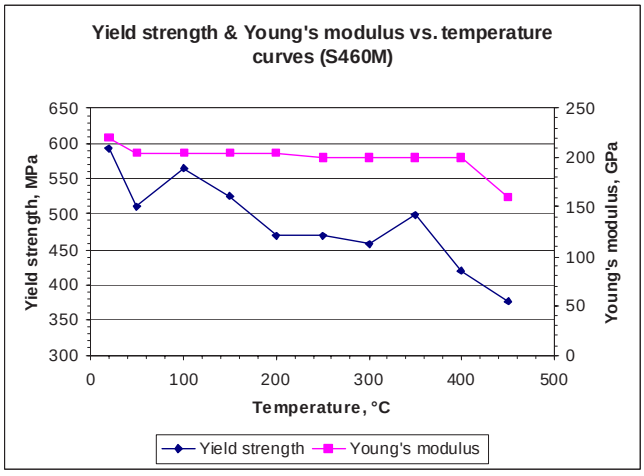

Fig. 31: Change in yield strength and Young's modulus with temperature for S460M steel

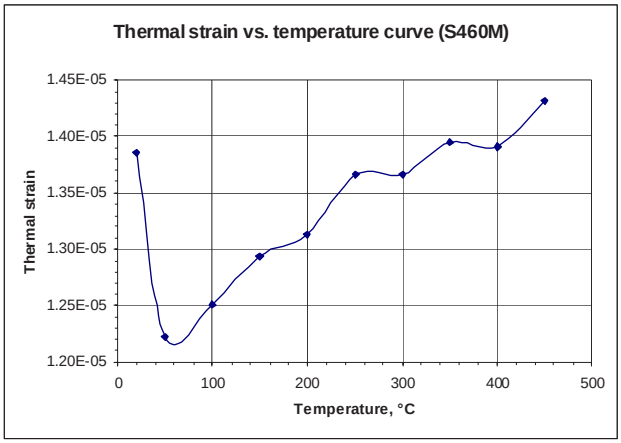

Fig. 32: Variation of thermal strain with temperature for grade S460M steel

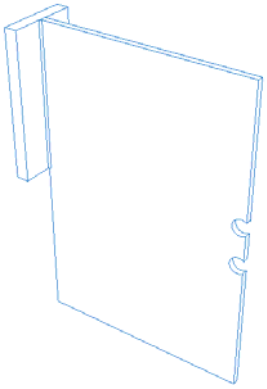

Fig. 33: Schematic of component used in Corus model of galvanising trial No. 1 conducted by TUKL.

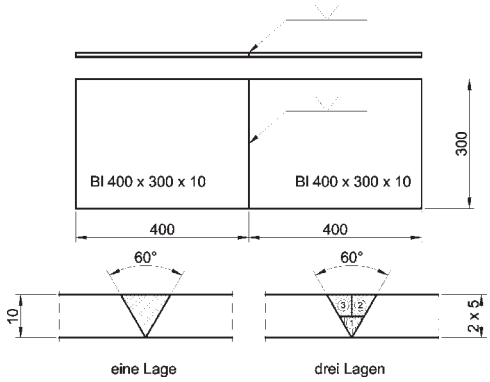

Fig. 34: Geometry used for validation of the welding process model at University of Kaiserslautern

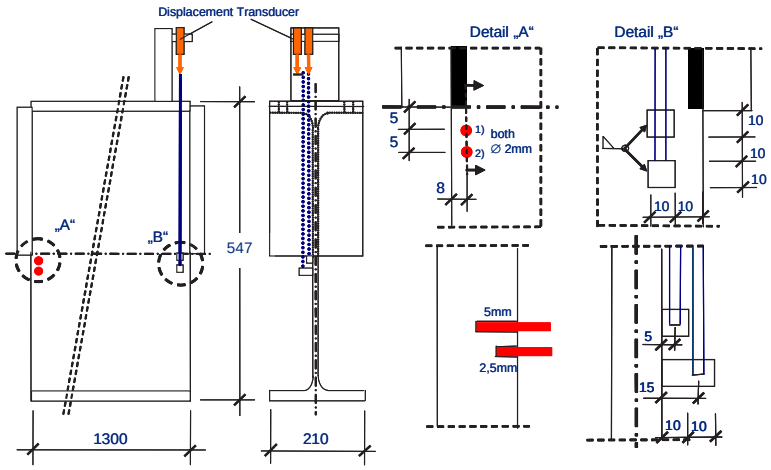

Fig. 35: TUKL validation Trial No. 3 - Geometry and application of measurement devices

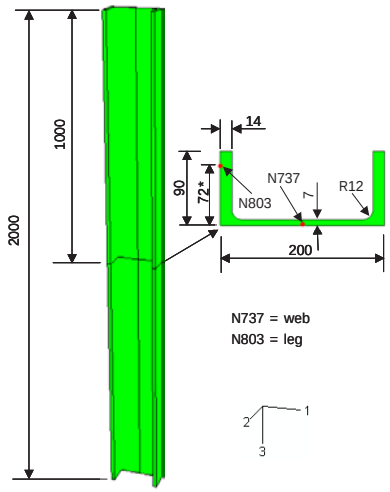

Fig. 36: Geometry of the channel section used in a galvanizing trial carried out by Corus for model development and validation

(a) test no. 1 (Zn bath)

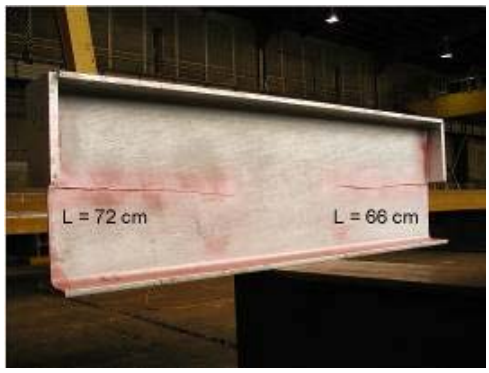

(b) Test no. 2 (Zn-Sn bath)

Fig. 37(a and b): Full-scale test. LMAC in Section of IPE 600A S450J0 (Steel J) – Rolling process: as rolled

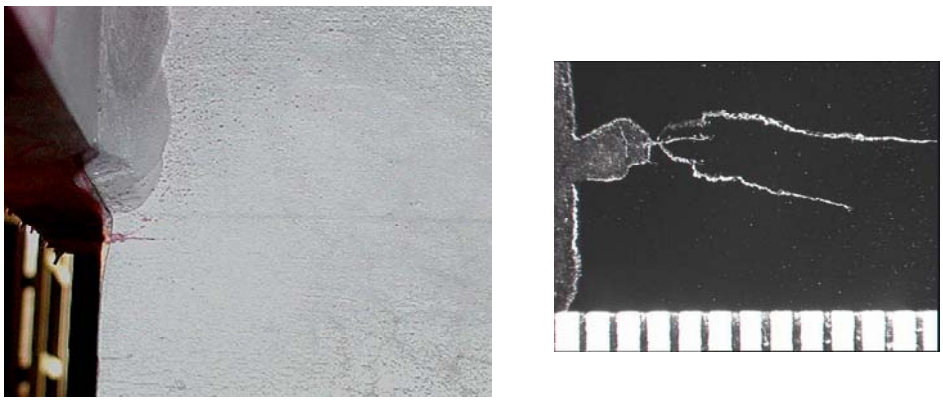

Fig. 38: Metallographic examination of small cracks

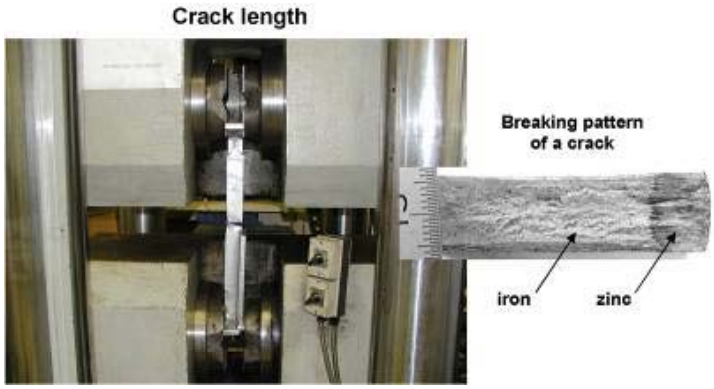

Fig. 39: Transverse tensile test used on full scale tests

Fig. 40: Full scale galvanizing test no. 3. Crack detection by magnetoscopic (magnetic particle inspection) technique

Location: Web

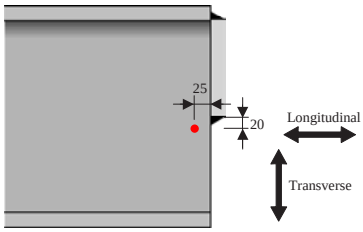

Thermal stress relieving (MPa)

	S 275 J0		S 450 J0	
	600°C	700°C	600°C	700°C
Web L	- 63	- 40	42	- 46
Web T	-121	- 65	- 71	-206
Edge L	98	7	13	31
Edge T	- 93	- 91	-155	-179

Location: Edge

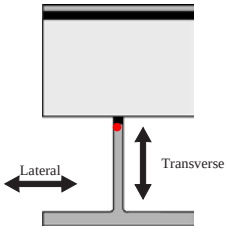

Mechanical stress relieving (MPa)

	S 275 J0		S 450 J0	
	Sand blasting	Stressonic	Sand blasting	Stressonic
Web L	- 113	-355	-134	-329
Web T	- 111	-334	-262	-378
Edge L	- 152	-457	-193	-432
Edge T	- 102	-347	- 43	-305

+ : tension
- : compression

Fig. 41: Measurements of residual stresses, X-ray techniques

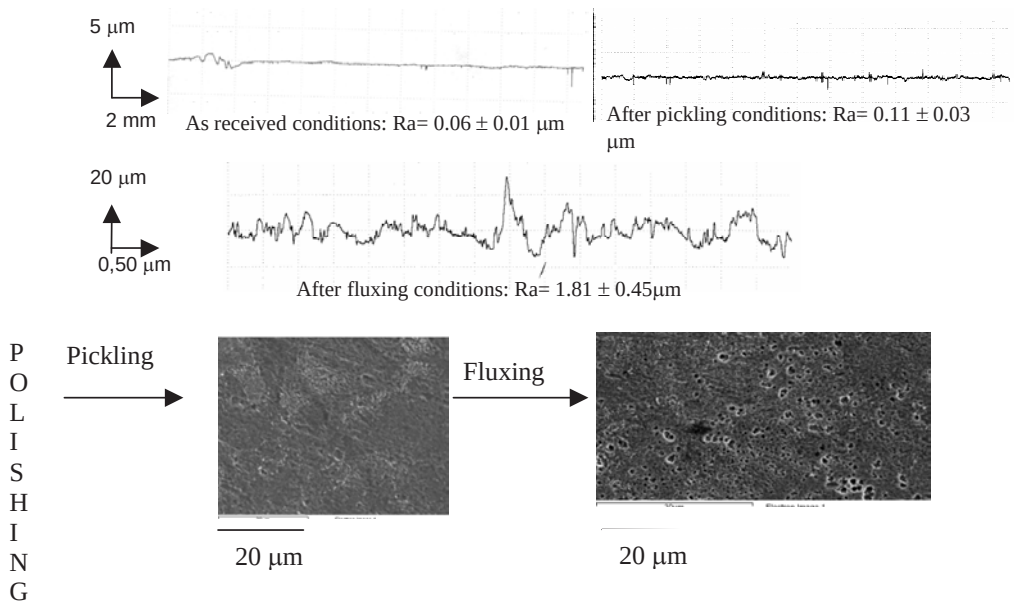

Fig. 42: Surface roughness tests for steel grade J

Fig. 43: Deposits on the surface of steel grade J after fluxing

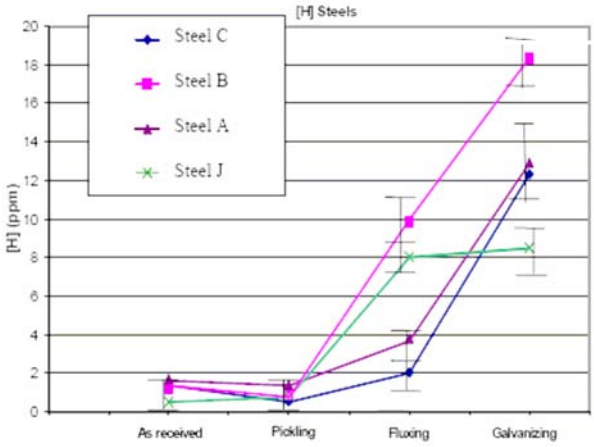

Fig. 44: Hydrogen concentration test results for different steel grades. H content after galvanizing includes hydrogen in the Zn layer over the steel.

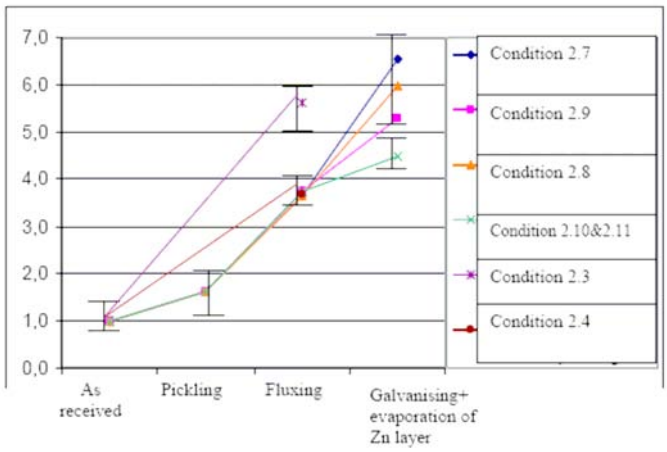

Fig. 45: Hydrogen concentration test results on steel grade J for different pre-galvanizing and galvanizing processes. H content after galvanizing does not include H in upper Zn layer.

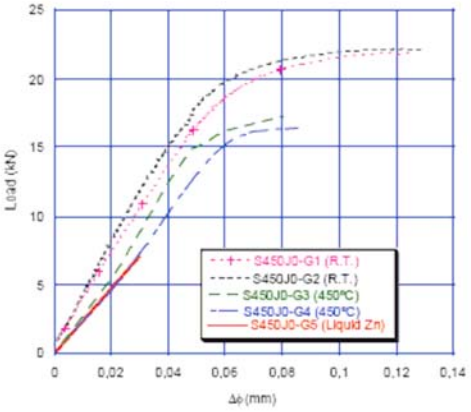

Spec.	Max. Load (kN)	$\Delta\phi_c$ (mm)
G1	21.8	0.126
G2	22.1	0.130
G3	17.2	0.080
G4	16.4	0.085
G5	7.1	0.030

Fig. 46: Results of J tests on CT specimens made of steel grade J

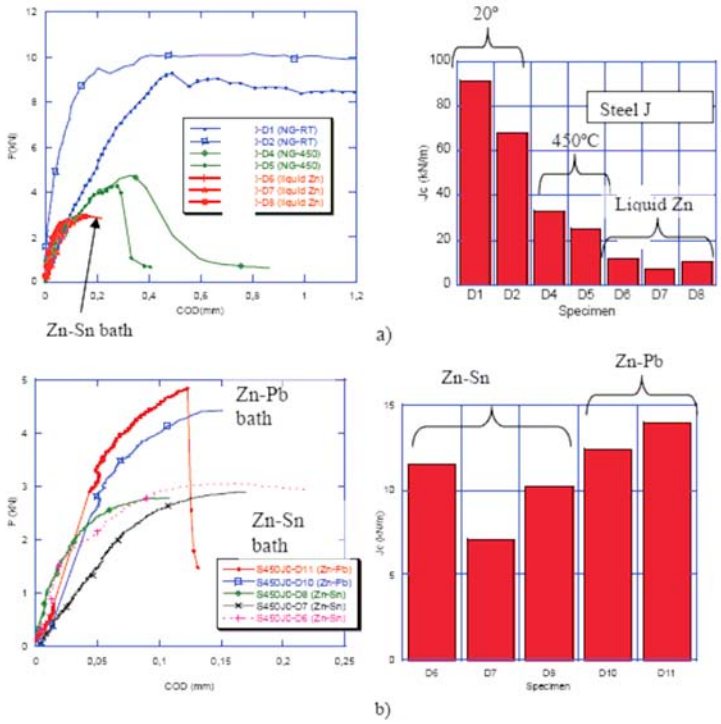

Fig. 47(a and b): Slow strain rate test results on specimens made of steel grade J.

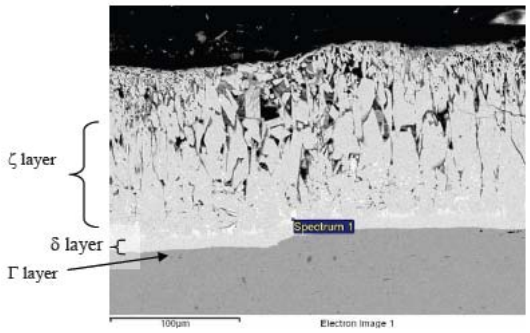

Element	Weight%	Atomic%
Al K	0.18	0.49
Fe K	6.25	8.33
Cu K	0.66	0.78
Zn K	70.55	80.48
Sn L	8.87	5.54
Pb M	14.23	5.13
Totals	100.0	

a)

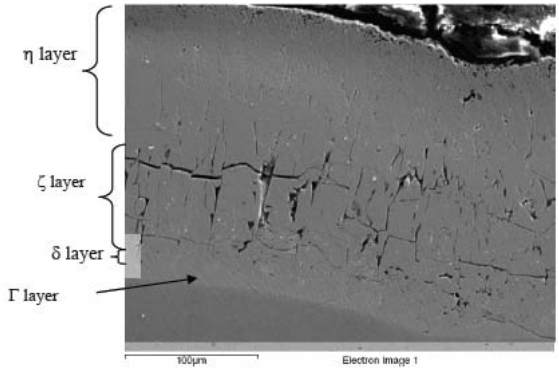

b)

Fig. 48: Microstructure of a Zn layer obtained with a Zn bath rich in Sn, and a EDS spectrum on a point rich in Sn and Pb (steel grade P).

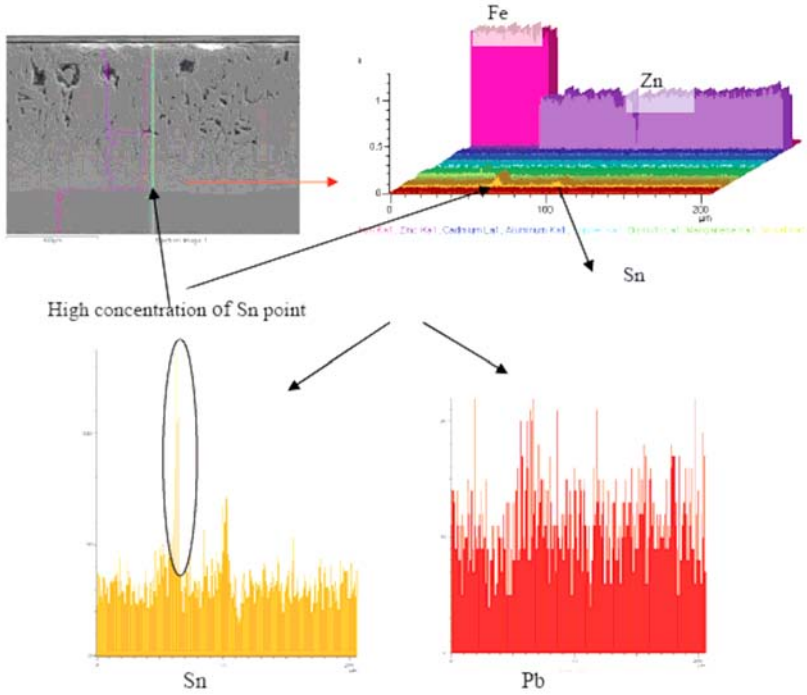

Fig. 49: Microstructure of a Zn layer. Chemical composition from the steel base to the surface of the Zn layer (Steel grade L).

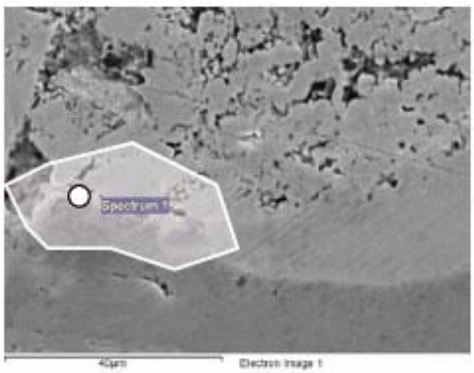

Element	Weight%	Atomic%
Mn K	0.20	0.27
Fe K	15.51	20.97
Zn K	54.59	63.09
Sn L	17.79	11.32
Pb M	11.74	4.28
Bi M	0.17	0.06
Totals	100.00	

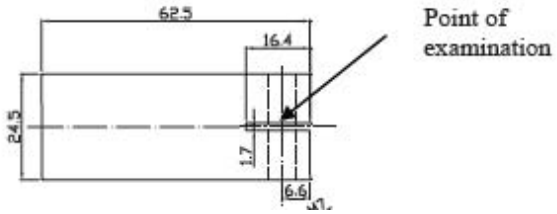

Fig. 50: Concentration of Sn and Pb on the steel base in a DCB specimen of steel grade B

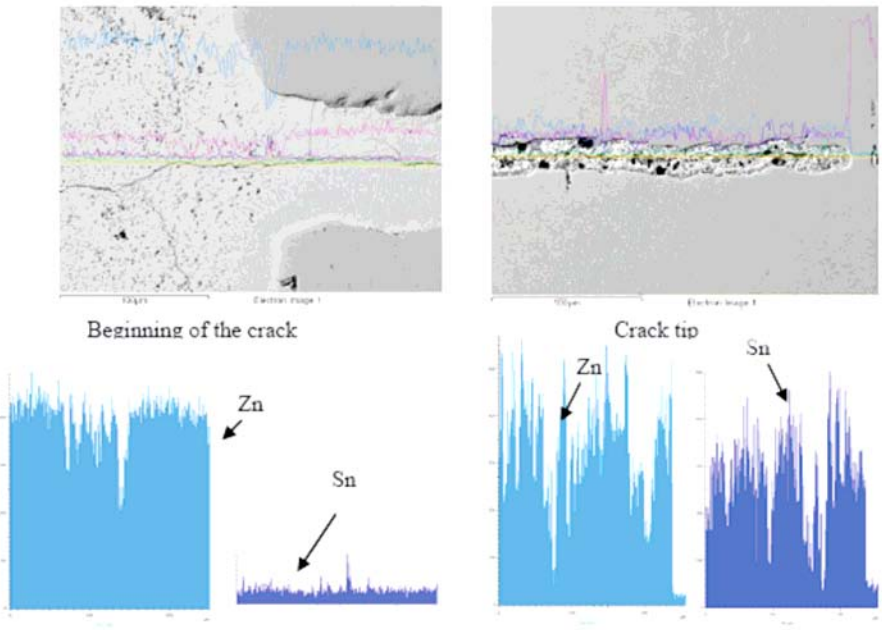

Fig. 51. Sn concentration on fatigue pre-crack of DCB test pieces. Steel B

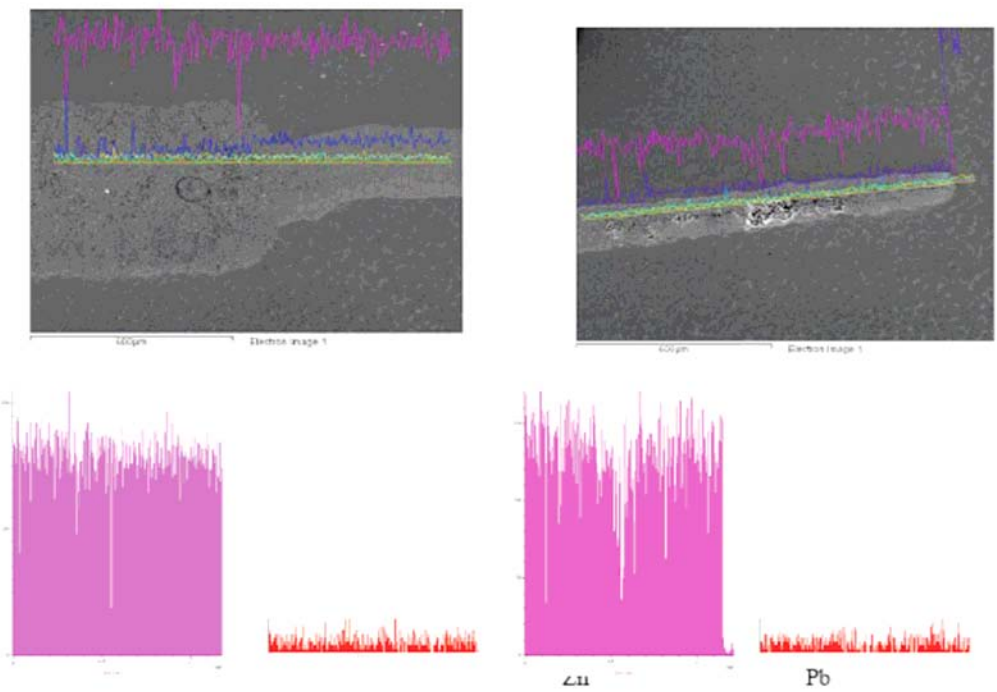

Fig. 52: Composition of Zn and Pb on pre-crack of DCB. Steel B

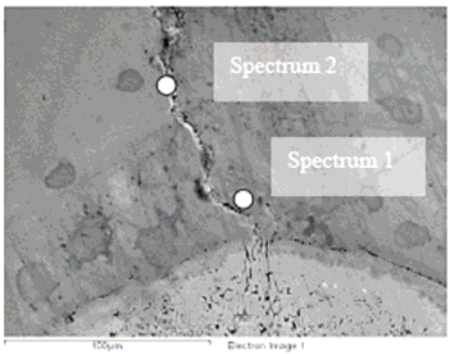

Spectrum 1		Spectrum 2	
Element	Weight%	Element	Weight%
S	1.22	S	1.79
Cl	1.65	Cl	1.23
Fe	14.74	Fe	18.28
Cu	0.34	Cu	1.72
Zn	62.22	Zn	75.33
Sn	8.76	Sn	0.39
Pb	11.06	Pb	1.26
Totals	100.00	Totals	100.00

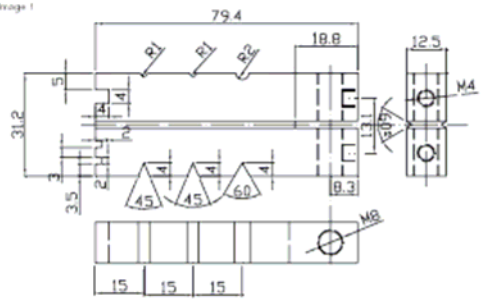

Fig. 53: Sn concentration in LMAC at point R1 in DCB test piece. Steel B

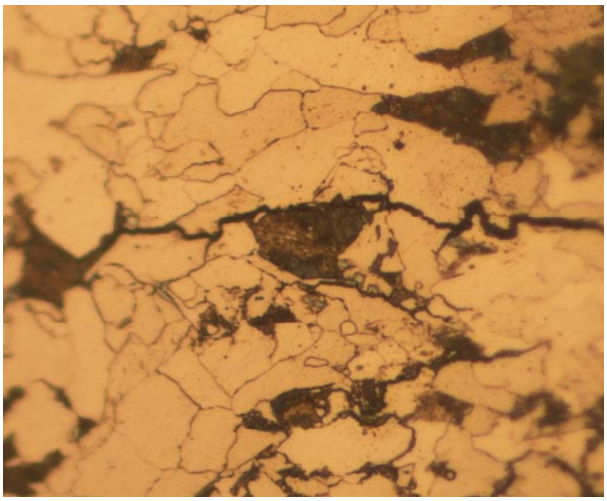

Fig. 54: Detail of the failure during galvanizing of Fig. 52, etched with 5% Nital

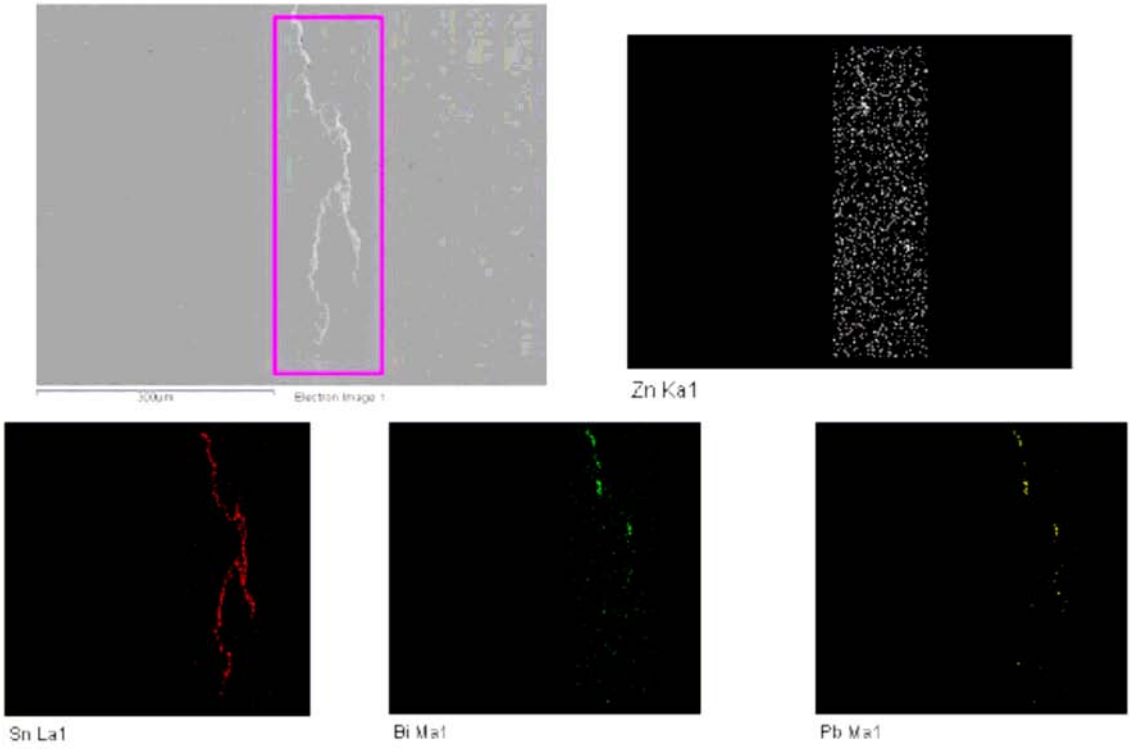

Fig. 55: Sn, Bi and Pb concentration on CT test piece after testing in liquid zinc. Steel C.

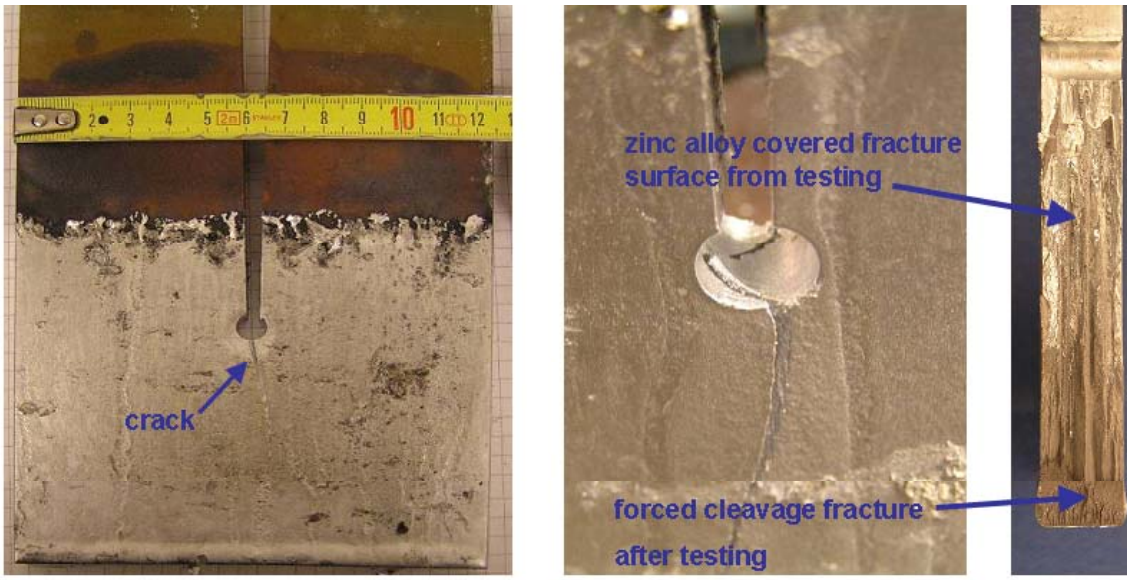

Fig. 56. Crack and fracture surface appearance after testing

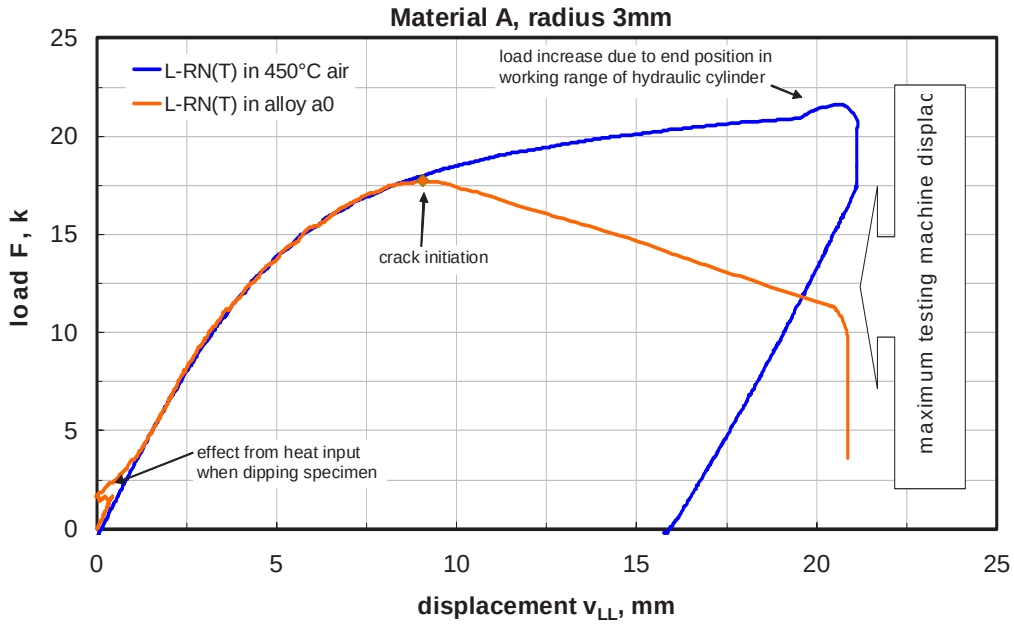

Fig. 57: Typical example for load-displacement plot from L-N(T) testing

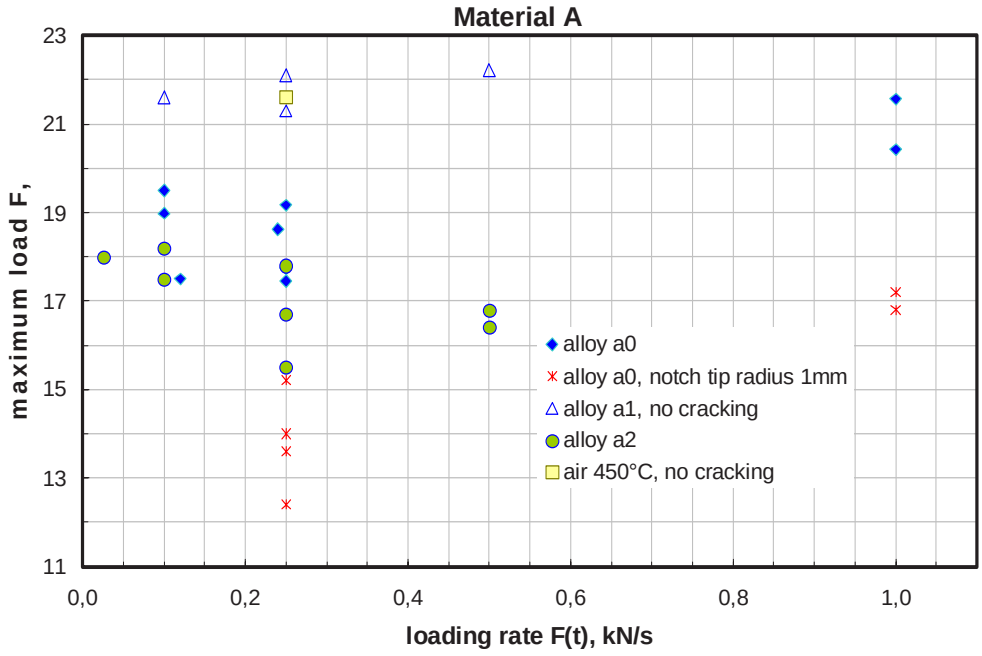

Fig. 58: Maximum load values in different loading rates, material A

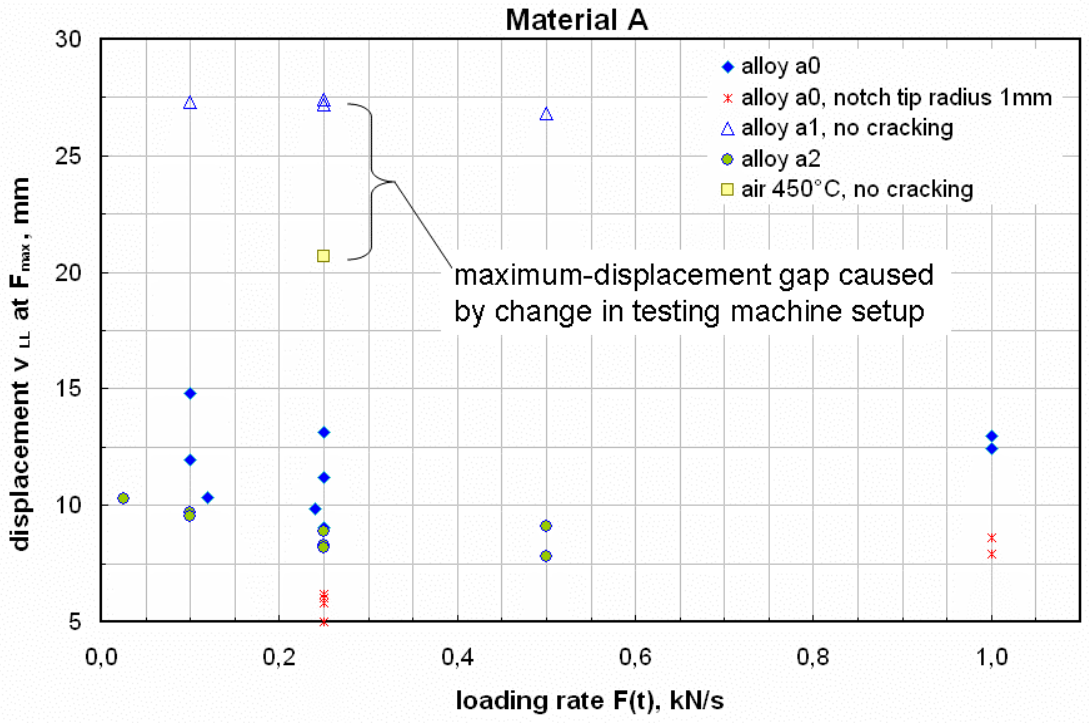

Fig. 59. Displacement at maximum load in different loading rates, material A

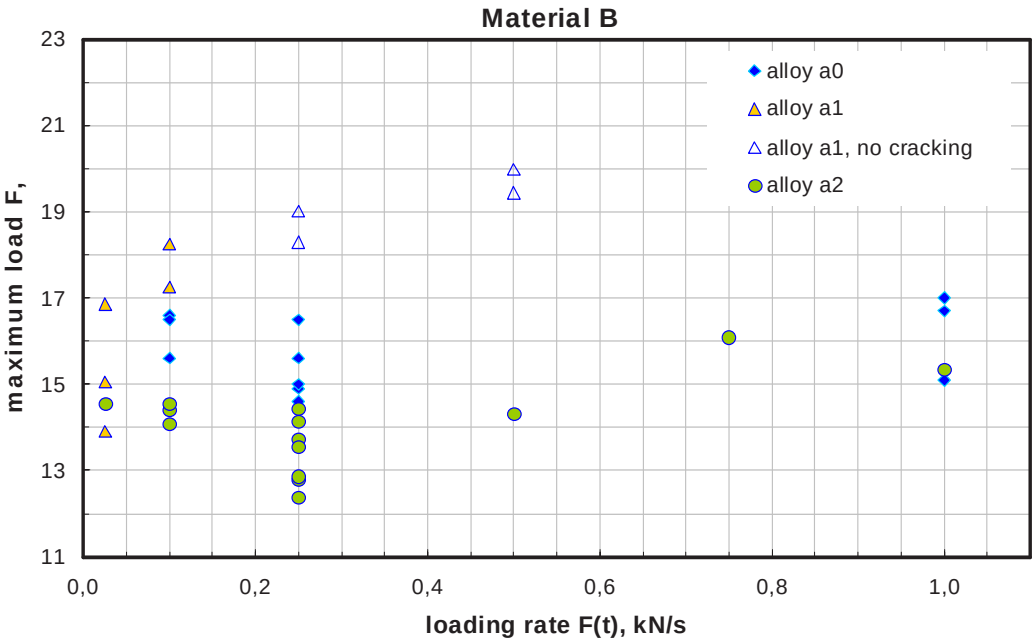

Fig. 60: Maximum load values in different loading rates, material B

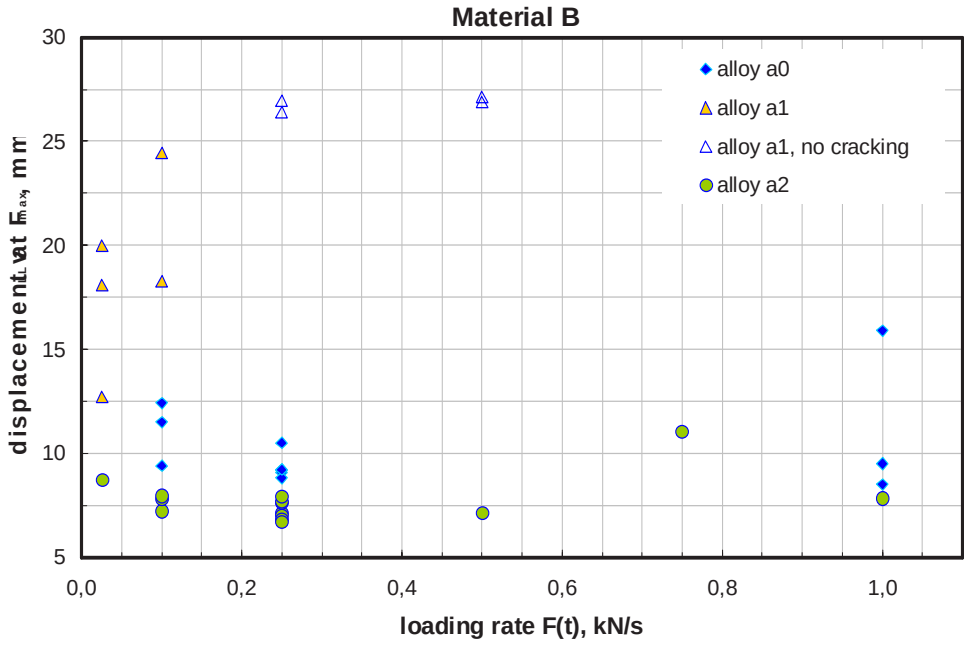

Fig. 61: Displacement at maximum load in different loading rates, material B

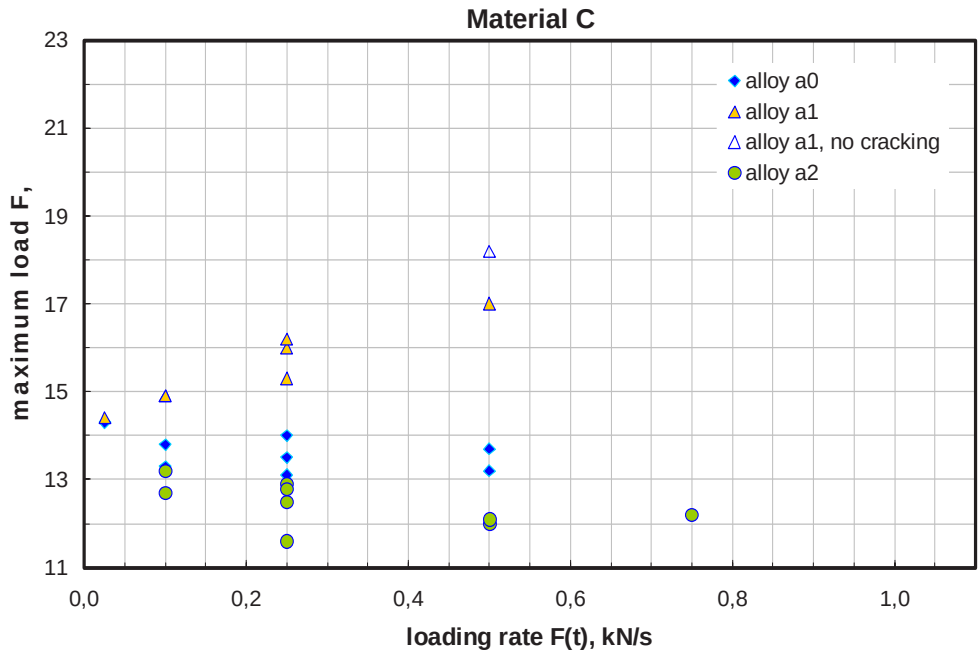

Fig. 62: Maximum load values in different loading rates, material C

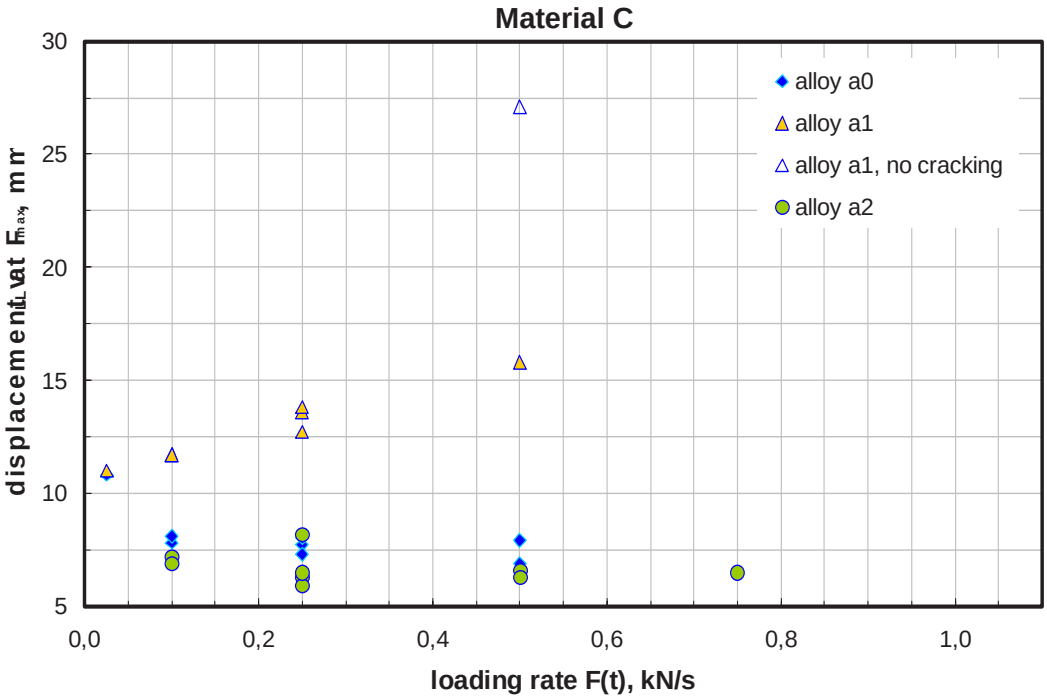

Fig. 63: Displacement at maximum load in different loading rates, material C

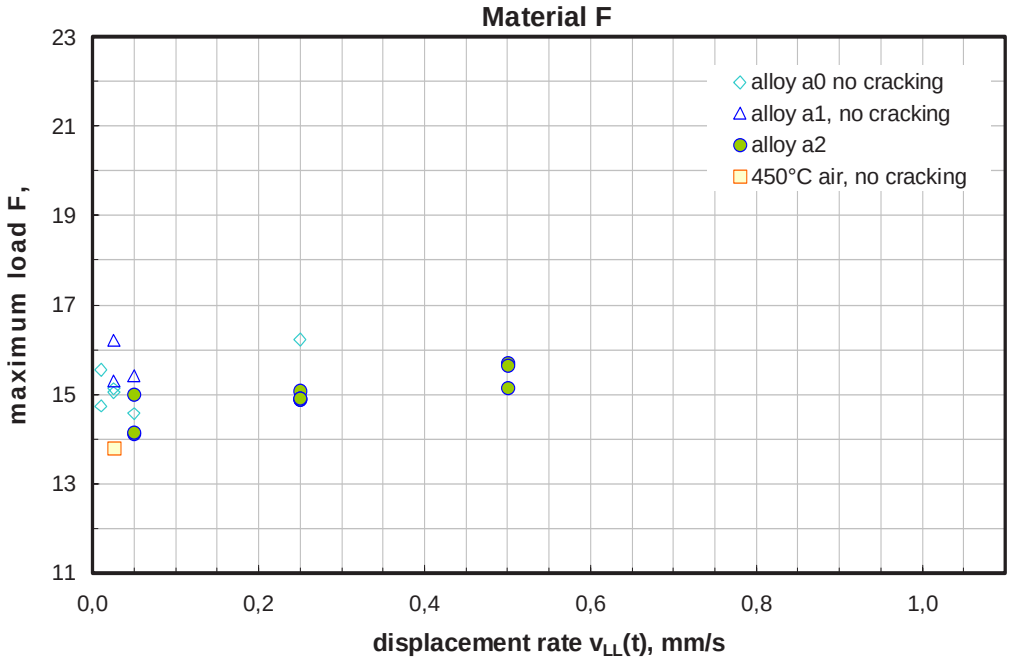

Fig. 64: Maximum load values in different displacement rates, material F

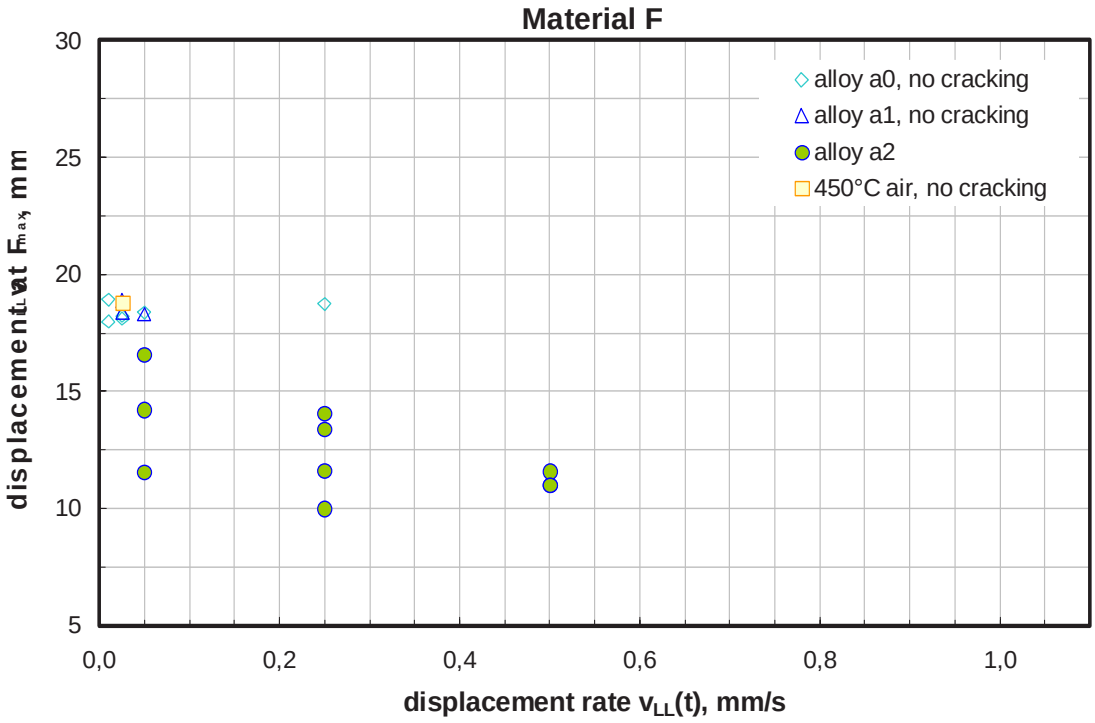

Fig. 65: Displacement at maximum load in different displacement rates, material F

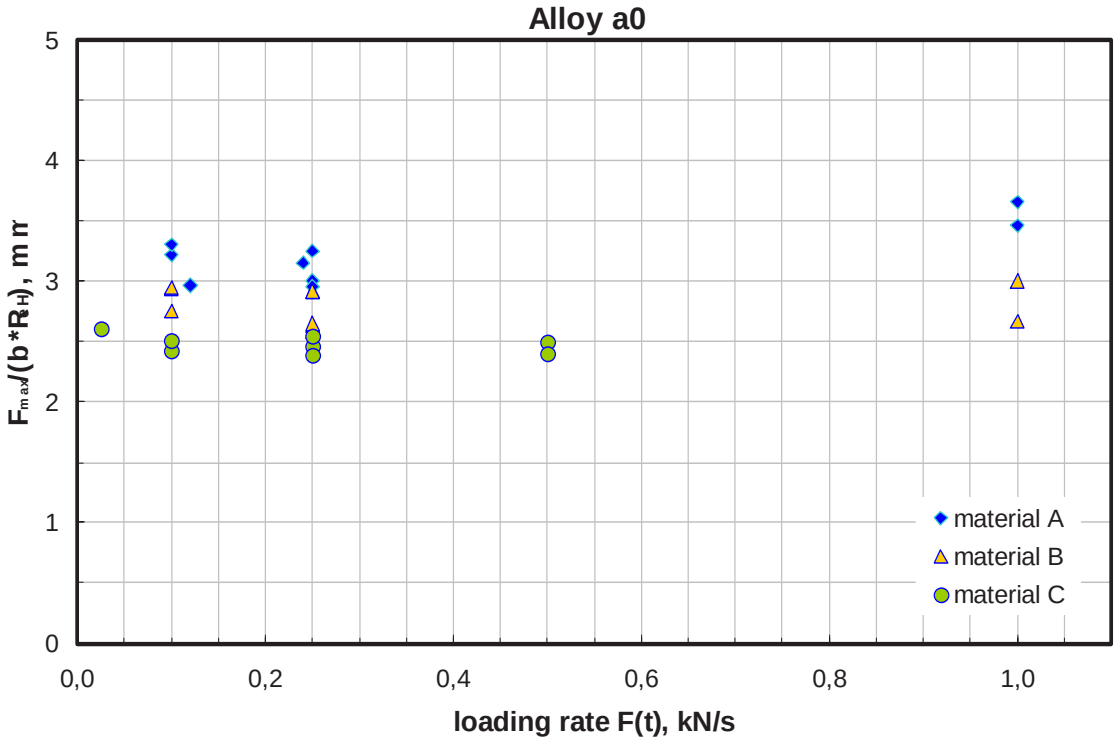

Fig. 66: Maximum loading values achieved for testing performed in alloy a0 divided by L-N(T) thickness b and upper yield R_{eH}

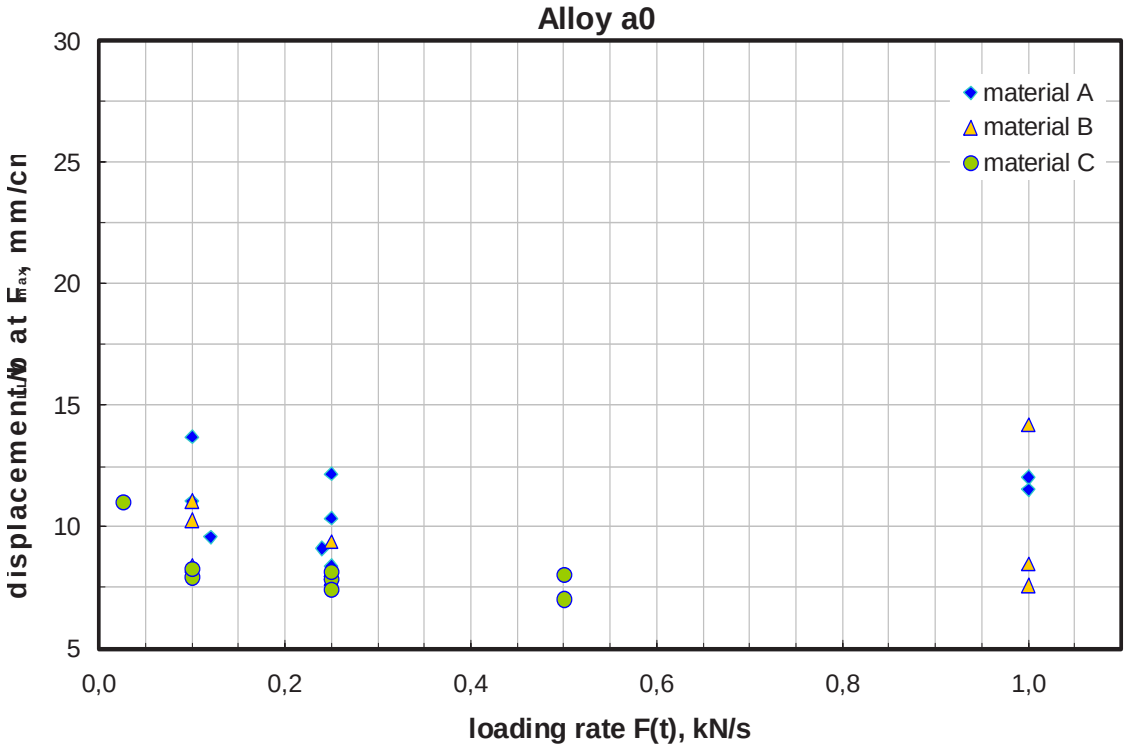

Fig. 67: Displacement values achieved corresponding to F_{max} divided by L-N(T) thickness b for testing performed in alloy a0

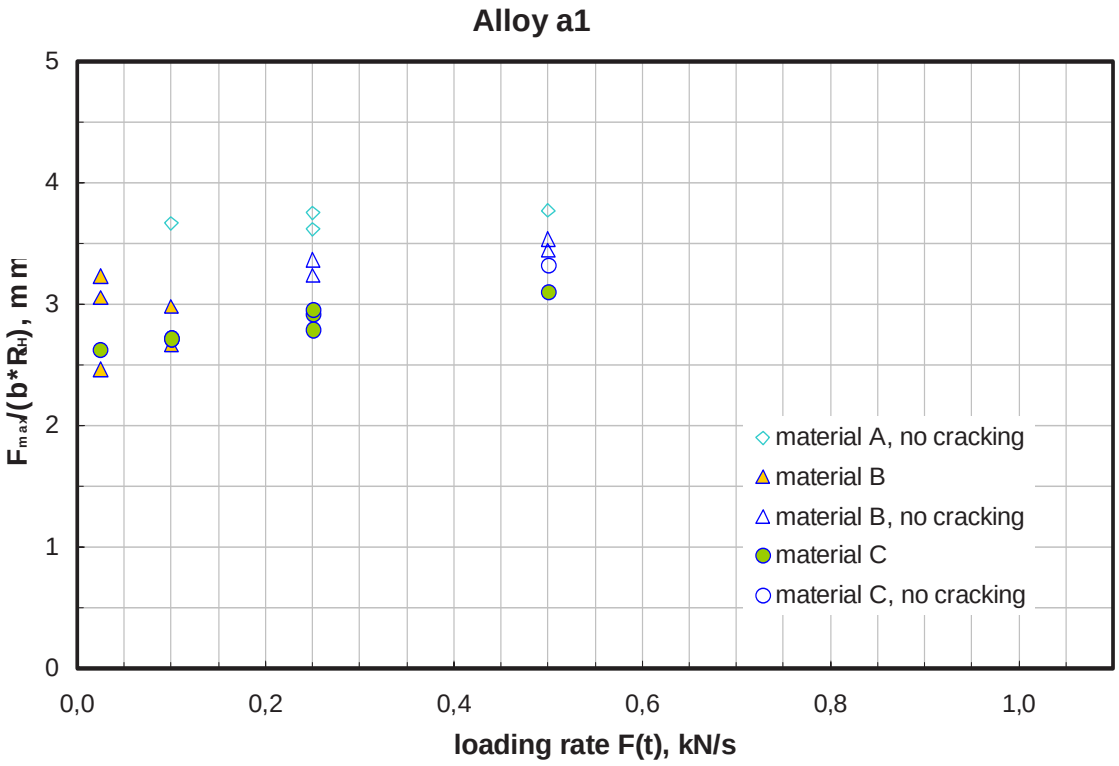

Fig. 68: Maximum loading values achieved for testing performed in alloy a1 divided by L-N(T) thickness b and upper yield R_{eH}

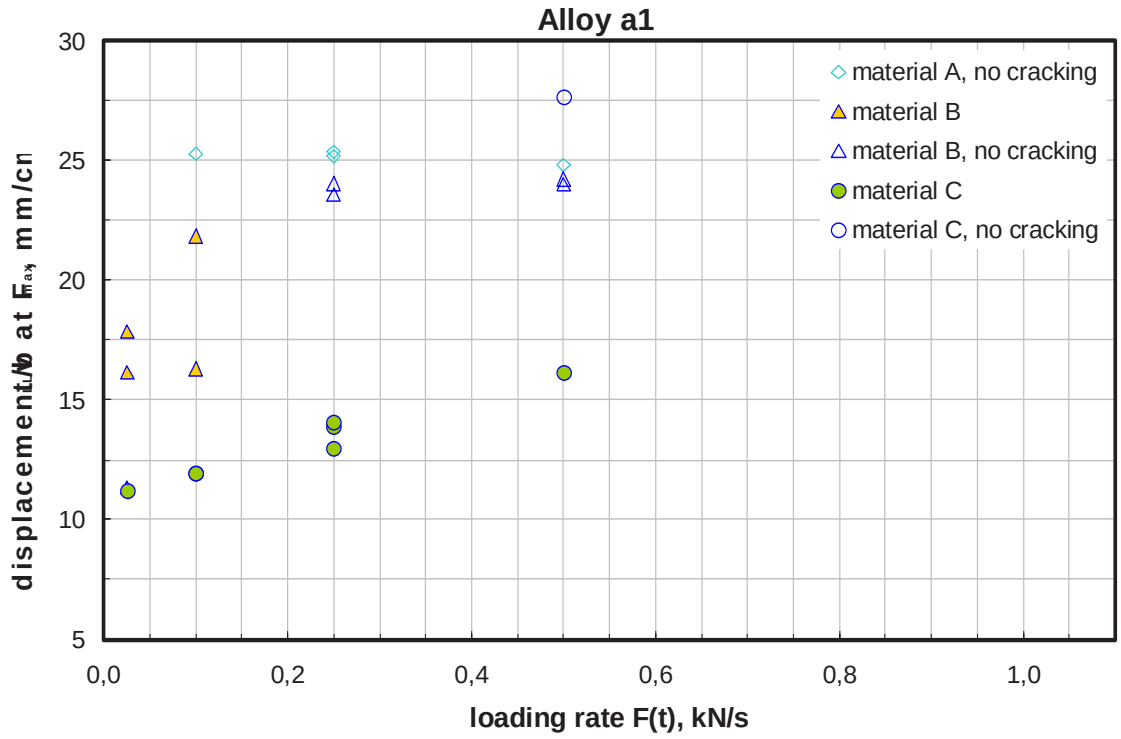

Fig. 69: Displacement values achieved corresponding to F_{max} divided by L-N(T) thickness b for testing performed in alloy a1

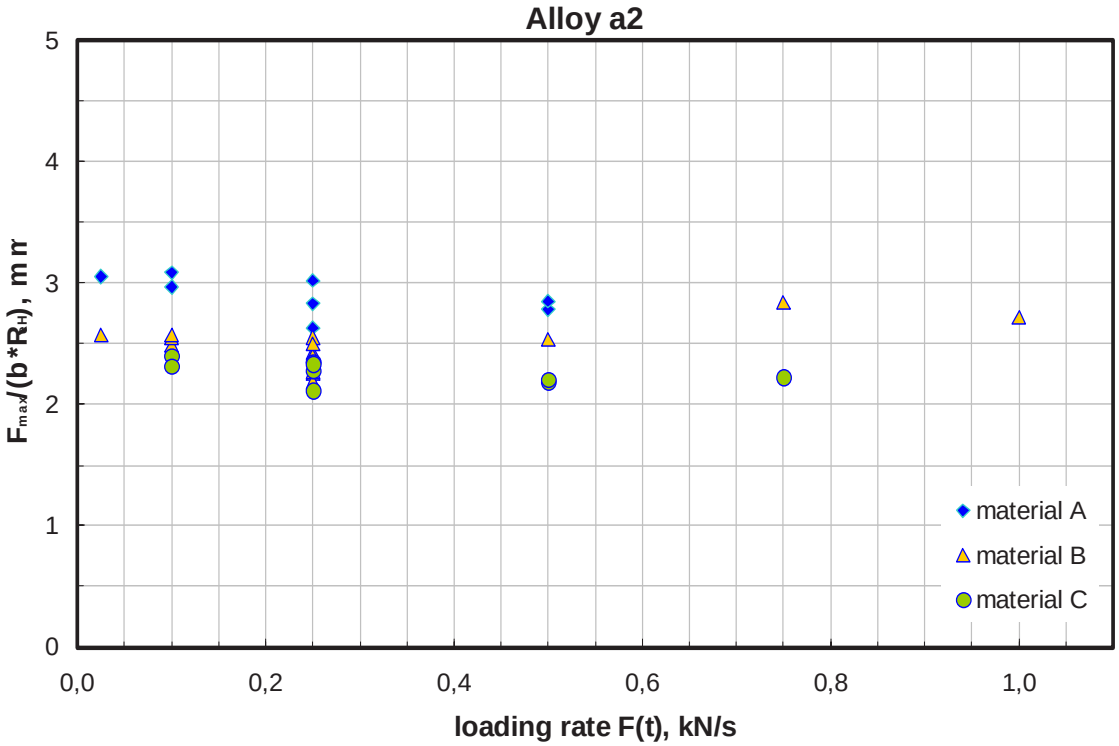

Fig. 70: Maximum loading values achieved for testing performed in alloy a2 divided by L-N(T) thickness b and upper yield R_{eH}

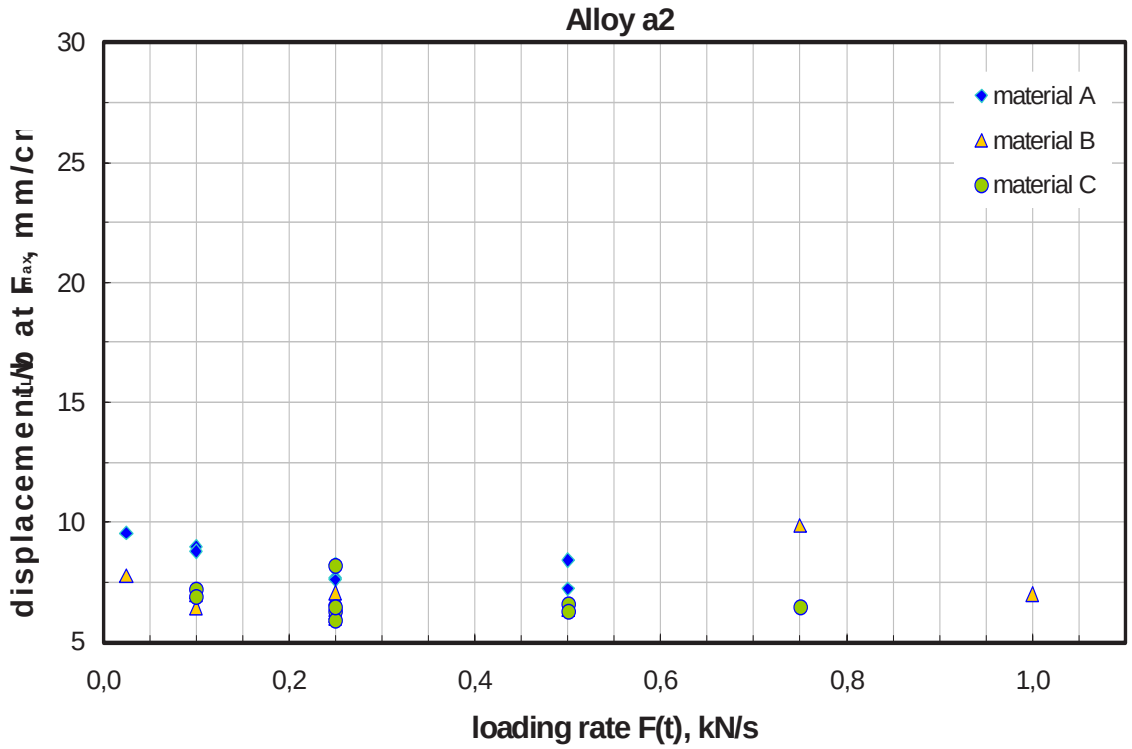

Fig. 71: Displacement values achieved corresponding to F_{max} divided by L-N(T) thickness b for testing performed in alloy a2

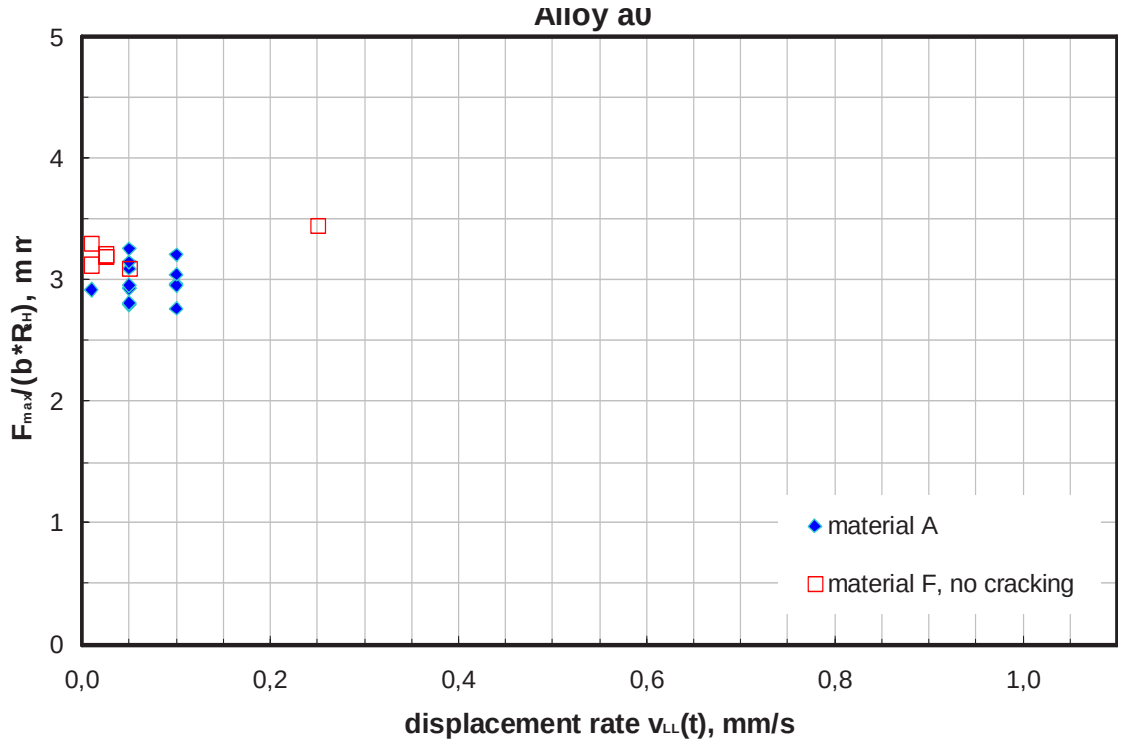

Fig. 72: Maximum loading values achieved for testing performed in alloy a0 divided by L-N(T) thickness b and upper yield R_{eH} (for material F from flange testing)

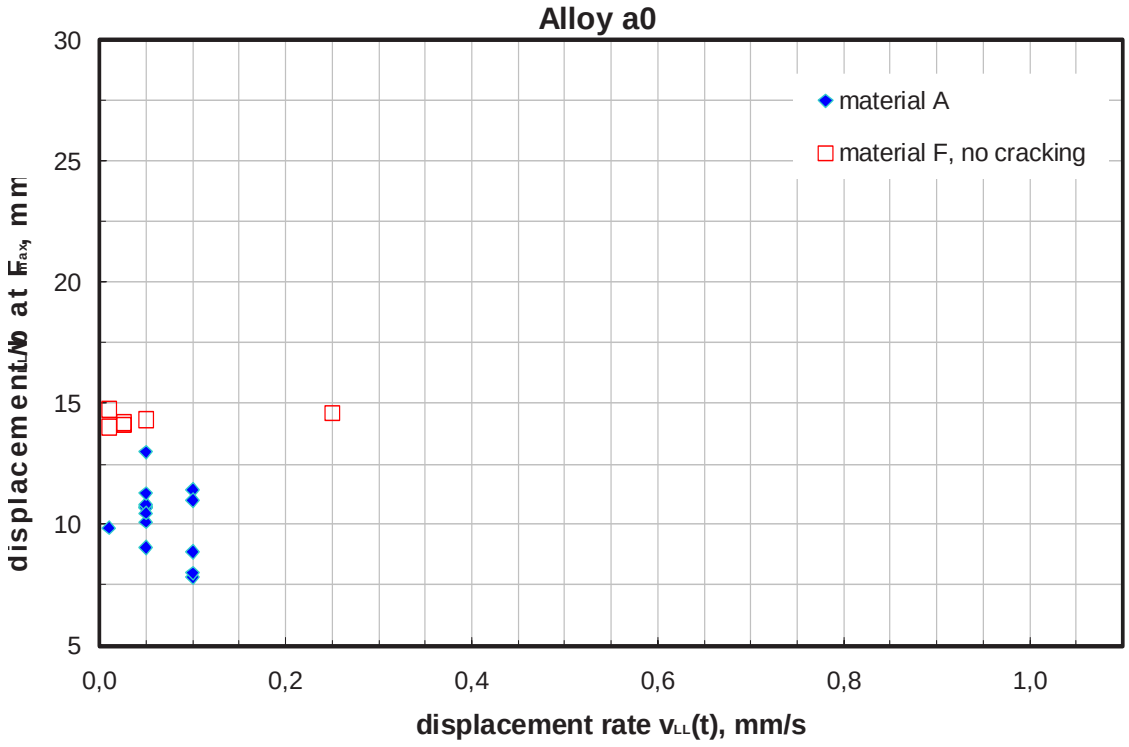

Fig. 73: Displacement values achieved corresponding to F_{max} divided by L-N(T) thickness b for testing performed in alloy a0

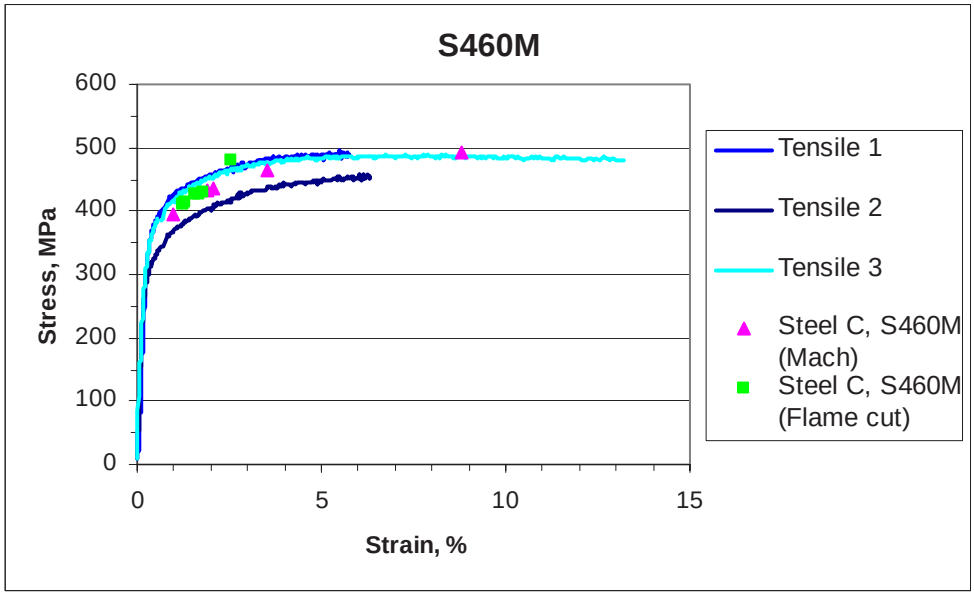

Fig. 74: CRD&T LMAC test results on steel C showing max stress compared to tensile results at 450°C

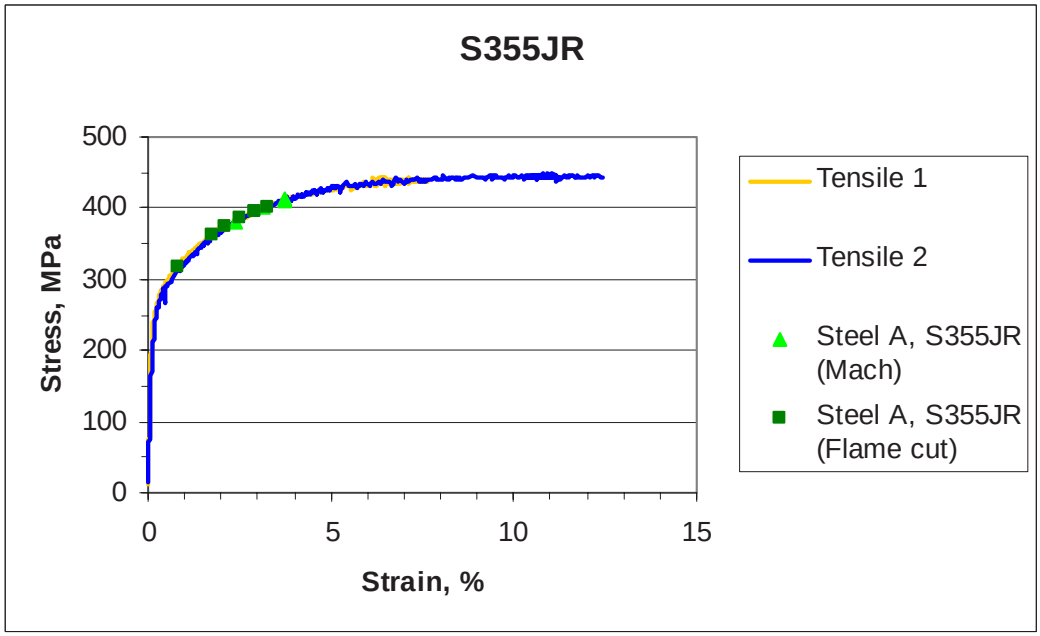

Fig. 75: CRD&T LMAC tensile test results on steel A showing max stress compared to tensile curves at 450°C

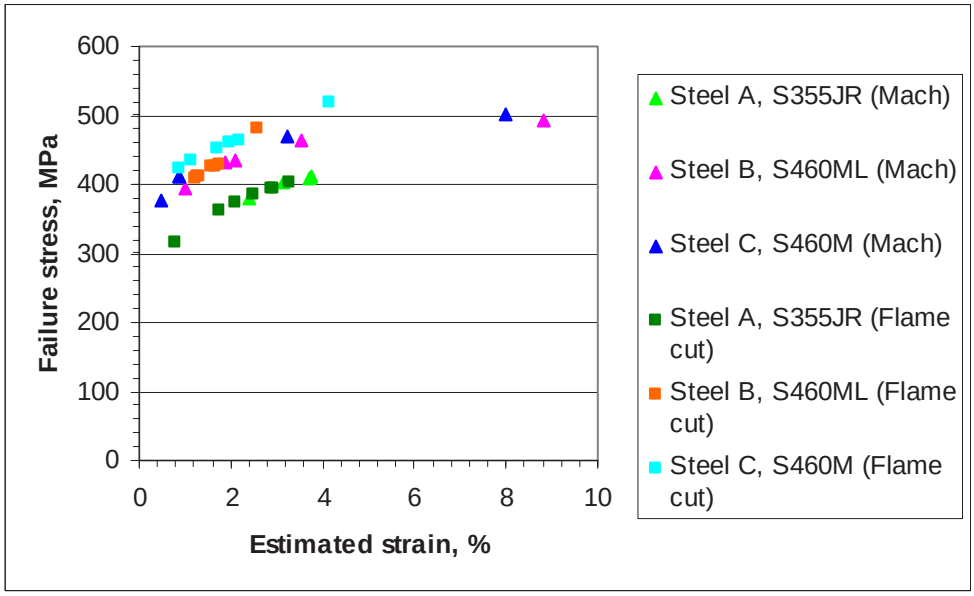

Fig. 76: CRD&T LMAC test results for machined and flame cut tensile test pieces

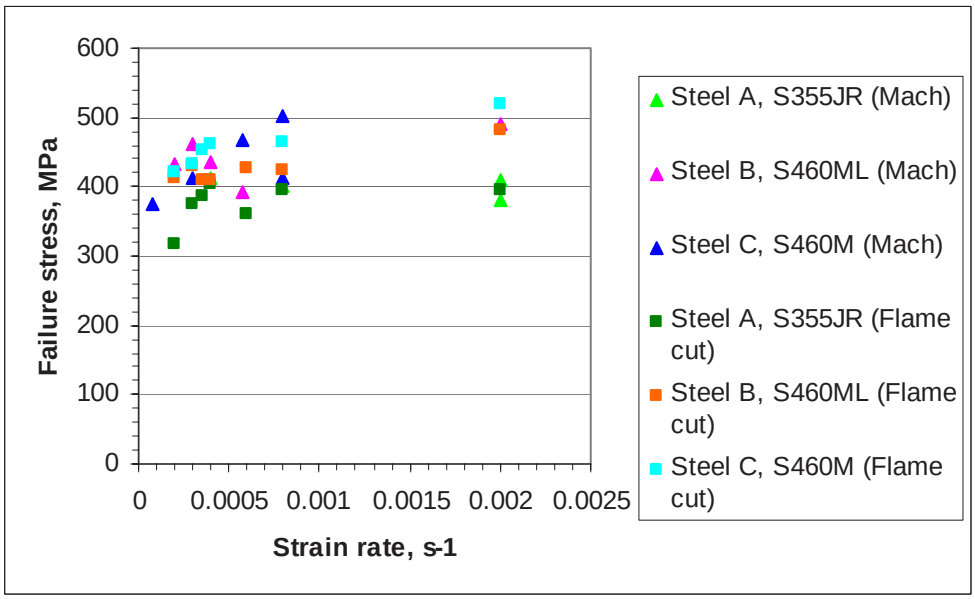

Fig. 77: Effect of strain rate on LMAC failure stress

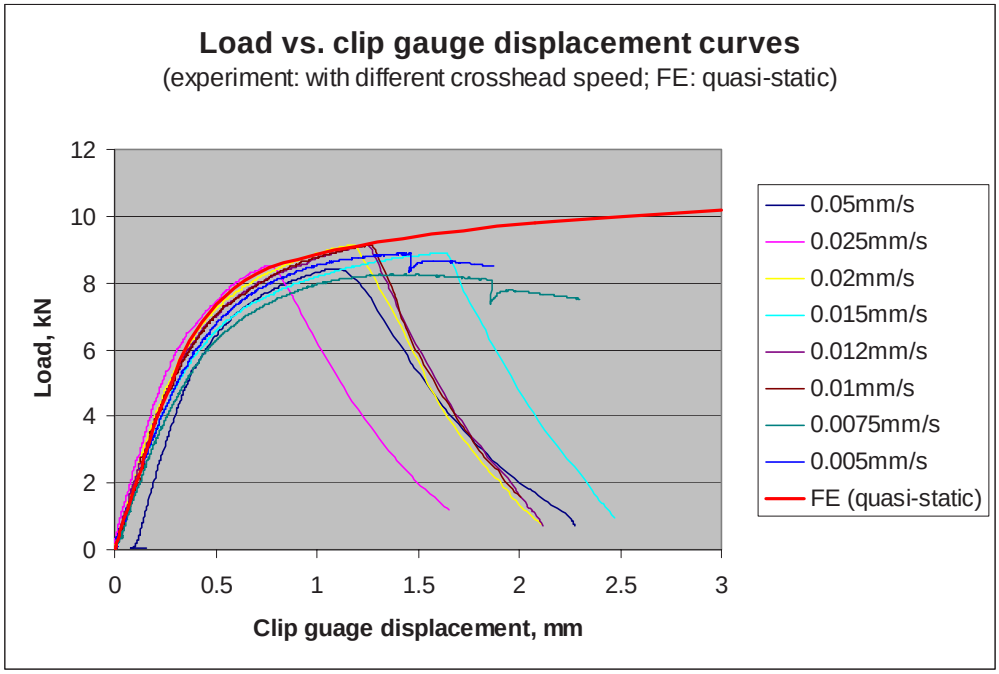

Fig. 78: LMAC tests on key-hole test pieces

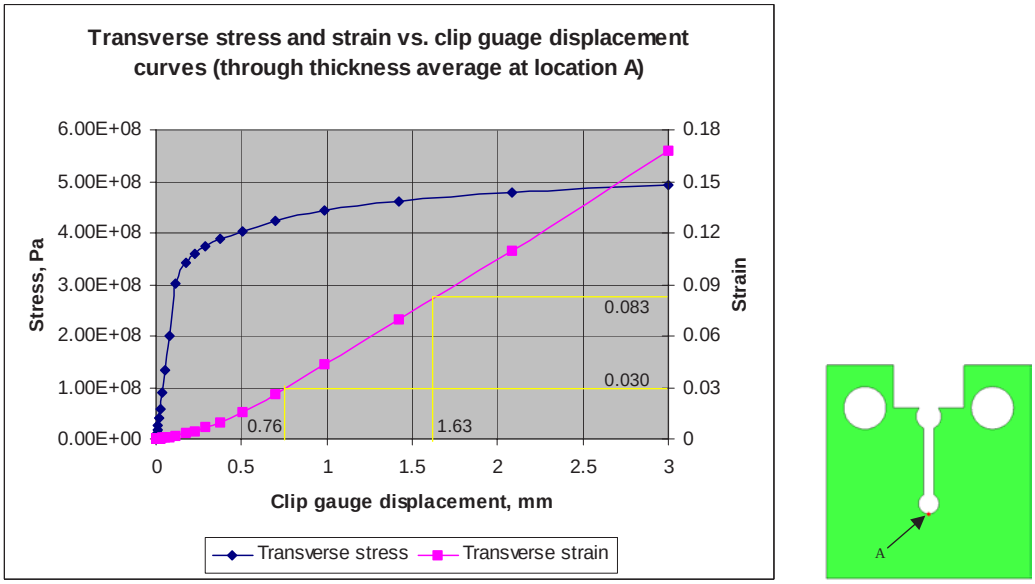

Fig. 79: Key hole results

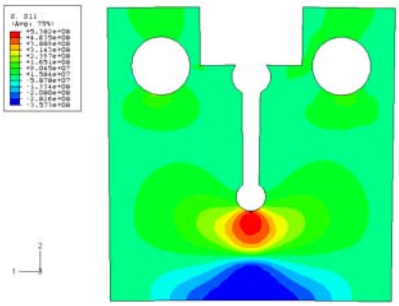

(a) Stress: clip gauge displacement of 0.99 mm

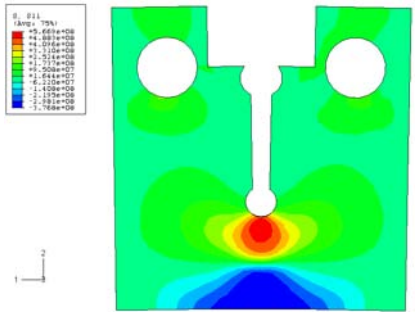

(b) Stress: clip gauge displacement of 1.43 mm

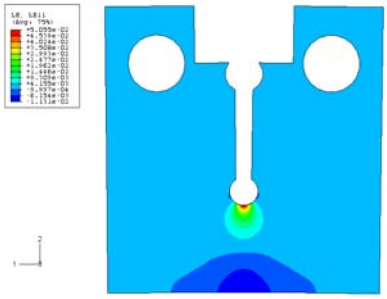

(c) Strain: clip gauge displacement of 0.99 mm

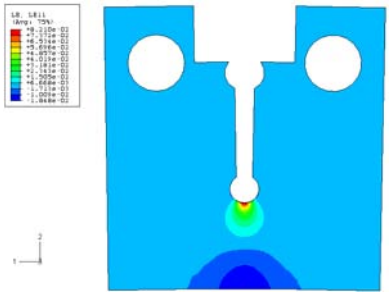

(d) Strain: slip gauge displacement of 1.43 mm

Fig. 80(a-d): FE prediction of transverse stress and strain distributions in the surface of the modified compact tensile specimen during testing at 450 °C

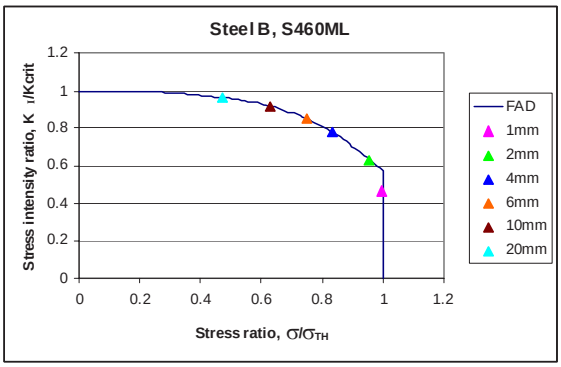

(a)

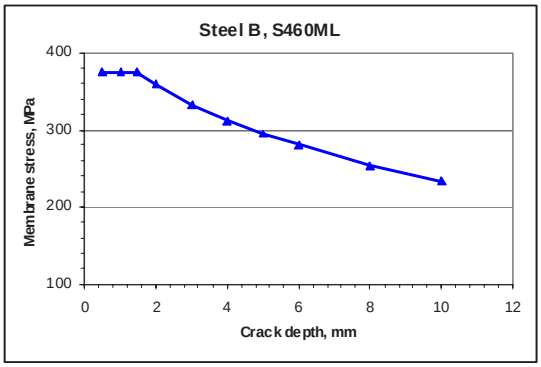

(b)

Fig. 81(a and b): Influence of long surface crack depth on LMAC (a) Level 2 FAD diagram for LMAC tests incorporating threshold stress and stress integrity (b) Dependence of critical stress on defect depth

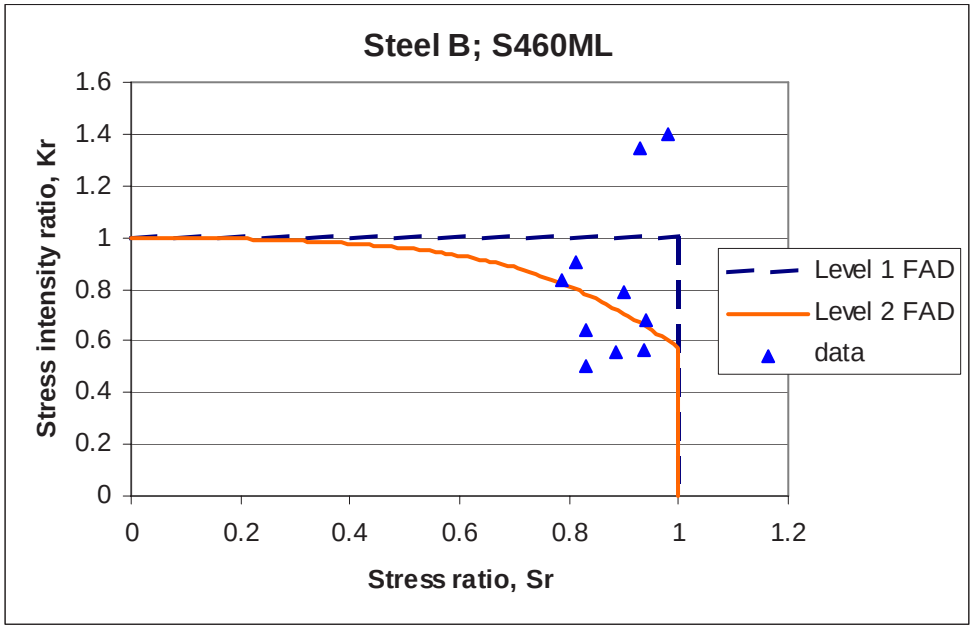

Fig. 82: Results of short crack tests

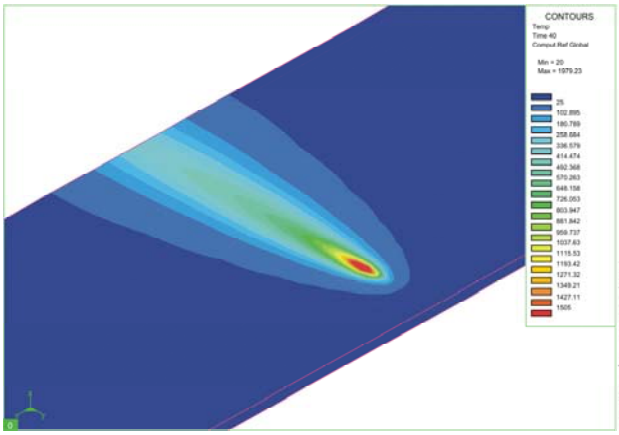

Fig. 83: Temperature field during the welding process of a butt weld connection of two plates

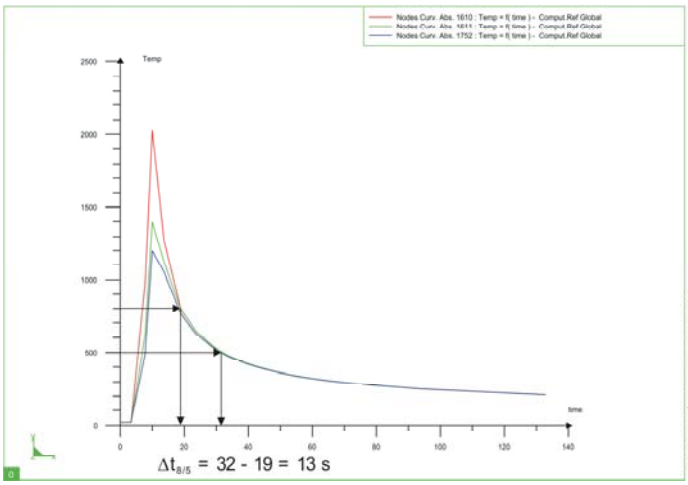

Fig. 84. Cooling curves in the middle of the weld

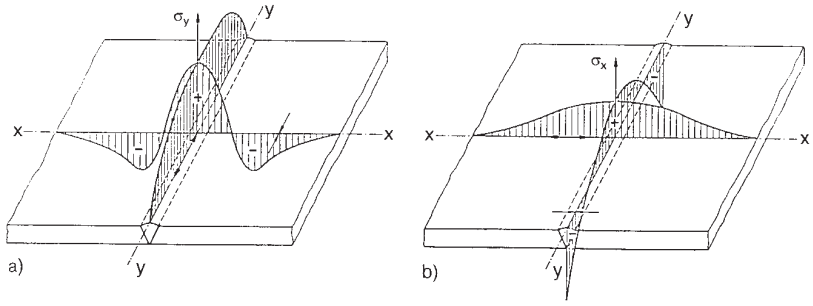

(a) (b)

Fig. 85(a and b): Qualitative distribution of longitudinal (a) and transversal stresses (b) in a butt weld connection after the welding process [8]

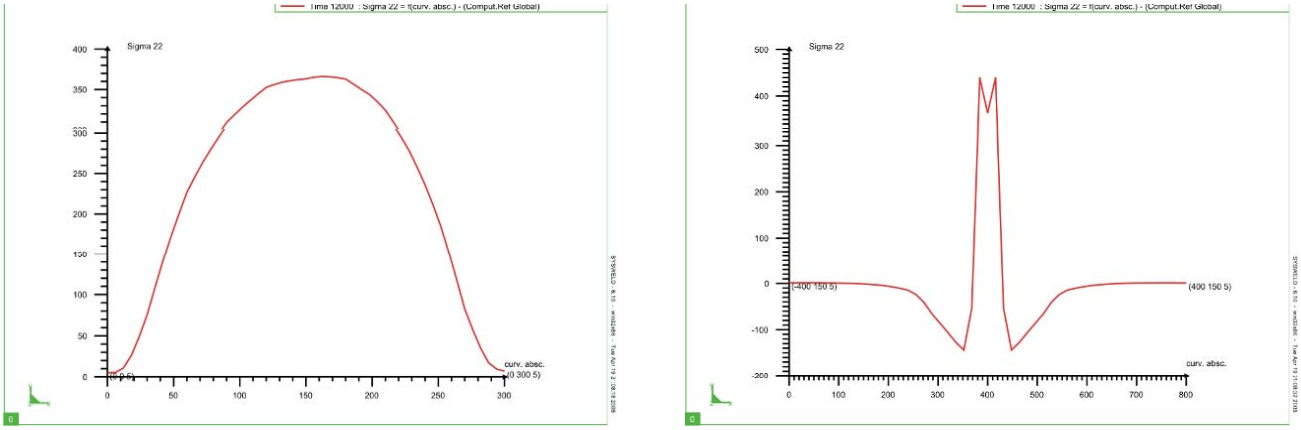

Fig. 86(a and b): Longitudinal stresses σy: (a) longitudinal cut, (b) lateral cut

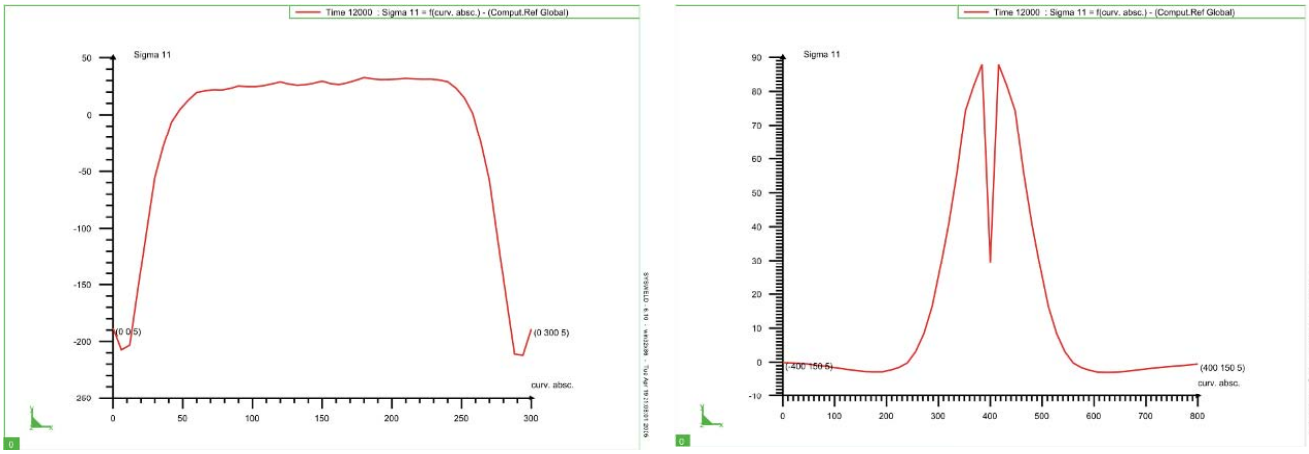

Fig. 87(a and b): Longitudinal stresses σy: (a) longitudinal cut, (b) lateral cut

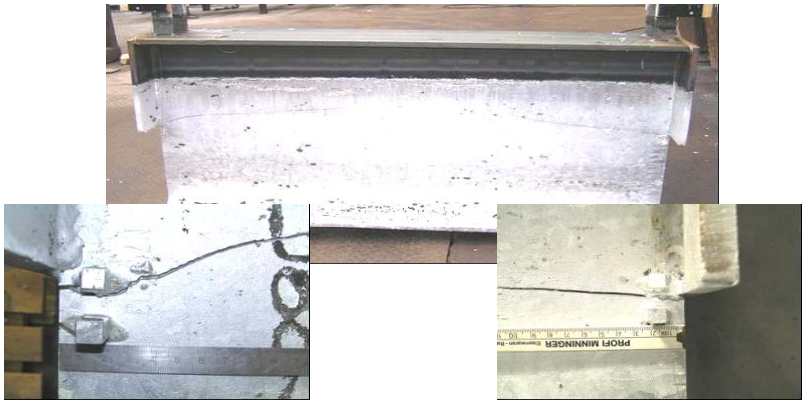

Fig. 88: Cracked section after TUKL validation trial

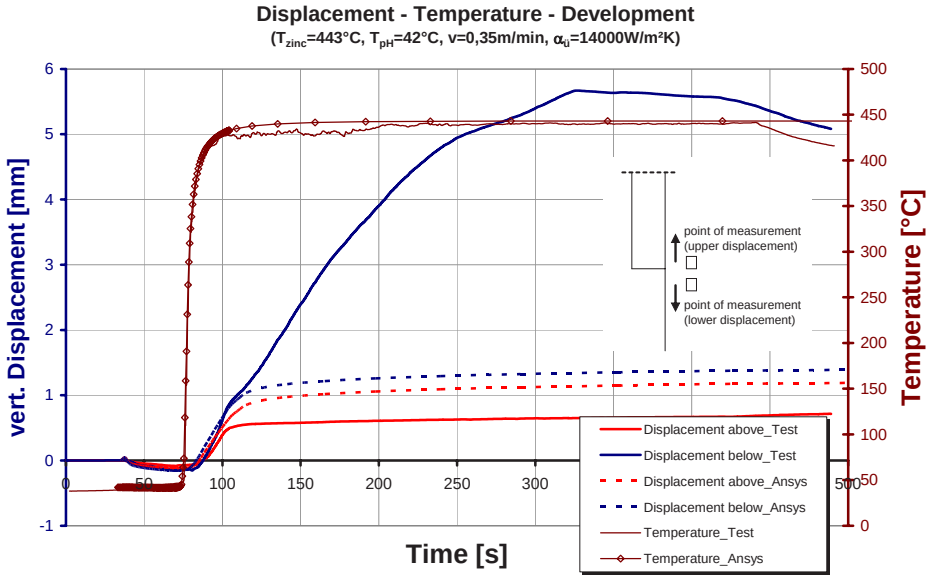

Fig. 89: Displacement and Temperature Development during the dipping process

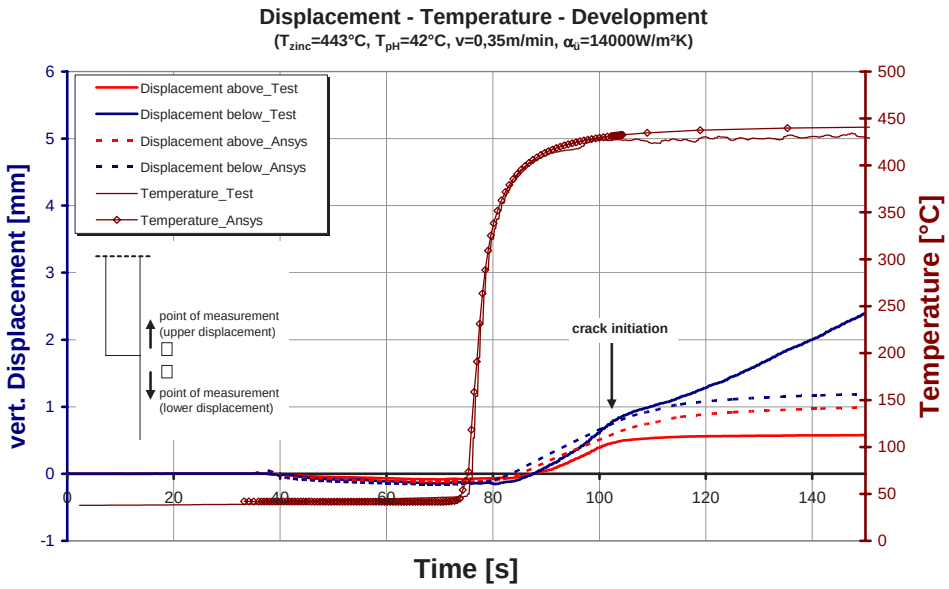

Fig. 90: Displacement and Temperature Development in the Time Range of Immersion

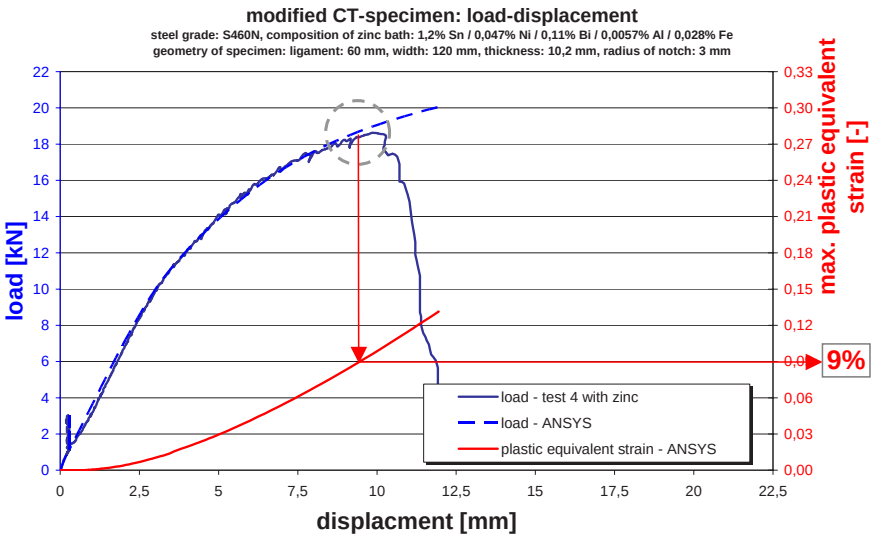

Fig. 91: Recorded and recalculated Load-Displacement-Development and calculated strain behaviour

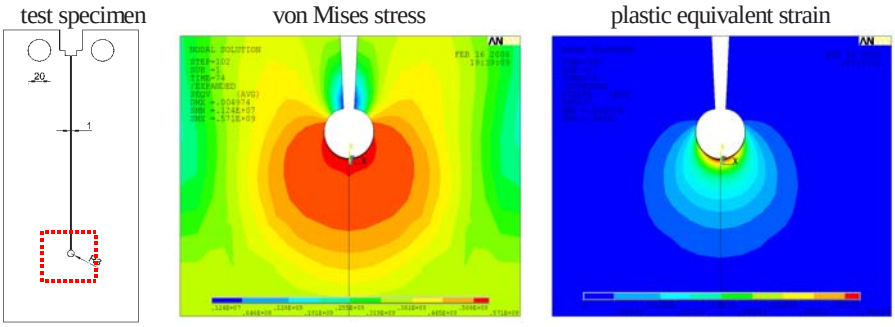

Fig. 92: stress and strain limit state at the point of crack initiation

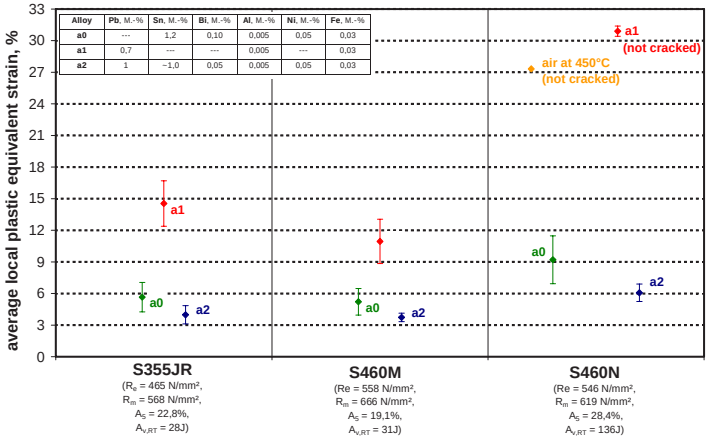

Alloy	Pb, M.-%	Sn, M.-%	Bi, M.-%	Al, M.-%	Ni, M.-%	Fe, M.-%
a0	---	1,2	0,10	0,005	0,05	0,03
a1	0,7	---	---	0,005	---	0,03
a2	1	~1,0	0,05	0,005	0,05	0,03

Fig. 93: Calculated limit strain in dependence of the bath composition and the material

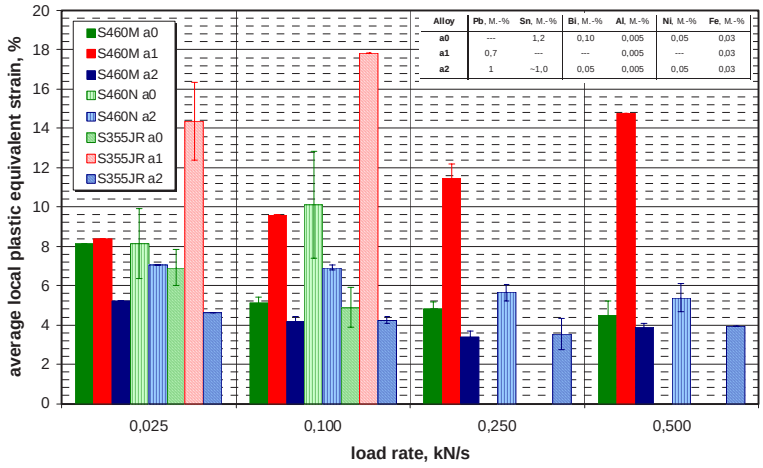

Fig. 94: Calculated limit strain in dependence of the loading velocity and the material

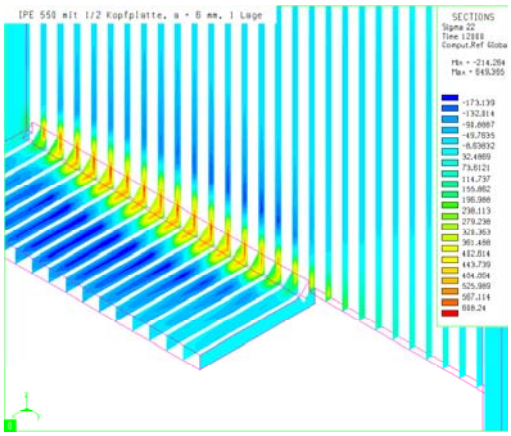

Fig. 95: Residual stress state in longitudinal direction (σ_y)

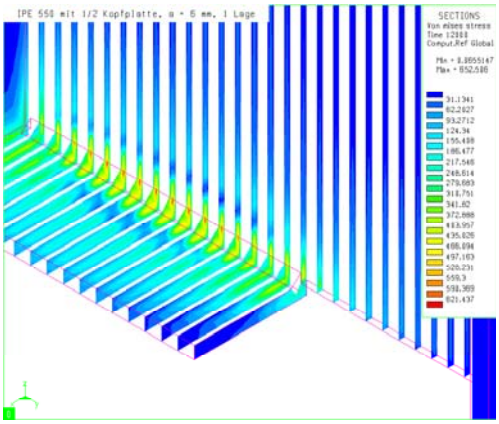

Fig. 96: Residual von Mises stress

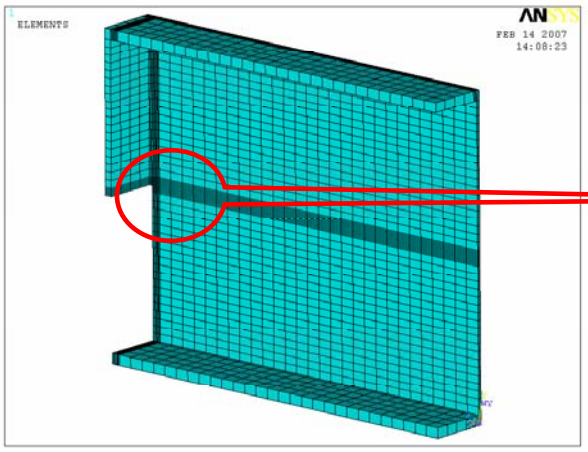

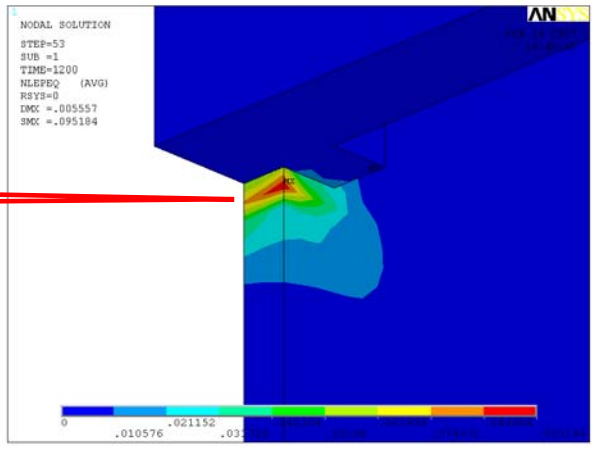

FE model **max. pl. equiv. strain during immersion: ca. 10%**

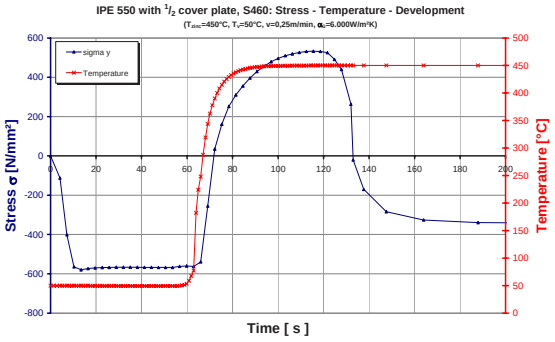

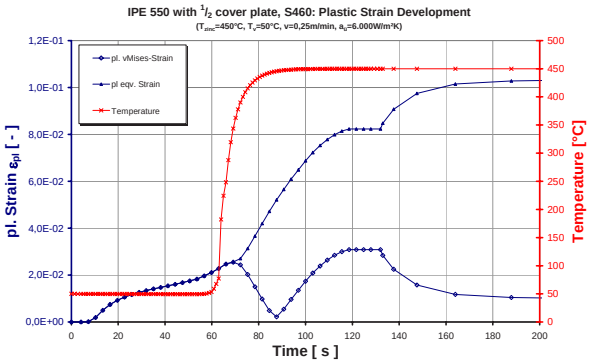

Fig. 97: Galvanizing Process Simulation of a Beam with Half Cover Plate – Results

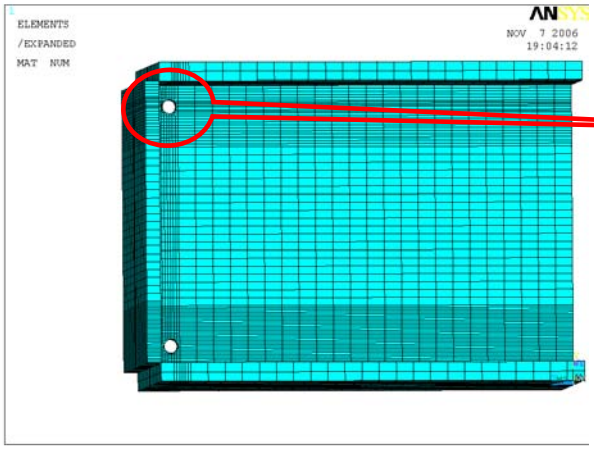

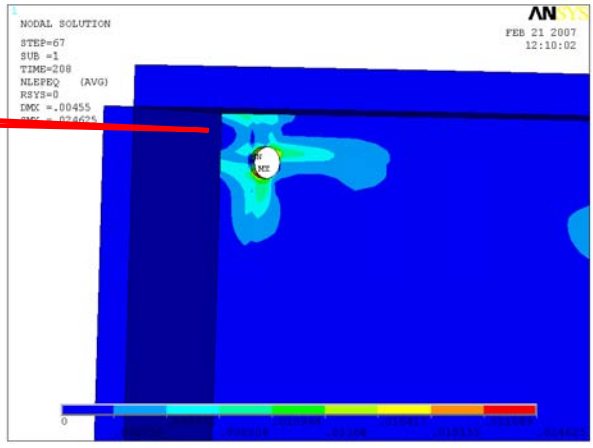

FE model **max. pl. equiv. strain during immersion: ca. 2,5%**

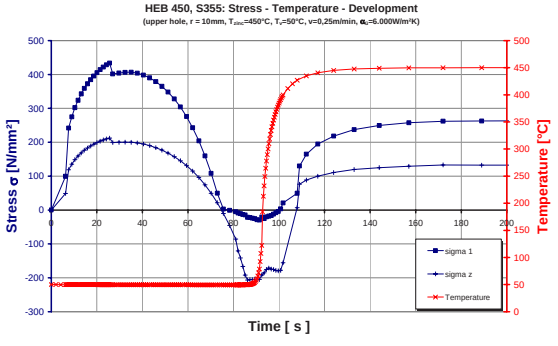

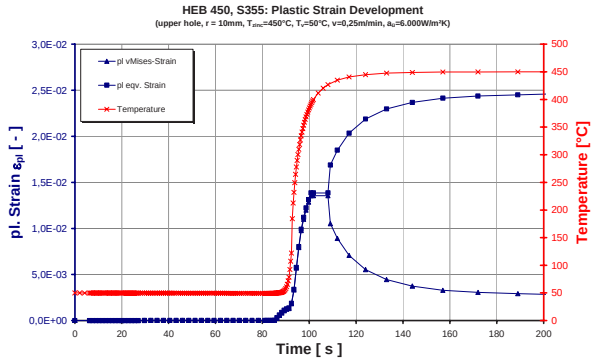

stress development during immersion **strain development during immersion**

Fig. 98: Galvanizing Process Simulation of a Beam with Full Cover Plate and Drilled Holes- Results

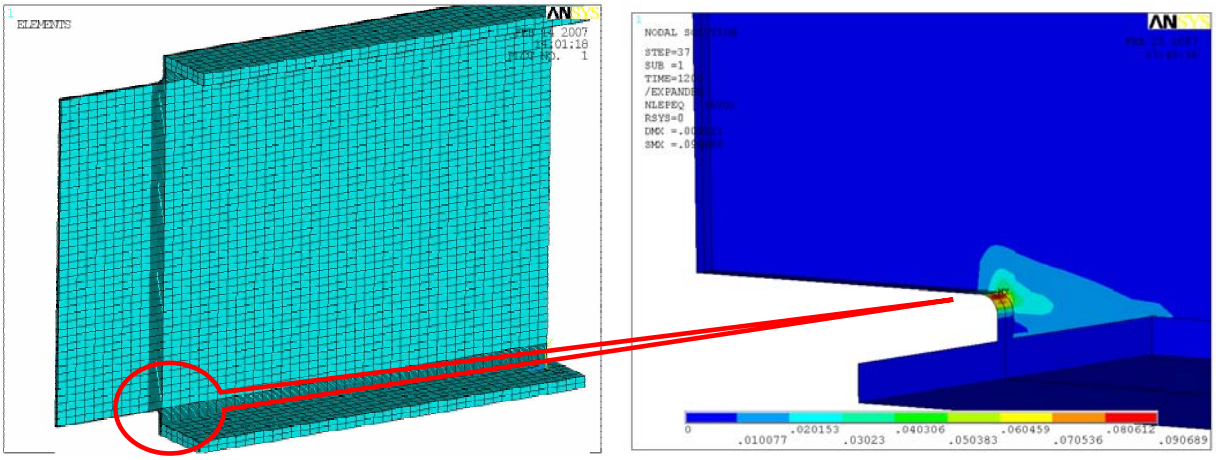

FE model **max. pl. equiv. strain during immersion: ca. 9%**

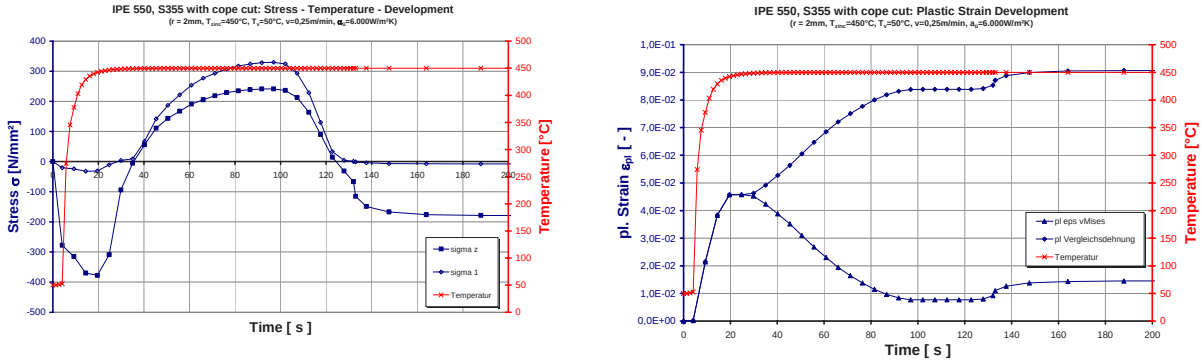

Fig. 99: Galvanizing Process Simulation of a Beam with Cope Cut- Results

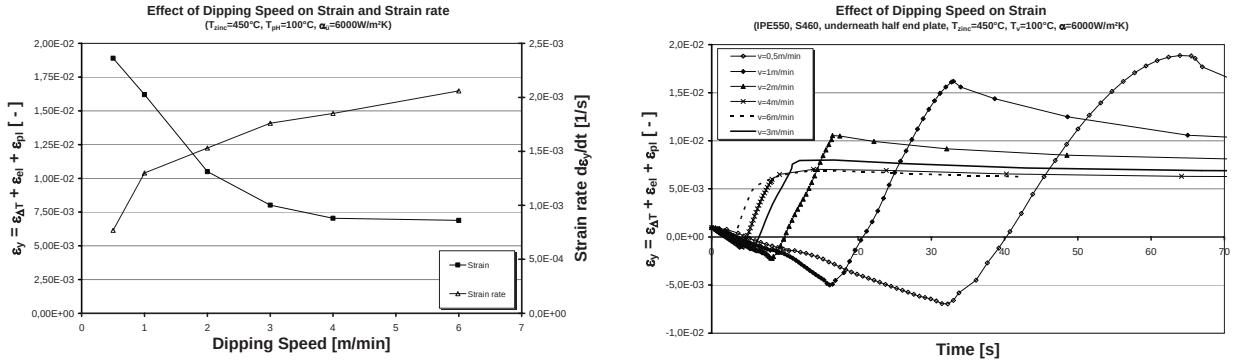

Fig. 100: Effect of the dipping speed on the maximum strain and strain rate

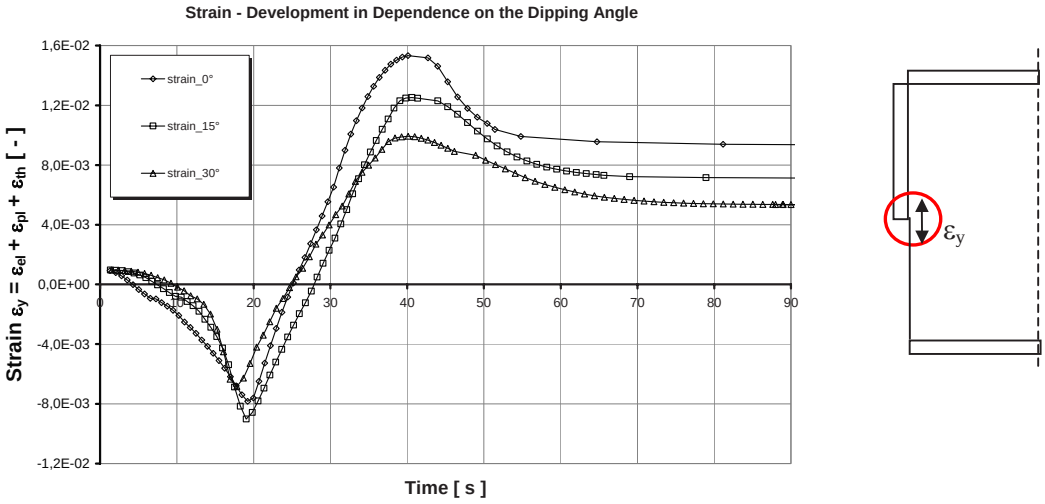

Fig. 101: Effect of dipping angle on the strain development

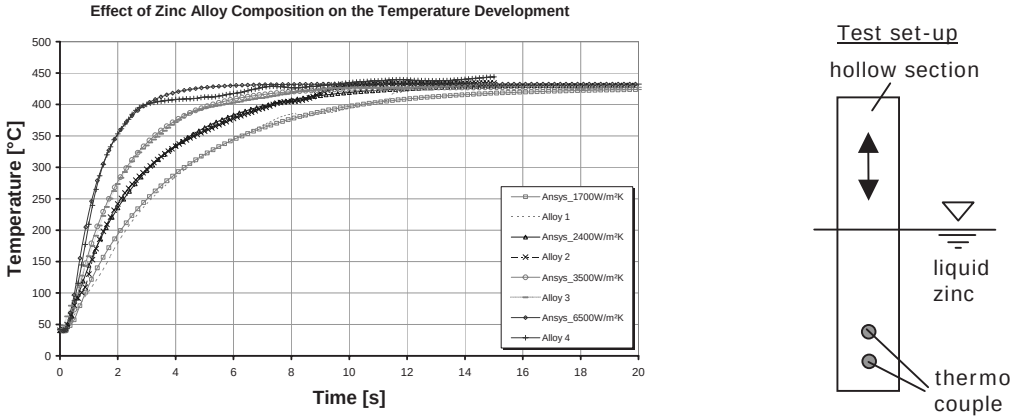

Fig. 102: Effect of Zinc Alloy Composition on the Heating Behaviour – Small Scale Test Results

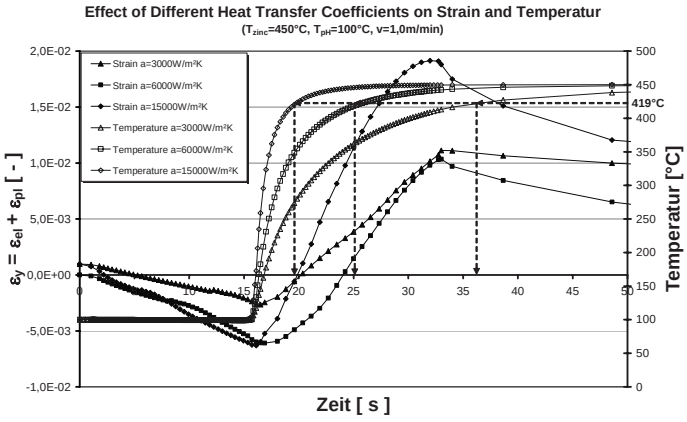

Fig. 103: Effect of Different Heat Transfer Coefficients on the Strain and Temperature Development During Immersion in the Zinc Smelter

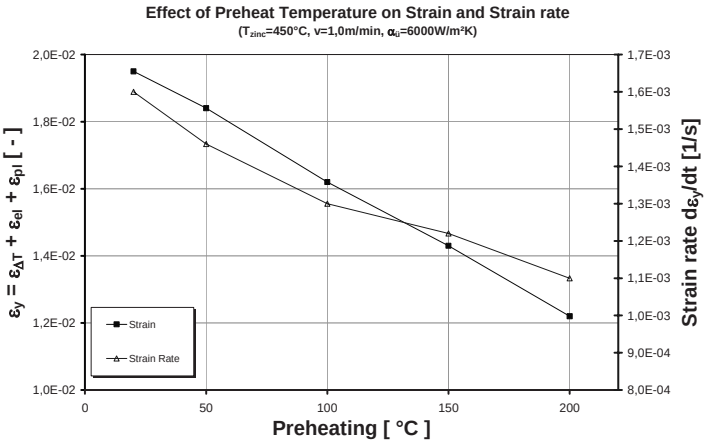

Fig. 104: Effect of Preheat Temperature on Strain and Strain rate
During Immersion in the Zinc Smelter

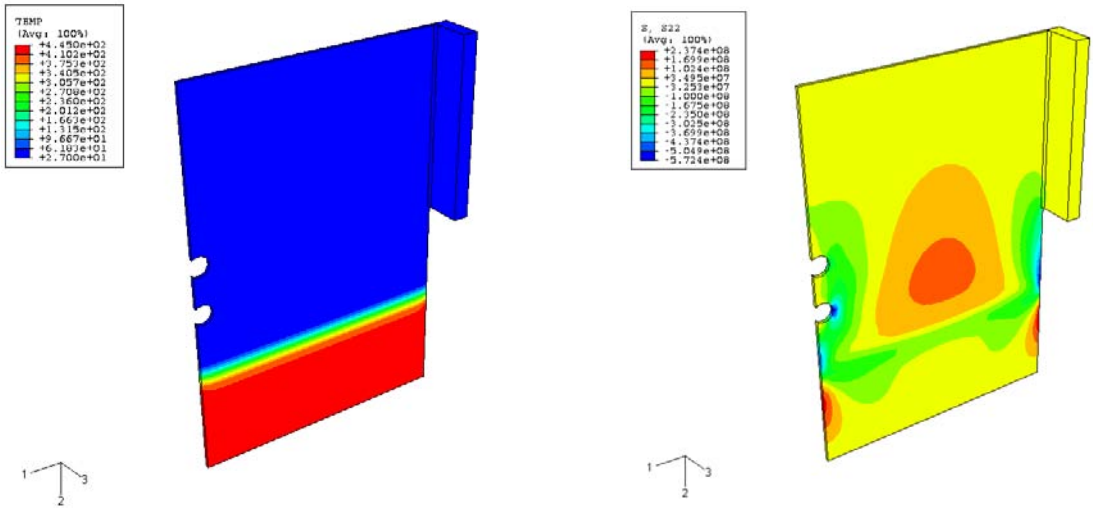

(a) (b)

Fig.105(a and b): Temperature (a) and longitudinal (S22) stress (b) development contours of the half-cover plate component during galvanizing (at 30 s) predicted by ABAQUS FE simulation (CRD&T).

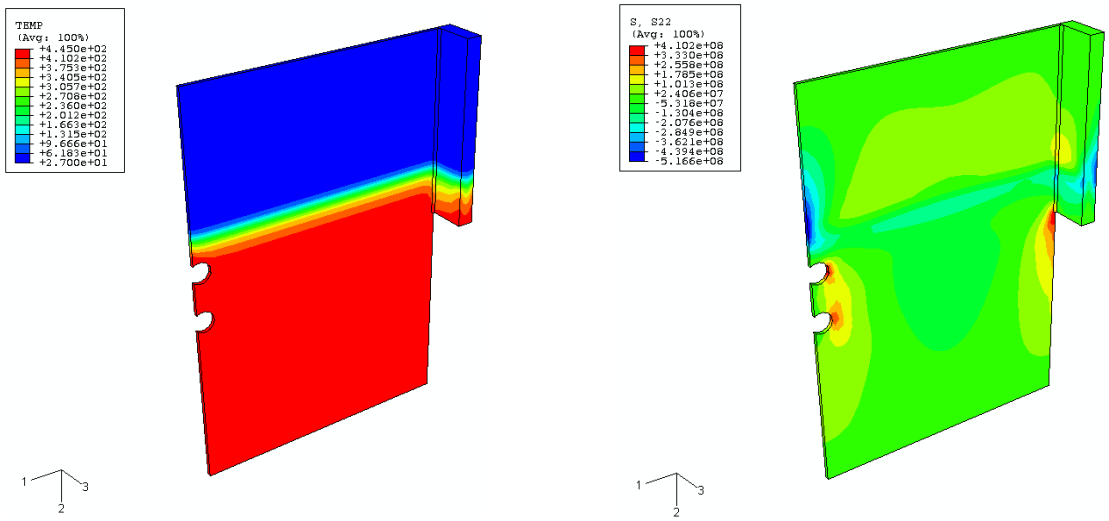

(a) (b)

Fig. 106(a and b): Temperature (a) and longitudinal (S22) stress (b) development contours of the half-cover plate component during galvanizing (at 69.5 s) predicted by the FE simulation.

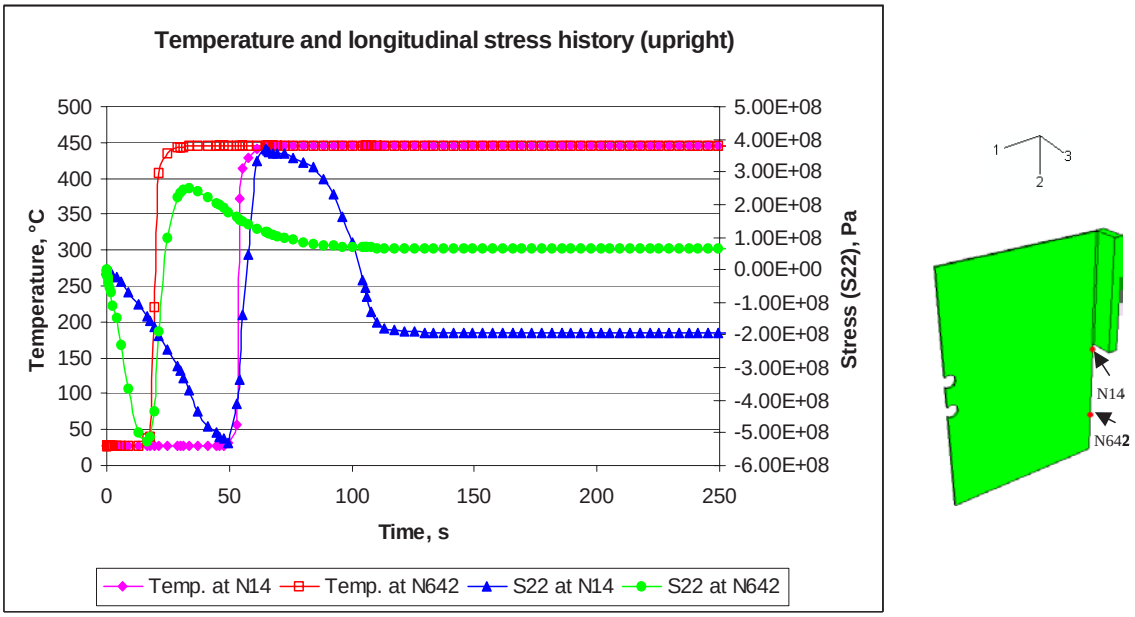

Fig. 107: Local temperature and stress history at nodes N14 and N642 during galvanizing of the half-cover plate predicted by the FE simulation (upright dipping)

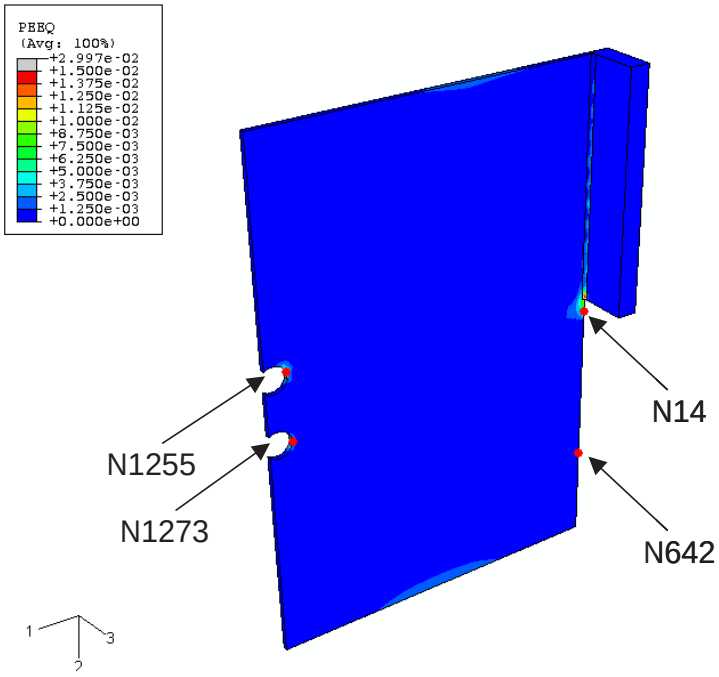

Fig. 108: Generalised plastic strain distribution of the half-cover plate after full immersion in the zinc bath predicted by the FE simulation, showing localised strain damage primarily in three areas (near nodes N14, N1255 and N1273).

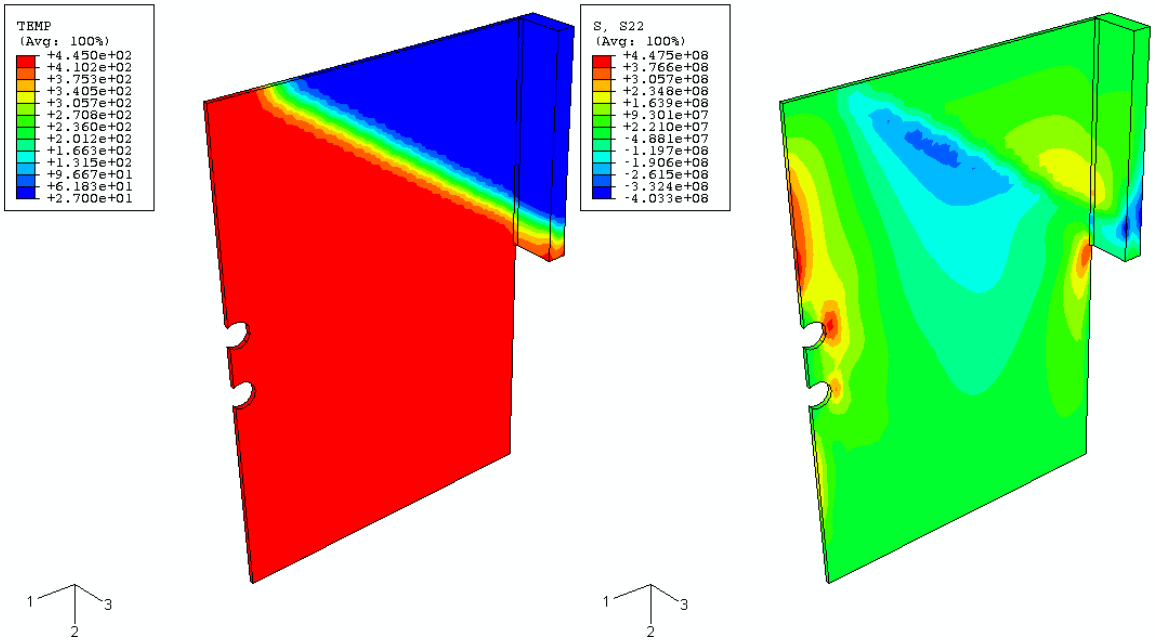

(a) (b)

Fig. 109(a and b): Temperature (a) and longitudinal (S22) stress (b) development contours of the half-cover plate component during galvanizing (at 165 s, 45-degrees dipping) predicted by the FE simulation.

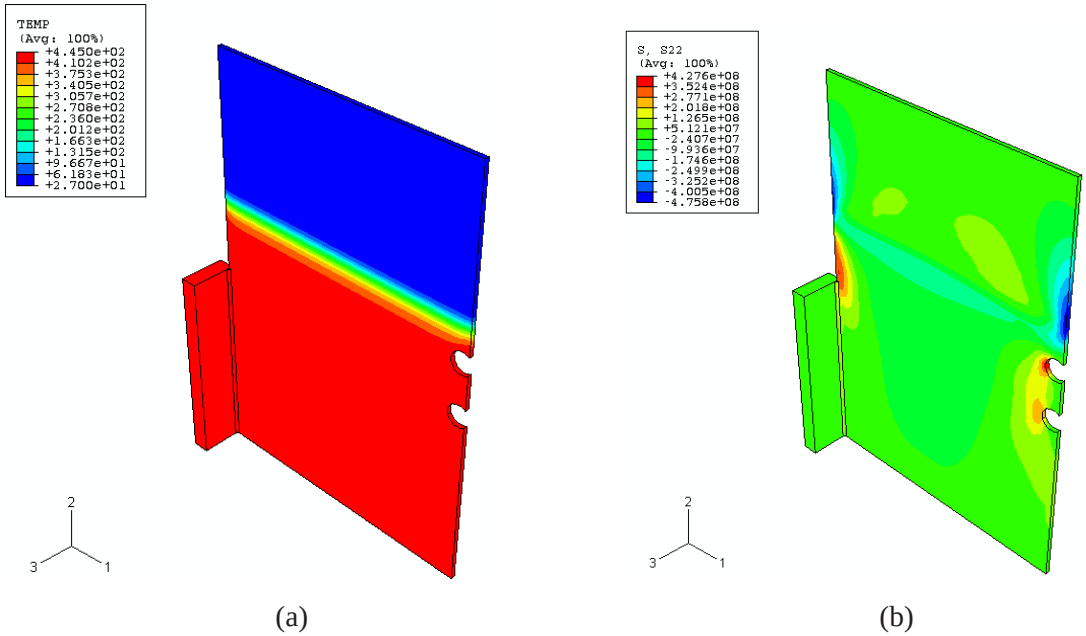

(a) (b)

Fig. 110(a and b): Temperature (a) and longitudinal (S22) stress (b) development contours of the half-cover plate component during galvanizing (at 70s, upside-down dipping) predicted by the FE simulation.

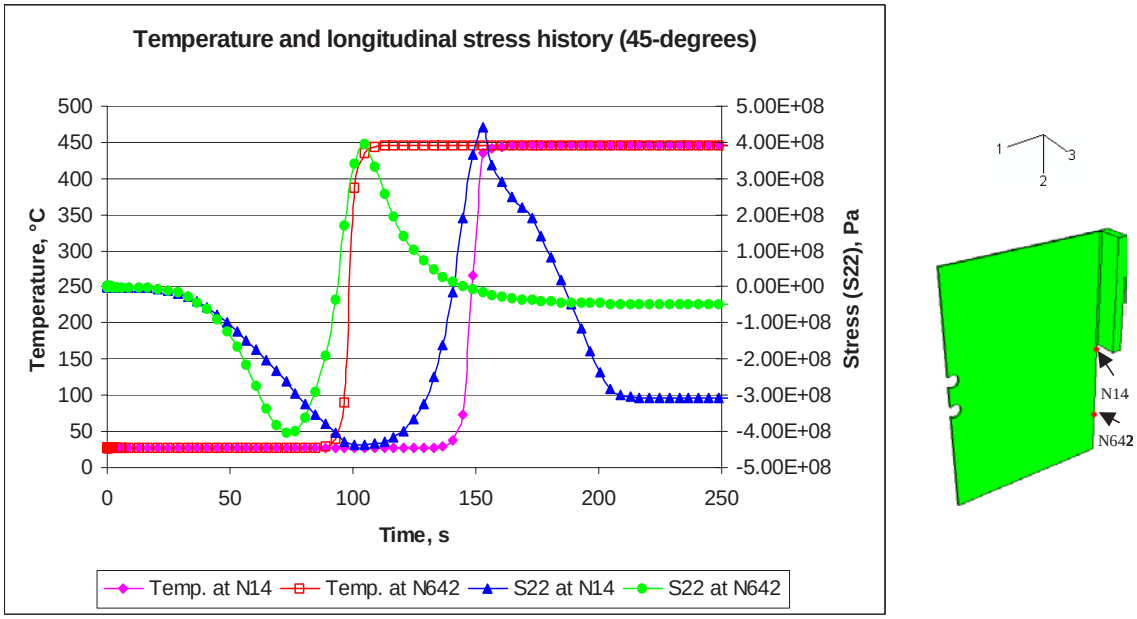

Fig. 111: Local temperature and stress history at nodes N14 and N642 during galvanizing of the half-cover plate predicted by the FE simulation (45-degrees dipping).

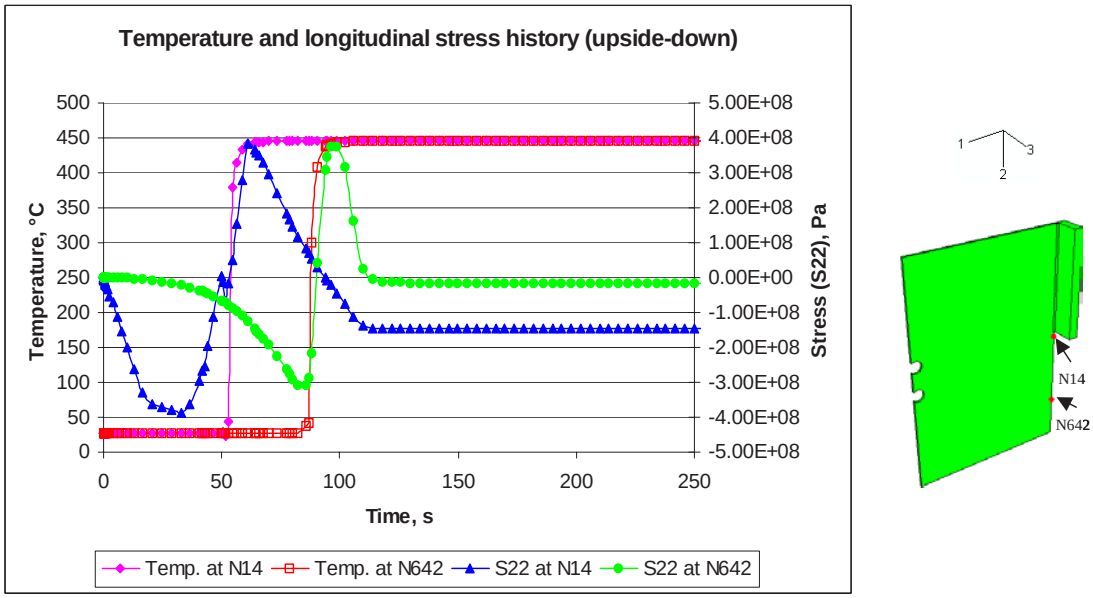

Fig. 112: Local temperature and stress history at nodes N14 and N642 during galvanizing of the half-cover plate predicted by the FE simulation (upside-down dipping).

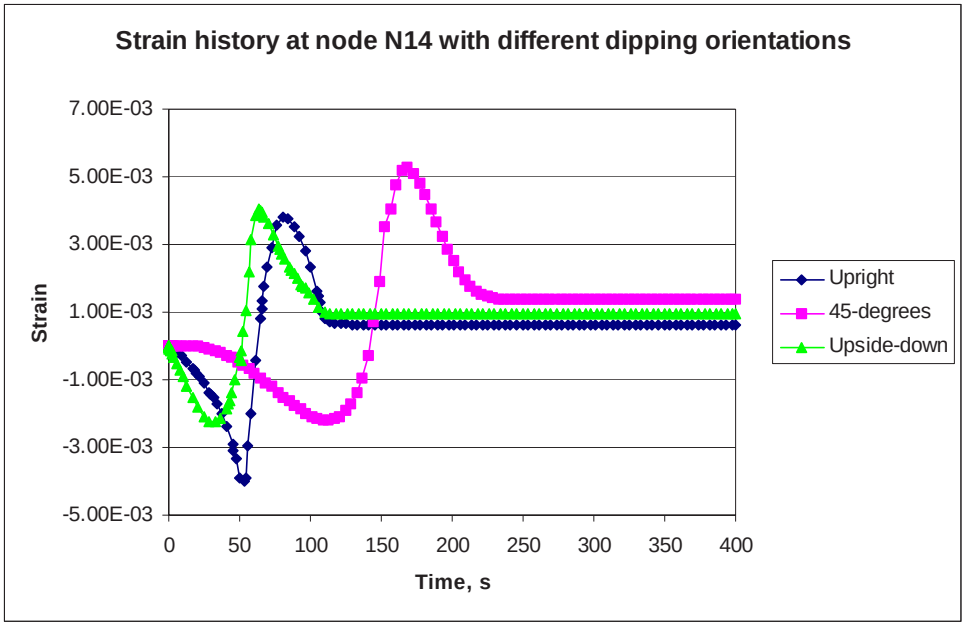

Fig. 113: FE prediction of strain history at node N14 with different dipping orientations.

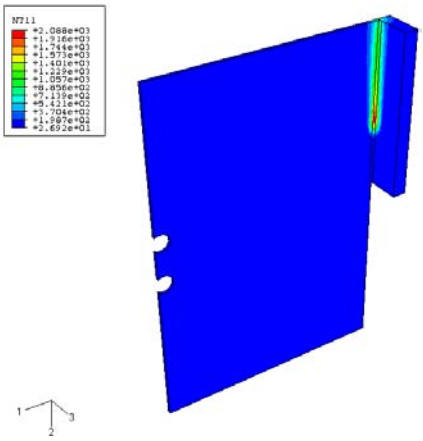

Fig. 114: FE prediction of temperature distribution during fillet welding.

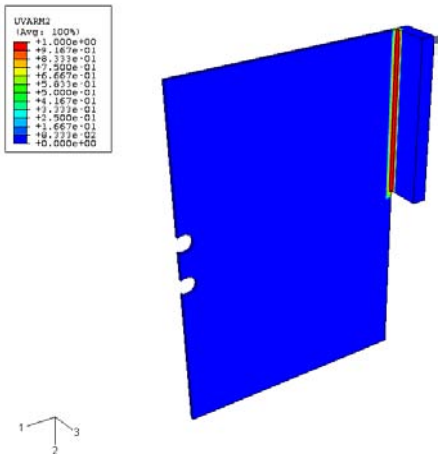

Fig. 115: FE prediction of HAZ index contours after fillet welding (contour value = 1.0: weld metal; contour value between 0.5 and 1.0: HAZ; contour value less than 0.5: parent material).

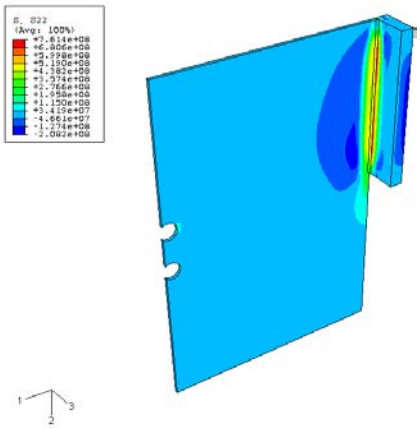

Fig. 116: FE prediction of longitudinal residual stress (S22) distribution after fillet welding.

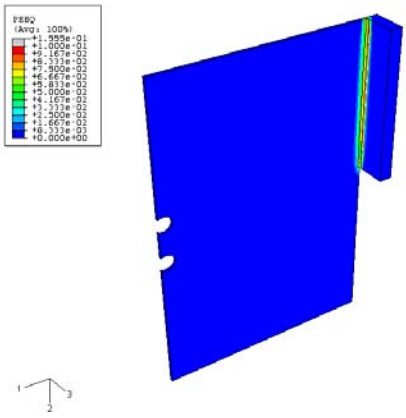

Fig. 117: FE prediction of generalised plastic strain distribution after fillet welding.

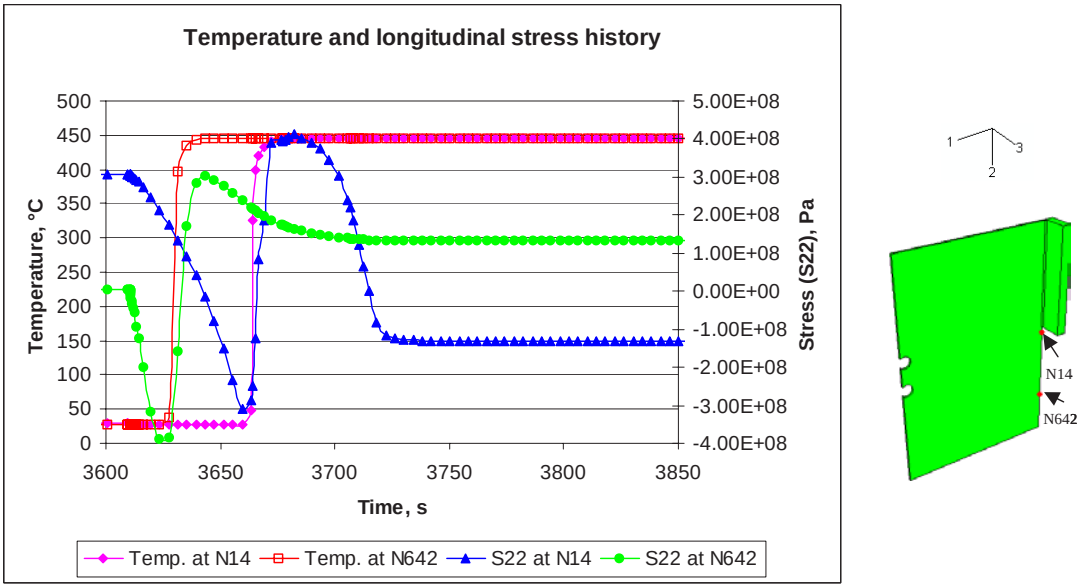

Fig. 118: Local temperature and stress history at nodes N14 and N642 during galvanising of the half-cover plate predicted by the FE simulation including the effect of weld induced residual stress and strain (upright dipping).

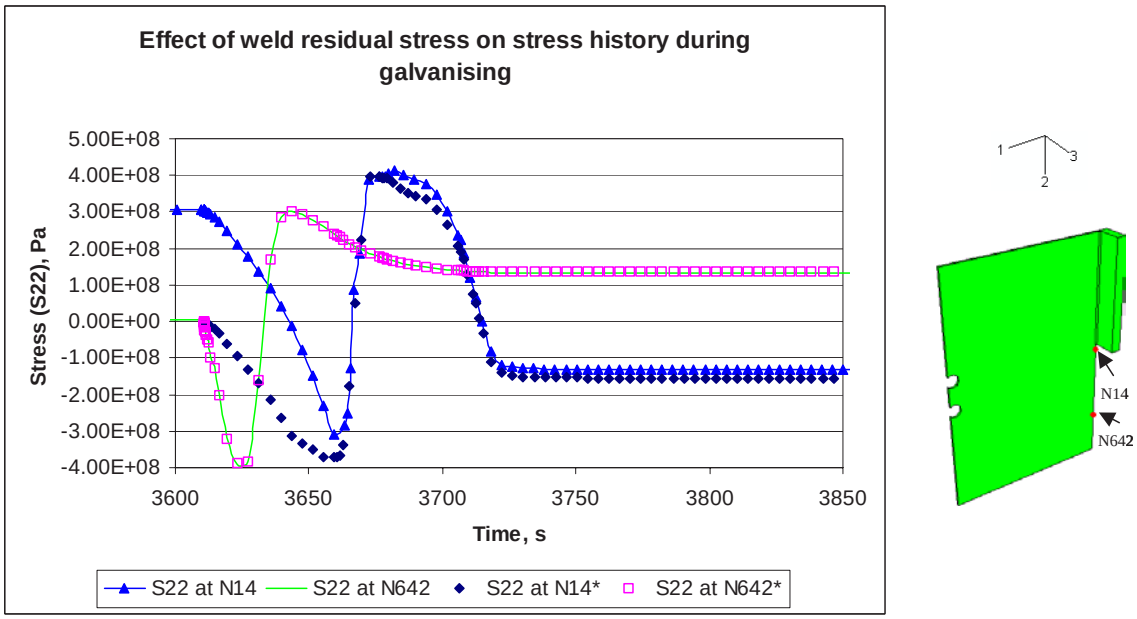

Fig. 119: Local stress history at nodes N14 and N642 during galvanising of the half-cover plate predicted by the FE simulation with (*) and without the effect of weld induced residual stress and strain (upright dipping).

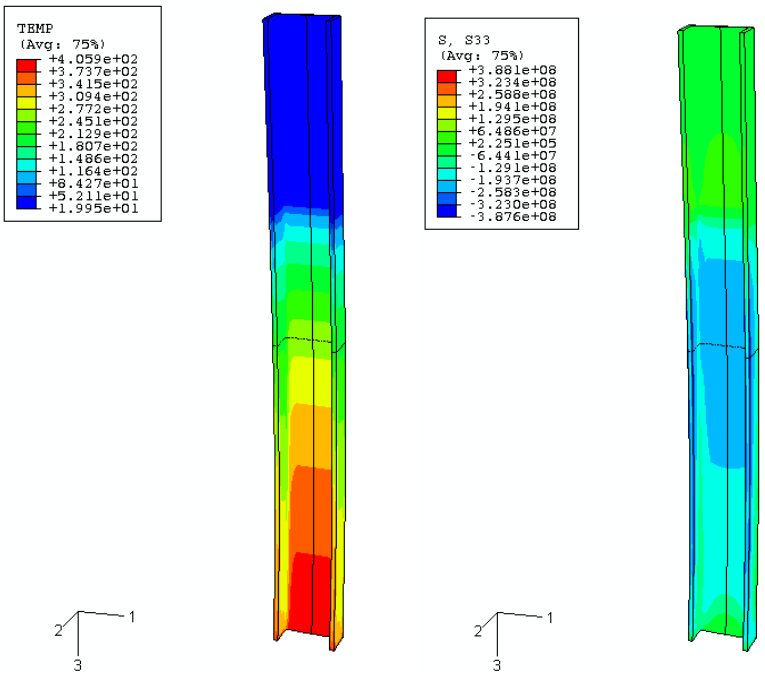

(a) (b)

Fig. 120(a and b): FE prediction of temperature (a) and longitudinal stress (S33) (b) distributions at 2.87 s of dipping during the channel section galvanizing process simulation (distorted geometry exaggerated by 10 times).

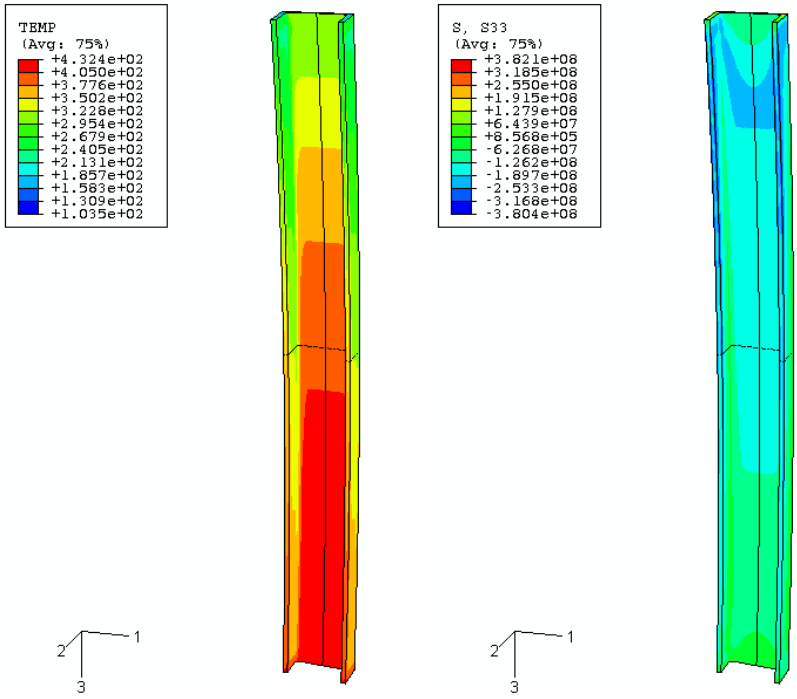

(a) (b)

Fig. 121(a and b): FE prediction of temperature (a) and longitudinal stress (S33) (b) distributions at 5.81 s of dipping during the galvanizing process simulation (distorted geometry exaggerated by 10 times).

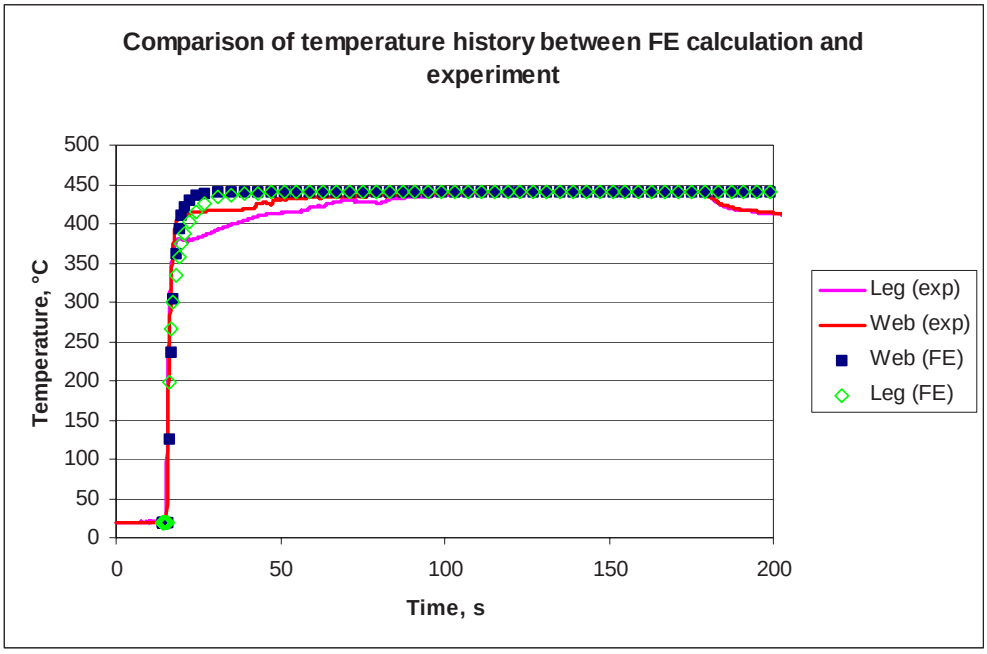

Fig. 122: Comparison of temperature history between FE prediction and experiment

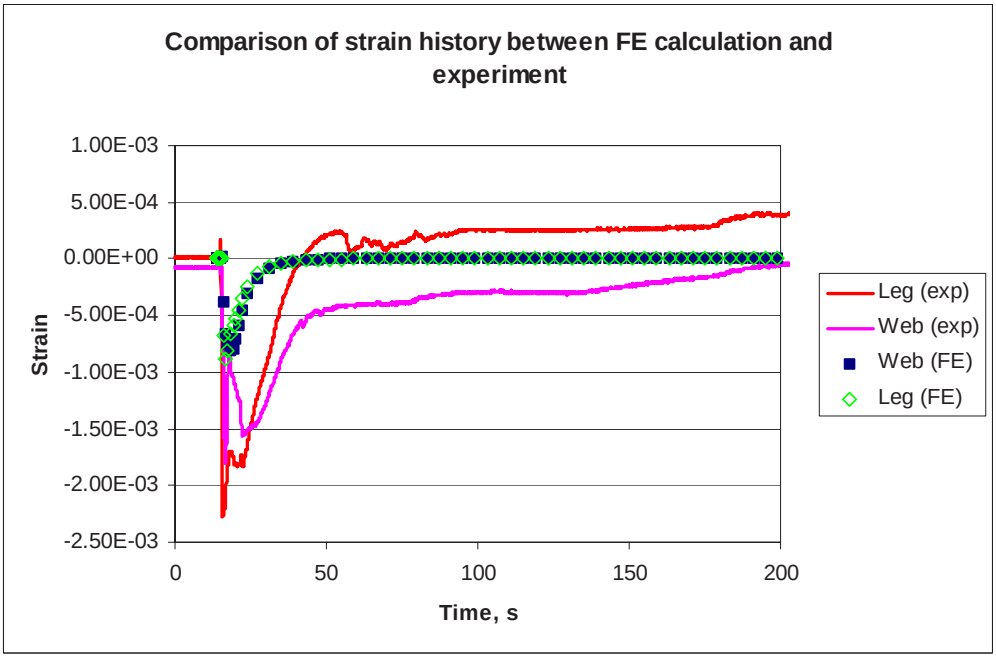

Fig. 123: Comparison of longitudinal strain history between FE prediction and experiment

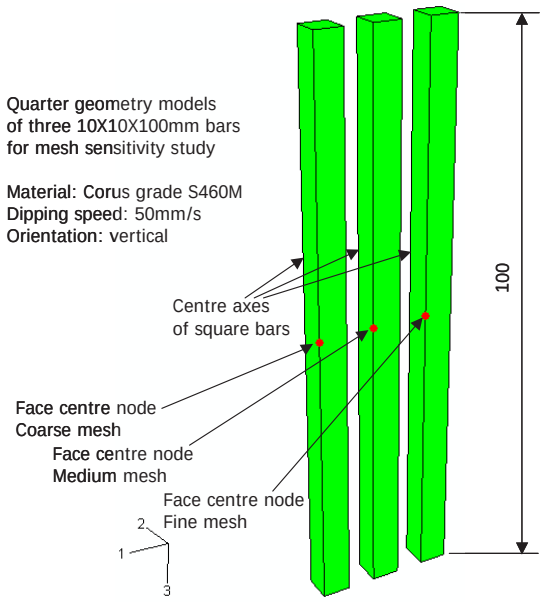

Fig. 124: Identical model geometry and different mesh density used in the FE mesh sensitivity study (face centre nodes are used for temperature and longitudinal strain history comparison).

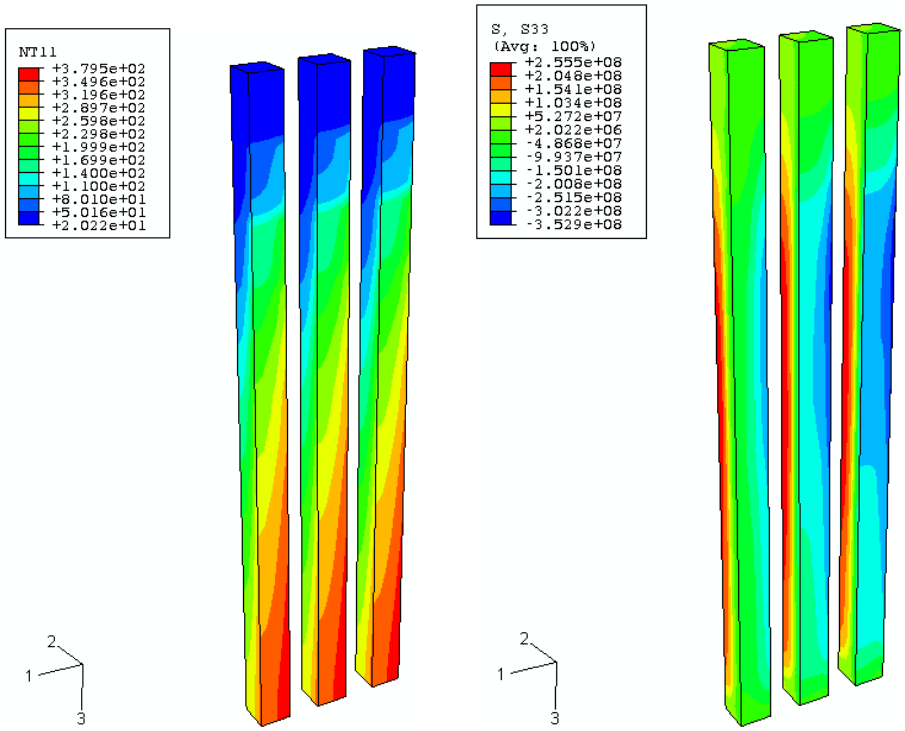

(a) (b)

Fig. 125(a and b): FE prediction of temperature (a) and longitudinal stress (S33) (b) distributions at 1.72 s of dipping during the galvanizing process simulation (mesh density increases from left to right).

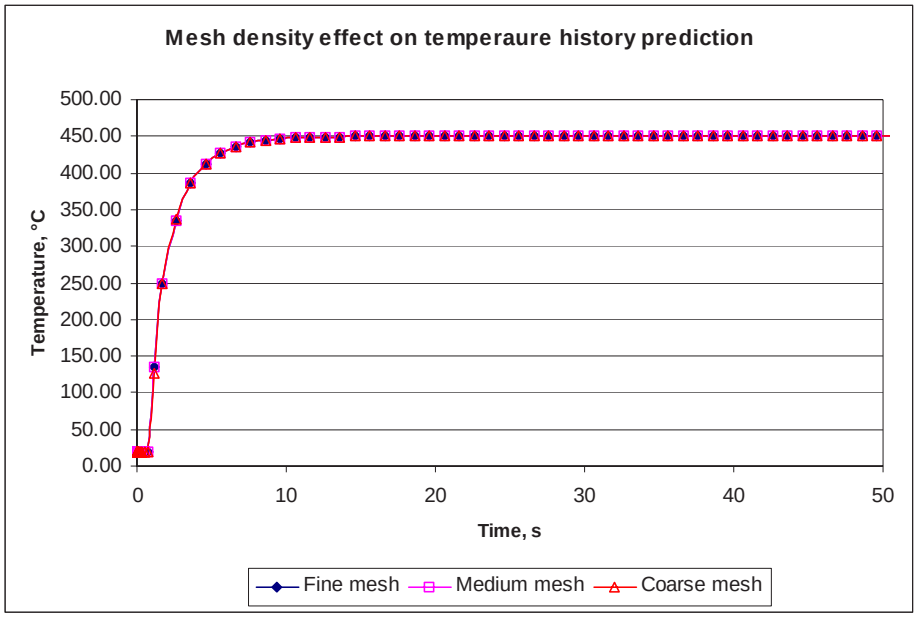

Fig. 126: FE prediction of temperature history at face centre nodes showing no effect of mesh density used in the FE simulation.

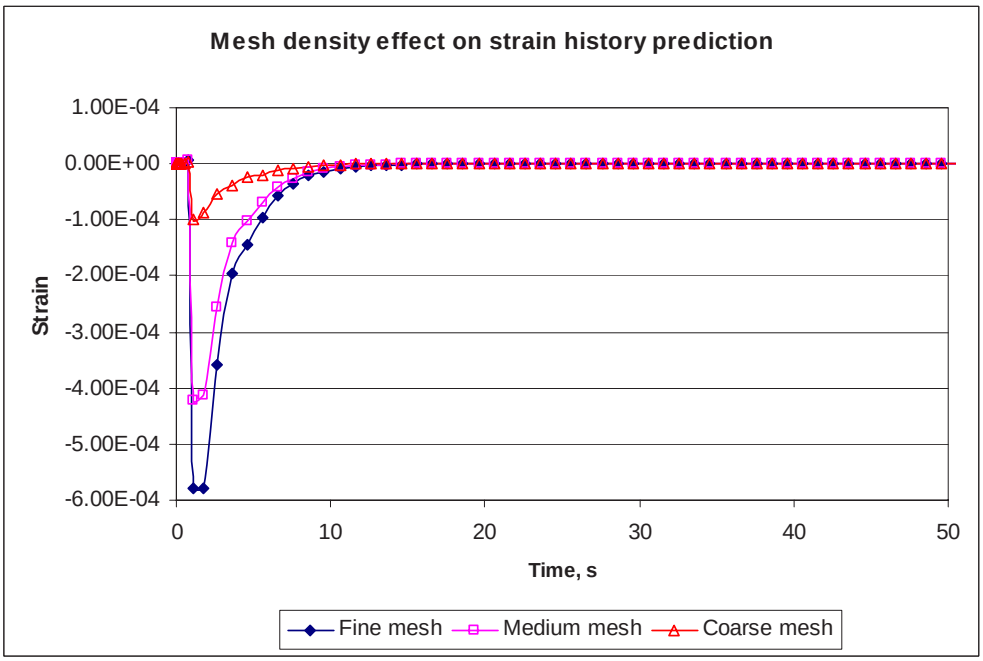

Fig. 127: FE prediction of strain history at face centre nodes showing the significant effect of mesh density used in the FE simulation.

European Commission

EUR 23195 — Failure mechanisms during galvanising

W. J. Rudd, S. W. Wen, P. Langenberg, B. Donnay, A. Voelling, T. Pinger, M. Feldmann, J. Carpio, J. A. Casado, J. A. Alvarez, F. Gutierrez-Solana

Luxembourg: Office for Official Publications of the European Communities

2008 — 138 pp. — 21 × 29.7 cm

Research Fund for Coal and Steel series

ISBN 978-92-79-08171-2

ISSN 1018-5593

Price (excluding VAT) in Luxembourg: EUR 20